ADVANCED TECHNOLOGY COMPOSITE
AIRCRAFT STRUCTURES

MONTHLY TECHNICAL PROGRESS REPORT NO. 25

FOR PERIOD MAY 1 - MAY 31, 1991

PREP \RED FOR

**NATIONAL AERONAUTICS AND SPACE ADMINISTRATION
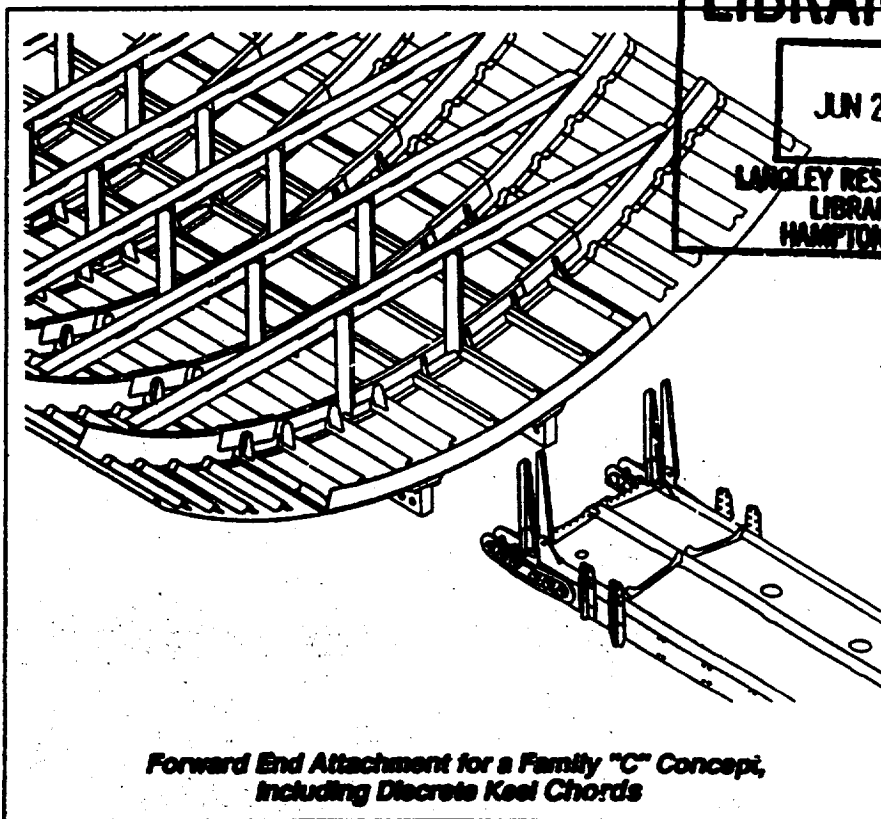LANGLEY RESEARCH CENTER
HAMPTON, VIRGINIA 23665-5225**

UNDER CONTRACT NAS1-18889

JUNE 14, 1991

*Forward End Attachment for a Family "C" Concept,
including Discrete Keel Chords*

**BOEING COMMERCIAL AIRPLANE GROUP
TECHNOLOGY AND PRODUCT DEVELOPMENT
P.O. Box 3707
Seattle, Washington 98124-2207**

38.

1-MR.JOSEPH W. OWENS, NASA CONTRACT ADMINISTRATOR M/S 126

8-MR.WILLIAM T. FREEMAN, TCHNICAL REPRSENTATIVE NASA M/S-241

1-MR.JOHN SAMOS NEW TECHNOLOGY REPRESENTATIVE M/S-139A

1-D. COURTNEY, AFPRO M/S 3C-84

1-T. GUTOWSKI, MASSACHUSETTS INSTITUTE OF TECHNOLOGY

1-J.T. QUINLIVAN M/S 9R-62

1-R.W.JOHNSON M/S 3K-65

1-P.J. SMITH M/S 3K-65

1-L.B. ILCEWICZ M/S 3K-65

1-T.H. WALKER M/S 3K-65

1-M.A. APELES M/S 3K-65

1-D.R. SEEMAN M/S 6P-78

1-D.E. HASTINGS M/S 76-67

1-D.H. GRANDE M/S 3K-65

1-K.S. WILLDEN M/S 57-09

1-M. MORRIS M/S 3K-65

1-K.H. SCHREIBER M/S 9R-62

1-D.L. GRANDE M/S 3T-CH

1-P.S. SAWCHUK M/S 3T-CH

1-D.P. MOONEY M/S 9R-62

1-C.K. GUNTHER M/S P30-31

1-R.E. HORTON M/S 3T-CH

1-G.G. CASSATT M/S K25-41

1-K. VENTERS M/S 3T-AX

1-B.L. MILLER M/S 6X-03

1-J. McCARTY

1-W.B. AVERY M/S 82-32

1-D. ARNOLD M/S 4H-98

1-K. MACKEY M/S 9R-64

1-S. METSCHAN M/S 3K-65

1-P. HARRADINE/M. SPENCER M/S 6R-MJ

1-B. COX-ROCKWELL INTL. SCIENCE CENTER

1-J. LAAKSO M/S 82-97

1-S. JOHNSTON M/S 7L-23

1-DR. RODERIC LAKES-UNIVERSITY OF IOWA

1-DR. J. AWERBUCH AND DR. A. WANG-DREXEL UNIVERSITY

1-DR. W.D. BASCOM-UNIVERSITY OF UTAH

1-M. KLOTZCHE-DOUGLAS AIRCRAFT CO.

1-J. SUAREZ-GRUMMAN AIRCRAFT SYSTEMS

1-A. JACKSON-LOCKHEED AERONAUTICAL SYSTEMS CO.

1-R.B. DEO-NORTHROP CORP.

1-S.P. GARBO-SIKORSKY AIRCRAFT DIV.

1-DR. K.Y. LIN-UNIVERSITY OF WASHINGTON

1-DR. J. SEFERIS-UNIVERSITY OF WASHINGTON

1-DR. M.E. TUTTLE-UNIVERSITY OF WASHINGTON

1-DR. FU-KUO CHANG-STANFORD UNIVERSITY

1-DR. T. KENNEDY-OREGON STATE UNIVERSITY

1-DRS. P. LAGACE AND M. GRAVES-M.I.T.

1-C. GRANT-HERCULES AEROSPACE CO.

1-R. HOLTHE-ICI FIBERITE

1-B. COXON-INTEC

1-R. NEFF-WRIGHT PATTERSON

1-J. SODERQUIST-FAA

1-R.HOLZWORTH-WRIGHT PATTERSON

1-M. FEDRO M/S P30-30

1-ATCAS TEAM GROUP FILE
DIRECT QUESTIONS ON DISTRIBUTION TO :   MARGE APELES
                                               393-9631 M/S 3K-65
                                               65 COPIES

ADVANCED TECHNOLOGY COMPOSITE AIRCRAFT STRUCTURES

MONTHLY TECHNICAL PROGRESS REPORT
NO. 25

FOR PERIOD
MAY 1 - MAY 31
1991

PREPARED FOR

NATIONAL AERONAUTICS AND SPACE ADMINISTRATION
LANGLEY RESEARCH CENTER
HAMPTON, VIRGINIA 23665-5225

UNDER CONTRACT NAS1-18889

JUNE 14, 1991

Prepared by: *[signature]* and *[signature]*
L.B. Ilcewicz   T.H. Walker
Principal Investigator   Structural Mechanics

Approved by: *[signature]*
FOR R.W. Johnson
Program Manager

BOEING COMMERCIAL AIRPLANE GROUP
TECHNOLOGY AND PRODUCT DEVELOPMENT
P.O. Box 3707
Seattle, Washington 98124-2207

TABLE OF CONTENTS

1.0 SUMMARY

This Twenty-fifth Technical Monthly Progress Report describes work performed during May 1991 on NAS1-18889 "Advanced Technology Composite Aircraft Structure" (ATCAS). The ATCAS "Concepts Assessment Review" was held in Seattle on May 15 and 16. Based on Phase A progress to date and plans for future ATCAS work, NASA decided to proceed with Phase B.

Crown. Local crown panel optimization of a Family C concept has occurred over the last nine months. The final crown design was projected to have cost and weight savings (relative to 1995 aluminum technology) of 18% and 45%, respectively. These savings are close to those quoted as ACT program goals.

The three main tasks supporting local optimization were each found to affect cost and weight. First, the enhanced tensile fracture performance of tow placed laminates was realized while collecting a material's database. This lead to lower cost and weight. Second, design variables were selected with the help of optimization software to minimize cost and weight. As discussed in previous months, stringer spacing was found to be the most significant variable affecting cost. This was found to ralate to the effect of stringer spacing on numerous manufacturing cost centers. The third task supporting local optimization, fabrication trials, were performed to demonstrate innovative processes which attack cost centers. This final activity continues to evaluate possible changes in crown panel manufacturing plans with a goal to further reduce costs.

A soft tooling trial was performed, yielding a curved panel with cocured hat stringers and cobonded frames. The trial variables included stringer mandrel type and edge trim. The panel will be inspected for defects and measured for warpage in June. Fabrication of crown manufacturing and test verification panels at Hercules remains behind schedule due to limited machine availability and delays in subcontract procurement.

The progressive damage modeling effort being conducted at Stanford University was reviewed, and a plan for the remainder of the contract was developed. This plan includes improvements to the plane-stress model to address multiple material zones, and verification of the model with several of the large crown test panels. Continued development of verification test plans resulted in elimination of two of the four flat post-buckling panels, since their response was not representative of the actual crown design.

Keel. Design work for global evaluation of keel panels continued with the release of several drawings. These included intercostals, and cargo floor frame details for Family D designs. Cargo floor details for the first Family C design were also completed. The design drivers for Family D and C keel concepts were identified during sizing exercises, indicating the need for materials and designs with balanced performance capabilities for compression, hoop tension, and shear in keel applications.

Work continued in developing manufacturing plans for keel panel designs. An installation plan was completed for the first Family D keel panel. A detailed pictorial of

this plan was included in Appendix G. Recurring and nonrecurring labor estimates were obtained for all cost components of the first Family D design with the exception of panel installation. Results obtained to date will be reviewed by the ATCAS DBT before documenting in a monthly report.

Work was started to initiate a second subcontract to study insitu foam processing of sandwich panels with the Sundstrand Corporation. This second study will consist of fabrication trials that address critical keel manufacturing issues such as thick sandwich facesheets, varying core thickness, and tapered skin thickness.

Results were presented for matrix splitting in unidirectional specimens of tough and brittle matrix composites, indicating a greater resistance to splitting in the former. Some temperature differences in the matrix splitting resistance of toughened materials were noted for specimens subjected to fatigue cycles. Matrix splitting is generally considered an attribute for tension damage tolerance of multidirectional laminates. Since hoop tension damage tolerance is still a design driver for the aft end of the keel panel, the tensile fracture of toughened systems considered for keel applications will need to be studied. Work at the University of Utah (Bascom ACT contract) will address the need for understanding the competing failure mechanisms of tough and brittle tow-placed laminates.

All impacts were completed for the designed experiment to identify critical impact threats for fuselage structure. Work began to characterize the damage created by impacts.

A research paper summarizing the effects of a negative Poisson's ratio on the mechanical performance of foam core materials was completed. A draft of this paper is included in Appendix H for NASA's review.

Frames and Attachment Details. Specimen fabrication was completed for the initial braided composite test matrix and frame material characterization tests. Specimens were sent to NASA Langley and mechanical tests have started.

The RTM tool to fabricate 3' frames was finished and sent to Fiber Innovations. These frames will be used in crown panel manufacturing demonstrations. A total of eight frames will be fabricated. Two of the frames will be used to make skin/frame adhesive bond test elements during June. A number of manufacturing and design variations will be screened in the initial tests which will be performed at Drexel University.

Cherry Textron demonstrated their thermoplastic rivet installation process at the May ATCAS program review with NASA. The next phase of work in this area is currently being planned.

Design Cost Model. Efforts continued to arrange subcontracts with Massachusetts Institute of Technology (MIT), Sikorsky Aircraft, Dow/United Technologies, and Northrop Corporation. Major differences exist between Boeing and MIT contract personnel. A trip by Boeing to MIT is planned in June to discuss the differences. Work began on the University of Washington subcontract with the identification of specific tasks to support "design constraints" and "software development".

2.0 INTRODUCTION

This report summarizes work performed during the 25th month on NAS1-18889, "Advanced Technology Composite Aircraft Structure." The primary objective of this program is to develop an integrated technology and demonstrate a confidence level that permits the cost- and weight-effective use of advanced composite materials in primary structures of future aircraft with the emphasis on pressurized fuselages. The program start date was May 12, 1989.

The current program master schedule is shown in Figure 25-1. The only tasks currently behind schedule relate to crown panel fabrication. These tasks continue to be delayed by problems in the procurement process and scheduling conflicts for the use of subcontract fabrication equipment.

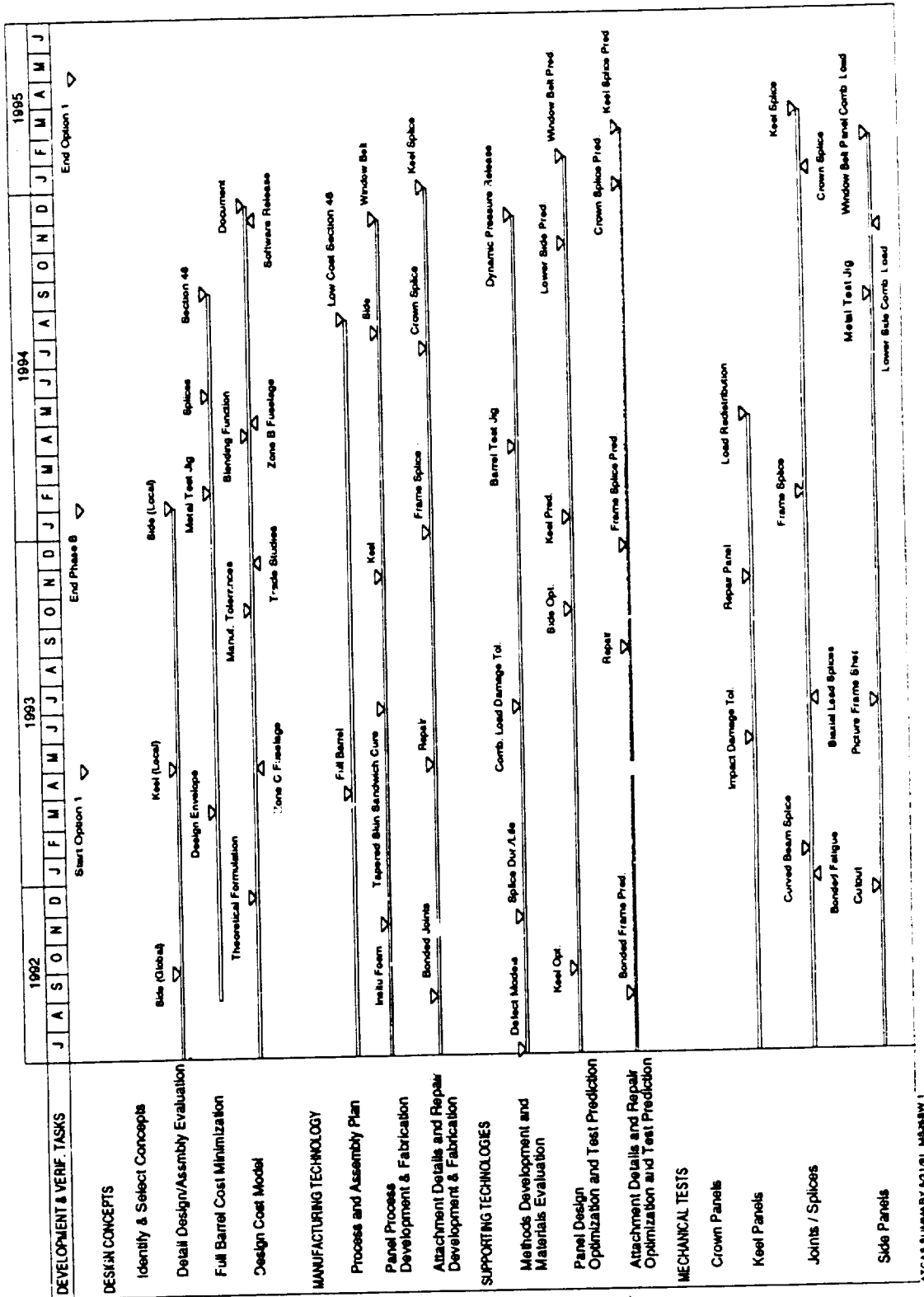This report covers the period starting May 1, 1991 and ending May 31, 1991.

Figure 25-1: BOEING/NASA ATCAS Program Summary Schedule (Sheet 1)
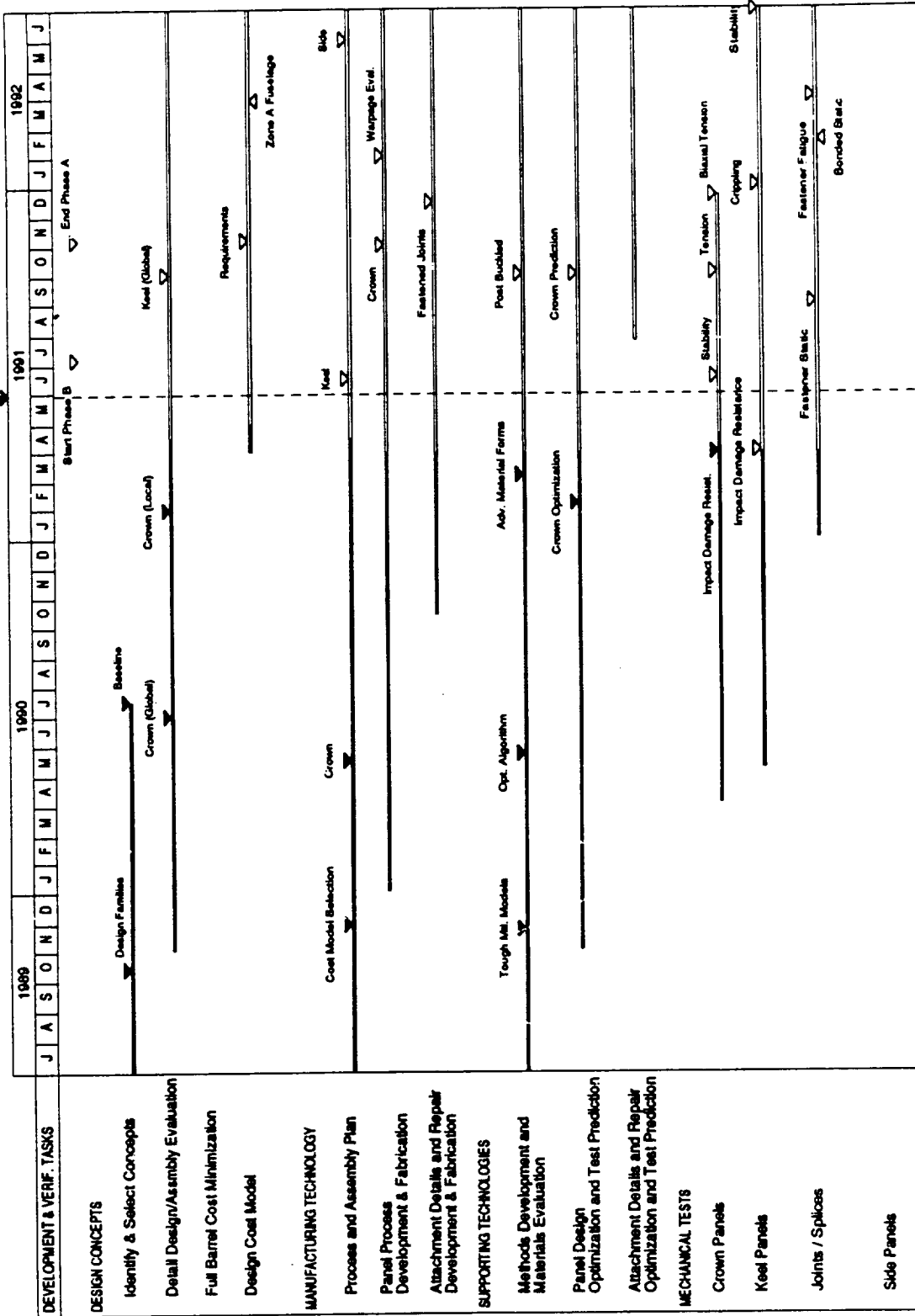
ATCAS SUMMARY 6/21/91 M3369W 1

Figure 25-1: BOEING/NASA ATCAS Program Summary Schedule (Sheet 2)

3.0 PROGRAM PERSONNEL

Program Manager: R. Johnson

Engineering Technology Manager: P. Smith

Principal Investigator: L. Ilcewicz

Business Management: M. Apeles

Engineering Personnel:

 Structural Design: M. Morris (Lead)
    K. Griess
    M. Schram
    S. Metschan

 Manufacturing R&D: K. Willden(Lead)
    T. Davies
    K. Goodno
    V. Starkey

 Material Technology: D. Grande
    W. Avery (BA&E)
    C. Gunther (BH)
    P. Grant (BH)
    M. Fedro (BH)

 Operations Technology: J. Valdez
    P. Keys

 Structural Mechanics: T. Walker (Lead)
    E. Dost
    G. Swanson
    B. Flynn

 Cost Modeling: K. Venters (Lead)
    D. Tervo
    L. Witonski

 Computing and Analysis Support: S. Johnston
    R. Lundquist

 Technical Support: W. Waltari
    T. Le

4.0 PROGRAM STATUS AND PLANS

The ATCAS "Concepts Assessment Review" (per Section 5.1.6 of the Statement of Work for NASA contract NAS1-18889) was held at Boeing, Seattle on May 15 and 16. Detailed progress and plans for the ATCAS program were presented at the review to "provide the necessary data base for NASA's decision to proceed with Phase B". The NASA and DoD group reviewing ATCAS gave a positive assessment of the program and decided to proceed with Phase B.

Handouts for each presentation given at the May 15 and 16 review are available upon request. A comprehensive outline for these talks appeared in Appendix B of the previous monthly report (MTPR #24, April, 1991).

In the following discussions, reference is frequently made to design families. These families have been previously reported. For reference, a pictorial of each family is included in **Appendix A.**
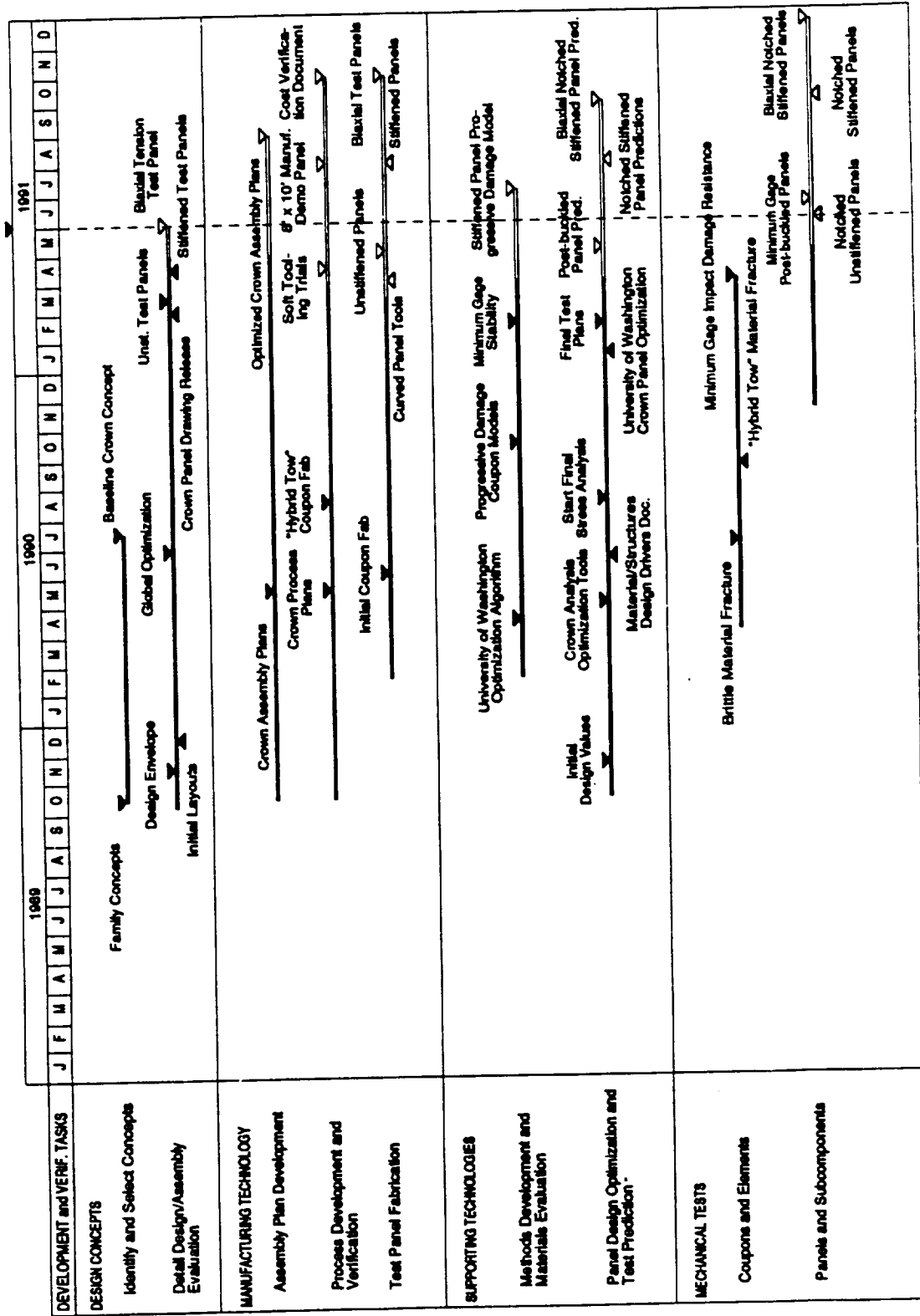
4.1 Crown Panels

The schedule for activities associated with crown panels is shown in Figure 25-2. The subcontract work related to curved tool fabrication, soft tooling trials, and unstiffened panel tests remains behind schedule. Procurement of most of the Hercules subcontracts needed to do these tasks has been achieved. Delays in fabricating unstiffened fracture test panels relates to conflicts in scheduling the Hercules tow placement machine. Some delays also continue in test prediction tasks due to manpower limits.

Local optimization of Family C crown panel design and manufacturing plans has occurred over the last nine months. As discussed in the past, the goals of this design phase is to attack cost centers and optimize within a family. Three main tasks are performed in support of local optimization; (1) generation of a material database, (2) design cost tool trade studies, (3) fabrication trials. The following discussion will update status for crown local optimization and discuss the effect of each task on projected cost and weight.

For the purpose of review, Figure 25-3 shows the final results from crown global evaluation studies performed last summer. A detailed description of the ATCAS DBT approach and crown global evaluation results were documented in a low-number contractor's report (currently being published by NASA Langley) and in a paper presented at the First Advanced Composite Technology Conference. Note the lower cost of one of the Family C designs shown in Figure 25-3 as compared to original results.   This is due to an improved process plan for long discontinuous fiber/thermoplastic frames obtained from the DuPont Company.

Figure 25-2: Crown Panel Development and Test Verification

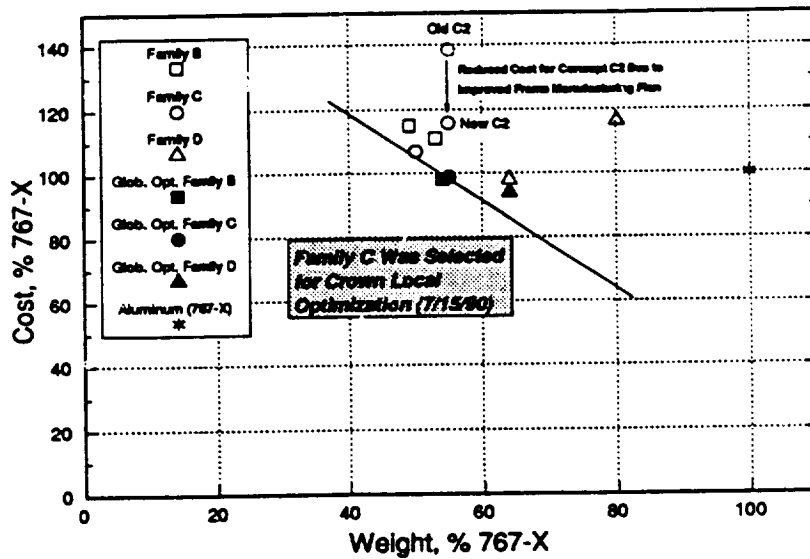| DEVELOPMENT and VERIF. TASKS	1989 J F M A M J J A S O N D	1990 J F M A M J J A S O N D	1991 J F M A M J J A S O N D

DESIGN CONCEPTS

Identify and Select Concepts — Family Concepts · Baseline Crown Concept

Detail Design/Assembly Evaluation — Design Envelope · Initial Layouts · Global Optimization · Crown Panel Drawing Release · Unst. Test Panels · Stiffened Test Panels · Biaxial Tension Test Panel

MANUFACTURING TECHNOLOGY

Assembly Plan Development — Crown Assembly Plans · Optimized Crown Assembly Plans

Process Development and Verification — Crown Process Plans · "Hybrid Tow" Coupon Fab · Soft Tooling Trials · 8' x 10' Manuf. Demo Panel · Cost Verification Document

Test Panel Fabrication — Initial Coupon Fab · Curved Panel Tools · Unstiffened Panels · Biaxial Test Panels · Stiffened Panels

SUPPORTING TECHNOLOGIES

Methods Development and Materials Evaluation — University of Washington Optimization Algorithm · Progressive Damage Coupon Models · Minimum Gage Stability · Stiffened Panel Progressive Damage Model

Panel Design Optimization and Test Prediction — Initial Design Values · Crown Analysis Optimization Tools · Start Final Stress Analysis · Material/Structures Design Drivers Doc. · University of Washington Crown Panel Optimization · Final Test Plans · Post-buckled Panel Pred. · Biaxial Notched Stiffened Panel Pred. · Notched Stiffened Panel Predictions

MECHANICAL TESTS

Coupons and Elements — Brittle Material Fracture · "Hybrid Tow" Material Fracture · Minimum Gage Impact Damage Resistance

Panels and Subcomponents — Minimum Gage Post-buckled Panels · Notched Unstiffened Panels · Biaxial Notched Stiffened Panels · Notched Stiffened Panels

CROWN PANEL 03161 CP251W1

Figure 25-3: Review of Results from Global Crown Evaluation
(Reprinted from ATCAS Contractor's Report)

The global optimized Family C concept was selected for local optimization studies. As shown in Figure 25-4, this concept was projected to have potential for additional cost and weight savings.
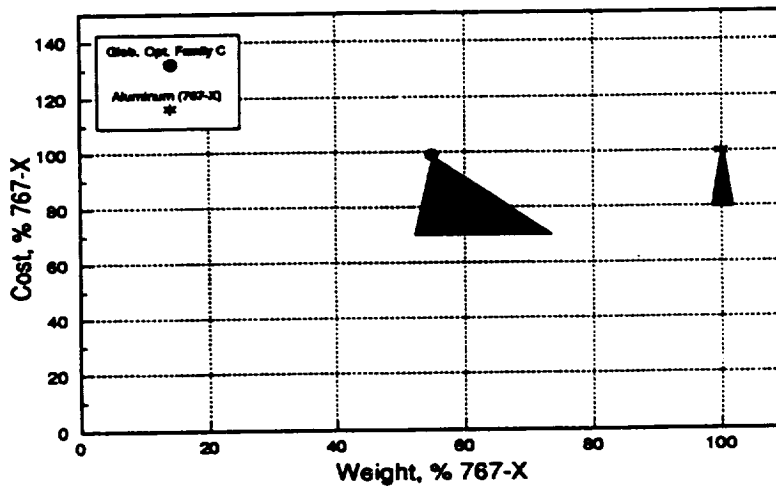
Figure 25-4: Local Optimization Potential for Family C Crown Panels
(Reprinted from ATCAS Contractor's Report)

Local optimization progress obtained during the last six months is summarized in Figure 25-5. The final crown design is projected to have 18% cost savings and 45% weight savings, relative to the aluminum 767-X benchmark. Each of the three tasks supporting local optimization were found to have a significant effect on the projected cost and weight of composite crown structures. In addition, design criteria were also found to have a significant effect.

Following global evaluation, the tension damage tolerance criteria for failsafe conditions was modified to account for larger notches and severed frames. It was then determined that the original Family C design had a negative margin of safety for failsafe considerations. As shown in Figure 25-5, redesigning the concept (i.e., increasing the skin gage) for sufficient damage tolerance results in both cost and weight increases.

Process/material relationships need to be understood in order to ensure the performance, repeatability, and optimization of structures fabricated by innovative methods. In ATCAS, mechanical tests are performed during local optimization to generate a database for selected materials and processes. This database yields more accurate information on the mechanical behavior of new material forms fabricated by the selected processes. Depending on the results of mechanical tests, designs are modified during local optimization.

As discussed in previous monthly reports, tow-placed laminates were found to have improved tensile fracture characteristics as related to tape laminates consisting of the same constituents. Figure 25-5 shows that the improved properties of tow-placed laminates result in significant decreases in both cost and weight. It was not possible to decrease cost and weight by eliminating skin plies in direct proportion to the increased tension damage tolerance performance of tow-placed laminates, because other considerations (e.g., minimum panel stiffness and stability) became the design drivers for portions of the crown panel.

A design cost tool (UWCODA) developed at the University of Washington was used to optimize cost and weight for the Family C crown design. Relationships between manufacturing cost and design parameters (e.g., stringer spacing, material costs, number of skin plies) were developed and input into UWCODA, together with crown panel design constraints. Figure 25-5 shows that both cost and weight were reduced significantly during UWCODA design optimization. As discussed in previous monthly reports, stringer spacing was found to be the dominate cost driver in these trade studies.

The final local optimization task involves fabrication trials to further attack cost centers and optimize manufacturing plans. This activity is still in progress for the crown panel (see discussions in Section 4.1.2). Figure 25-5 shows an estimated reduced cost for optimized manufacturing plans on the order of 10%. Cost savings identified to date include (a) reduced number of tools for stringer and frame fabrication, (b) lower material costs for stringer fabrication (tow instead of tape), (c) increased tow band width for tow-placed skin layup (increased to 6 in. width), and (d) soft tooling concepts to minimize labor costs for panel bagging. Additional modifications will be made to the crown manufacturing plans based on the results of fabrication trials during the summer of 1991.
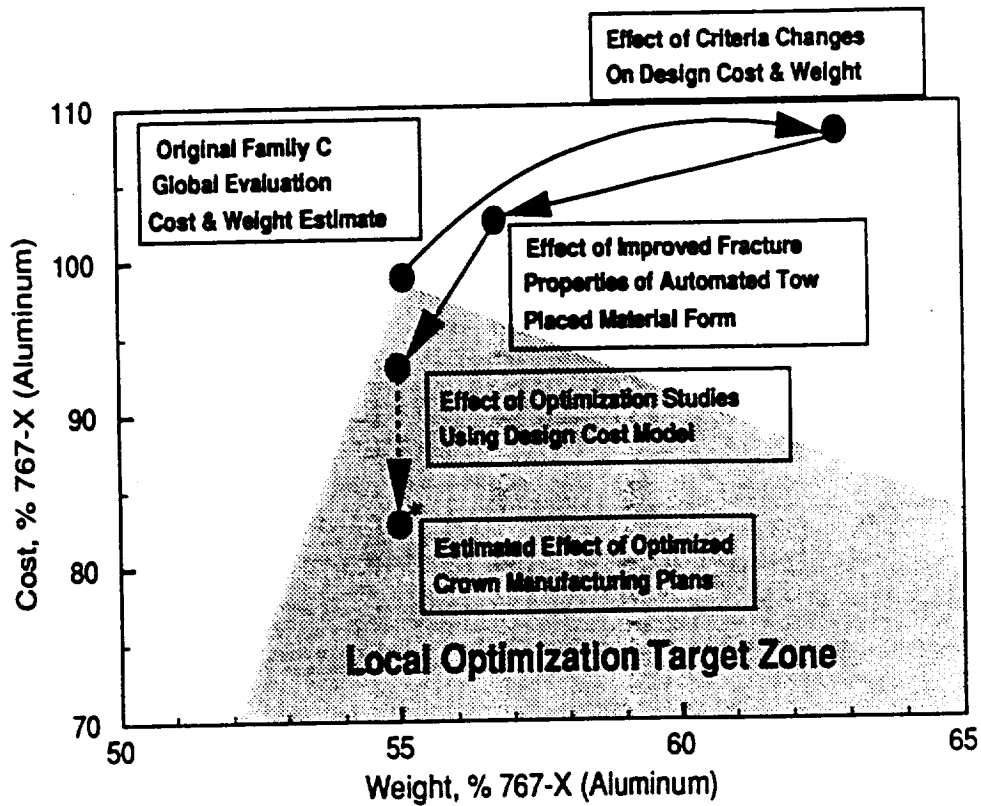
Figure 25-5: Summary of Individual Factors Affecting Local Crown Optimization

4.1.1 Design Concepts

Current Progress: The results of the stringer element cost study referred to in Monthly Technical Progress Report #24 (April 1991) are presented in Figure 25-6. As previously reported, the result of this study indicate that large increases in stringer cost relative to the original cost estimate have little or no effect on the stiffened panel design, with maximum stringer spacing being the dominant design driver. Costs relating to the number of stringers overshadow the costs relating to stringer fabrication and material costs.

Efforts continued toward the completion of the drawings and purchase orders for the crown verification test program. The current status is shown in Figure 25-7. Efforts during May focussed on refining the stringer, frame and stringer/frame intersection details for the curved manufacturing demonstration articles (3' x 5' and 7' x 10') as well as the curved biaxial tension panel (#12). In addition, some progress has been made toward completion of the purchase order for the flat stiffened panel (#9).
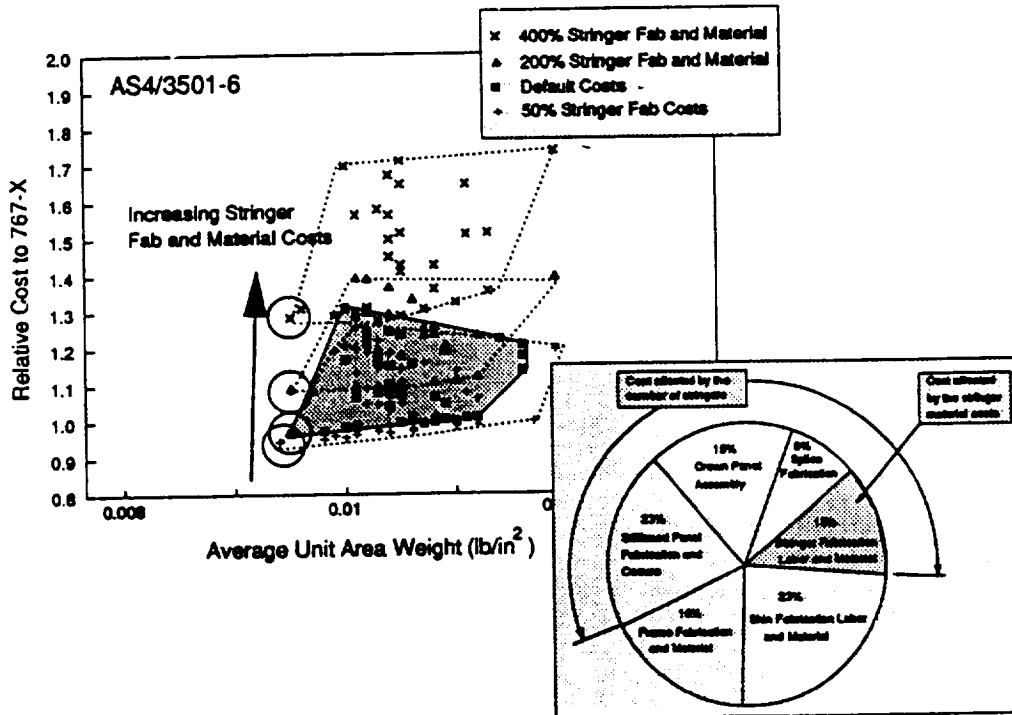
Figure 25-6: Effect of Increasing Stringer Element Cost on a Crown Panel Design

Description	Drawing	Engineering Purchase Request	PR Approval	Purchase Order	Panel Fabrication
#1: Biaxial, AS4, 2/4/6	●	●	●	●	O
#2: Biaxial, 90-deg Hybrid	●	●	●	●	●
#3: Biaxial, AS4 Optimized	●	●	●	●	O
#4: Biaxial, 25% Hybrid Optimized	●	●	●	●	O
#5: Flat Uniaxial Unstiffened, Hoop, AS4	●	●	●	●	O
#6: Flat Uniaxial Unstiffened, Axial, AS4	●	Hercules ACT Contract Requirement			O
#7: Flat Uniaxial Unstiffened, Axial, 25% Hybrid	●	Hercules ACT Contract Requirement			O
#8: Undefined	O	O	O	O	O
#9: Flat Uniaxial Stiffened, Axial, AS4	●	●	●	⊗	O
#10: Flat Uniaxial Stiffened, 25% Hybrid	●	Hercules ACT Contract Requirement			O
#11: 8' x 10' Manufacturing Demo	⊗	O	O	O	O
#12: Curved Biaxial, AS4, Optimized	⊗	Hercules ACT Contract Requirement			O

O = Not Started   ⊗ = In Work   ● = Completed

Figure 25-7: Test Panel Drawing, Purchase and Fabrication Status

Problems and Recommendations: No problems are currently foreseen and there are no recommended changes in plans or schedules at this time.

Near Term Plans: Documentation of the local optimization studies will be initiated.

Work will continue on the drawings for the 3' x 5' and 7' x 10' manufacturing demonstrations articles, as well as the biaxial tension panel (#12). Purchase Orders will be expedited as required to avoid delay in the manufacturing progress.

4.1.2 Manufacturing Technology

Current Progress: Figure 25-8 shows a curved panel (two "I" frame/two hat stringer) that was fabricated and cured with the new modified soft tooling concept. This 74" radius panel was cured with 150 psi on a steel OML cure tool. The panel shown in Figure 25-8 was the second fabrication trial used to develop an optimal soft tooling approach for the crown manufacturing plans. Additional trials are planned using 3' x 5' panels and the final concept will be demonstrated with the 7' x 10' crown verification panels.

ORIGINAL PAGE
BLACK AND WHITE PHOTOGRAPH
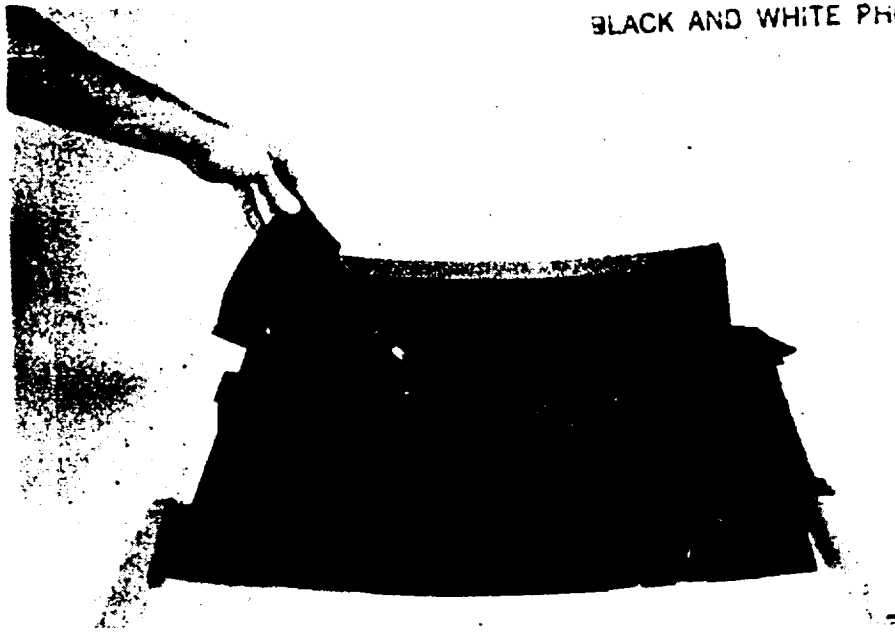
Figure 25-8: Curved Family C Design Concept Fabricated Using a New Soft Tooling Concept.

The modified soft tooling concept used to fabricate the panel in Figure 25-8 is shown schematically in Figure 25-9 for the current crown design (i.e., J-frames). Figure 25-10 shows two types of hat stringer cure tools which were compared in the fabrication trial.

The cure tool for the first hat was a silicon mandral. A low coefficient of thermal expansion (CTE) flex mandral was used as a cure tool for the second hat. Both mandrals were extracted over a tapered skin (0.10" buildup over 3") to evaluate scale-up production requirements. Soft tooling was fabricated on a flat panel mockup which reflected the stringer cross sections and panel taper. Stringers were drape-formed ar . edges were trimmed with an ultrasonic knife as shown schematically in Figure 25-11.
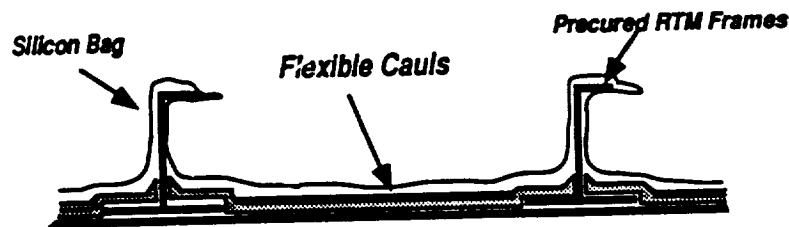
Figure 25-9: Cross Section of the Soft Tooling Concept

Stringer Edge

Stringer Mandrel

Silicone   Low CTE Flex Mandrel
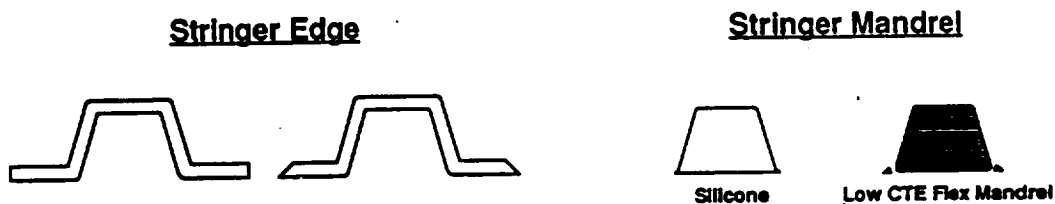
Figure 25-10: Stringer Tooling Combinations

Following panel fabrication, the straight (90°) and tapered cut stringer flanges were inspected and indications show that the soft tooling minimized the resin pooling for both the 90° and tapered flange edge cuts. Figure 25-12 shows the results of this inspection schematically. The 90° edge had some edge defects from stringer mislocation and/or stringer edge trimming accuracy. Figure 25-12 illustrates that the tapered stringer edges proved to be more tolerant for locational and trimming inaccuracies.

Limitations of hat stringer mandral extraction and stringer gage thickness control are currently under evaluation. The low CTE flex mandrals were found to extract easier than the silicon mandral. The typical skin thinning which has been observed between the webs of hat stringers in past fabrication trials occured in the current study with both the silicon and low CTE flex mandrals. The low CTE flex mandral yielded a more consistent hat cross sectional shape than the silicon mandral. More measurements along the length of the stringer will be taken after nondestructive inspection is completed.

Drape Form Charge   Trim Cut   _Cured Hat_

Figure 25-11: Trim of Drape Formed Stringers

An analysis will be conducted to determine costs of the low CTE flexible mandral. One added cost to the low CTE mandral is that of an added radius noodle.

90° Cut

Fiber Wrinkles
(Over cut)

Resin Pool
(Under Cut)

Skin Thinning

Tapered Cut

Skin Thinning
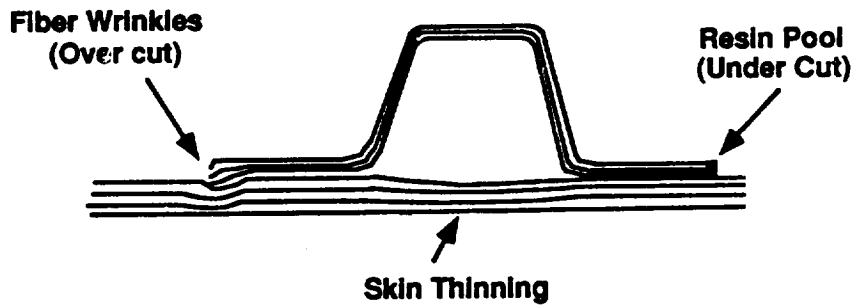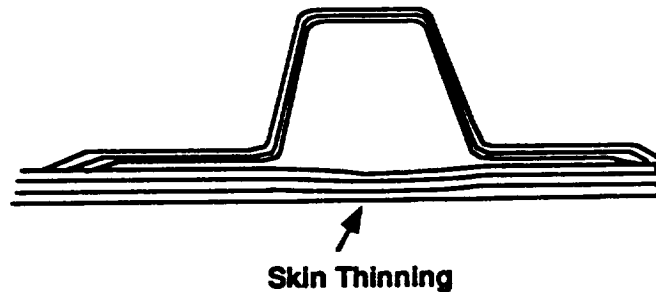
Figure 25-12: Schematic of Stringer Details Resulting from Soft Tooling Fabrication Trial

The winding tool for the 3' x 5' and 7' x 10' demonstration panels is still under fabrication and will be completed and shipped to Hercules in the middle of June. Fabrication of the outside mold line (OML) cure tool has had schedule delays and will be finished at the end of July. Cure mandrals and soft tooling material are on order for the 3' x 5' panels. A mock-up to build the 3' x 5' soft tooling is being designed to handle both the 3' x 5' and 7' x 10' demonstration panels. The panel mock-up will be made of a flat graphite/epoxy plate with metal stringers and graphite/epoxy frames. Fabrication of the 3' x 5' skins will begin by the end of July.

Work began on the fabrication of the crown verification test hardware. The first two flat panels for unstiffened uniaxial (small coupons) and biaxial tension tests were tow-placed at Hercules, Inc. The first panel (#1) was scrapped due to an improper cure cycle caused by a thermocouple failure. This panel will be remade. The second panel (#2) was subsequently cured successfully.

Problems and Recommendations: Fabrication of the crown manufacturing and test verification panels at Hercules, Inc. is significantly behind schedule. Delays are due to both limited machine availability and the amount of procurement paperwork flow. A new fabrication schedule will be developed during June to understand the influence of these delays.

Near Term Plans: The intricate bond panel produced in a soft tooling trial (Figure 25-8) will be ultrasonically inspected and warpage tests will be conducted. After inspection, the panel will be sectioned and measured to evaluate the panel dimensional accuracy. Planning will continue for additional, larger, soft tooling trials. All soft tooling and assembly designs for the 3' x 5' and 7' x 10' panels will be finished and tool fabrication will begin.

During June, fabrication of the crown verification tests will continue. The remaining panels to support small coupon and biaxial tension fracture testing will be tow-placed and cured.

4.1.3 Supporting Technology

Current Progress: A meeting was held between Boeing personnel and Dr. Chang from Stanford University to discuss the progressive damage modeling being developed there. After reviewing the progress, it was determined that a plate implementation of the model would not be possible by the contract-end date (September 1991), limiting applications to the current plane-stress implementation. Methods to avoid numerical instability for large damage zones have been implemented. During the remainder of the contract, the following activities will be completed.

1. Analytical studies to investigate the ability of transverse ply strength, fiber/matrix shear strength, and fiber strength differences to account for experimentally-observed improvements in tension fracture performance of tow-placed laminates when compared to tape laminates

2.   Modifications to the model to allow for zones of differing materials and thicknesses

3.   Verification of the model's predictive capability, conducted using test results obtained from:

    a.   previously completed and future 10" x 30" flat unstiffened uniaxial tension panels with 2.5" notches

    b.   40" x 40" flat unstiffened, biaxial tension panels with notches of approximately 2.5"

    c.   60" x 150" flat unstiffened, uniaxial tension panels with notches of approximately 14"

    d.   30" x 100" flat uniaxial tension panels with co-bonded or co-cured tear straps representative of stringer and/or frame flanges. The notches in these tests will be approximately 8". Several locations of the notch relative to longitudinal and transverse tear-straps will be included.

Parallel to the Stanford University work, Boeing and NASA personnel will compare predictions using alternative methods (e.g., Poe-Sova, Whitney-Nuismer, Mar-Lin, alternate progressive damage models) to unstiffened and tear-strap experimental results. The finite element method (FEM) will be used as required to accommodate multiple material zones, extend these models to stiffened structural configurations. Predictions of the *stiffened* panels (both uniaxial and biaxial tension) will be made with the most promising of the methods evaluated, again using FEM as required. If the Chang model appears encouraging, the plane-stress implementation will be used for further predictions. Although the underlying plane-stress assumptions will be violated in the configured structure, such attempts will indicate whether the use of these simplifying assumptions can provide sufficiently accurate predictions.

Work began on the PATRAN datasets of two impact-DOE three-stringer panels for use in the non-linear finite element analyses which will support the experimental tests. One hat-stiffened panel and one blade-stiffened panel typical of the crown region are being investigated.

Work was also initiated on a PATRAN model of the flat, unstiffened biaxial tension specimens. This model will be used to determine doubler thickness and aid in failure predictions.

Problems and Recommendations: No problems are currently foreseen and there are no recommended changes in plans or schedules at this time.

Near Term Plans: Stanford University efforts will continue in the progressive damage model development. The model will be used to predict the observed differences between tow-placed and tape laminate tension fracture performance.

Work will continue on the finite element modeling effort in support of planned flat three-stringer panel buckling tests (Section 4.1.4).

Work will also continue on the modeling of the flat, unstiffened biaxial tension panels. Doubler requirements will be defined during June.

4.1.4 Mechanical Tests

Current Progress: Work continued on the interpretation of tension-fracture coupon results. Due to manpower restrictions, efforts to finish reducing the intraply hybrid design-of-experiments (DOE) results have been delayed.

Plans are under development to refocus the University of Utah (Bascom) subcontract to address the failure mechanism differences between tape and tow-placed laminates. The detailed plans will be reported in future reports. As an initial step, some tensile fracture coupons of 50% AS4 / 50% S2-Glass hybrid material will be tested to identify the failure mechanisms. These specimens (3.5" wide with 7/8" notches) have been received by University of Utah.

The final report on the tension fracture behavior of IM7/977-2 has been received from San Jose State University and is being reviewed. Salient results will be presented in future monthly reports.

Development of the plans for crown verification tests continued. The cooperative effort with the Mechanics of Materials Branch (C. C. Poe) at NASA-Langley to test and evaluate the results from flat unstiffened biaxial tension panels appears on track. Checkout of the test fixture at Langley is nearly complete, with results indicating good grip alignment. Coordination with the Non-destructive Measurement Science Branch (J. Heyman) is continuing to use the laser speckle profilometer to obtain full-field in-plane displacement fields.

Testing of the flat unstiffened uniaxial and biaxial tension panels was originally scheduled for June and July. However, as mentioned in Section 4.1.2, fabrication is behind schedule. A new test schedule will be developed in June.

Planning for the compression testing of the flat three-stringer DOE panels is continuing. After further prediction of the expected failure modes using approximate solution techniques, it was decided to test only the panels with a skin thickness of 0.089". Detailed predictions indicated that the column instability of the thicker panels occurs shortly after skin buckling, a failure mode not representative of ATCAS fuselage designs (i.e., either forward-crown or aft-keel). The data obtained from such tests would not be applicable to crown panel verification. Therefore, one hat-stiffened and one blade-stiffened panel will be tested in compression. Cost estimates for panel preparation and testing are pending.

Work on the planning of curved, three-stringer panel compression post-buckling tests has been initiated. These panels are to be fabricated as manufacturing demonstrations and will reflect the crown panel design geometry.

Initial work on a crippling test program to validate the crown panel design details was initiated. Background information on crippling tests was gathered and evaluated. Concern for the crippling response of configured stiffeners and the effect of the test element length on the crippling data was emphasized. Currently, a test matrix is being formulated to address hat and blade stiffener geometries, both of which are being used in the crown panel design studies. Also, the effects of test element length for larger L'/p values, the effect of stringer damage, and the effect of a high temperature environment on the local buckling and crippling failure are being considered. Test elements are being obtained using the impact-DOE panels and the manufacturing demonstration panels.

Problems and Recommendations: No problems are currently foreseen and there are no recommended changes in plans or schedules at this time.

Near Term Plans: Work on the intraply hybrid DOE will continue as manpower and schedule allow.

Tests of the center notch hybrid coupons at the University of Utah should be starting in the next two weeks.

Review and interpretation of the test report on the notch size/shape testing at San Jose State University will continue.

A schedule for all the verification testing will be developed during June. Efforts will continue towards planning for these tests.

The preparation of the flat three-stringer panels for testing will be initiated during the next reporting period. Work will also continue on the curved three-stringer panel test plans and the crippling test matrix and test plans.

4.2   Keel Panels

The schedule for activities associated with keel panels is shown in Figure 25-13. Work which was reported as behind schedule last month (i.e., baseline concept design layouts and impact damage resistance tests) was completed during May. Design drawings and manufacturing plans for alternate concepts remain behind schedule.

4.2.1   Design Concepts

Current Progress: Work continued on the keel panel designs. The design status is shown in Figure 25-14, and the concept variables are contained in Figure 25-15. The intercostal drawing for both Design D1 and D2 is contained in Appendix B. The Design D1 cargo floor frame drawing is shown in Appendix C. The drawings of the frame details and cargo floor details are contained in Appendices D and E, respectively. The sizing of the C1 design is complete for the skin, stringer and discrete keel chords and the drawings are being prepared. The drawing for the cargo floor details for this design is contained in Appendix F. The sizing of the Design C2 skin, stringer, and smeared keel is still being developed.

Figure 25-13: Keel Panel Development and Test Verification

5-31

5 Year Span

DEVELOPMENT and VERIF. TASKS	1989	1990	1991	1992	1993	1994

DESIGN CONCEPTS

Identify Concepts

Detail Design/Assembly Evaluation

MANUFACTURING TECHNOLOGY

Assembly Plan Development

Process Development and Verification

Test Panel Fabrication

SUPPORTING TECHNOLOGIES

Methods Development and Materials Evaluation

Panel Design Optimization and Test Prediction

MECHANICAL TESTS

Coupon and Element

Panel and Subcomponent

Baseline Keel Concept
Design Envelope
Alternate Layouts
Stability Panels
Keel Panel Drw. Release
Load Redistribution Panel
Baseline Layouts
Global Optimization
Damage Tol. Panels
Repair Panel

Keel Assembly Plans
Opt. Keel Assembly Plans
Damage Resistant Tow Panels
Keel Process Plans
Foam Cored Sandwich NDE
Manufacturing Demo Panels
Tapered Skin Sandwich Cure
Cost Verification Document
In-situ Foam
Stability Panels
Damage Tol. Panel
Load Redistribution Panel
Panel Repair

Tough Material Models
Compression Strength
Warpage Analysis & Test
OSU Repair F.E. Analysis
Comb. Load Damage Tol.
Dual Resin Evaluation
Post-Buckled Structure
Drexel Defect Models
Univ. of Washington Impact Models
Initial Design Value
Stability Prediction
Damage Tol. Prediction
Load Redistribution Pred.
Doc. Design Drivers
Keel Panel Opt. Tools
Repair Pred.

U of Iowa Foam Indent.
U of W Impact
U of Utah Failure Mechanism
Crippling
Repair Concepts
Resin Content
Impact Damage Resistance
CAI
Panel Stability
Damage Tolerance
Repair Panel
Load Redistribution

KEEL PANEL DEVELOPMENT

25-20

Figure 25-14: Status of Keel Design Work

Figure 25-15: Keel Design Concept Variables

Work on keel panel cost estimating continued. To date, recurring and nonrecurring labor estimates have been obtained for the skin, cargo floor frame, cargo floor beam, intercostal, and keel frame of design concept D1. Estimates for D1 installation and material costs are in work. Recurring and nonrecurring labor estimates have also been completed for the D2 skin, cargo floor beam, and keel frame. Keel cost results will be summarized in future monthly reports, following review by the ATCAS DBT.

Problems and Recommendations: No problems are currently foreseen and there are no recommended changes in plans or schedules at this time.

Near Term Plans: Work will continue on the C1 and C2 skin, stringer and keel chord designs and the sizing of the remaining details will begin. All components of the cost estimate for Designs D1A and D1B will be completed.

4.2.2 Manufacturing Technology

Current Progress: The installation plan has been completed for the sandwich keel Designs D1A and D1B. Appendix G contains a pictorial sequence of the assembly to aid in visualization. The cured keel panel configuration is shown in Figure SK-1 in that appendix. The panel will be made using an inner moldline (IML) tool. The decision to use an IML tooling concept was largely driven by the thickness tolerance build-up possible in a 1.3" thick prepreg laminate (Figure SK-2). The rationale is to push the variations outside the airplane thereby eliminating their effect on the inside chord details.

The side panels are located and lapped under the keel panel and the longitudinal blade stringer positioned (Figures SK-3 through SK-5). Two tandem robots perform the panel fastening, with one drilling, countersinking and inserting the bolt and the other installing the lockbolt collar and tensioning the bolt. The same tandem robots used on the longitudinal lap splice will be used for the aft Section 46 splice (Figures SK-6 through SK-10).

The full depth cargo floorbeams are mechanically attached to the co-bonded chords on the keel panel and side panel frames (Figure SK-11). The keel intercostals are then mechanically attached to the co-bonded intercostal chords and one full-depth floorbeam stiffener (Figures SK-12 to SK-14). The details at the frame splice are then mechanically attached (Figures SK-15 to SK-18).

The forward splice is accomplished through the use of two titanium splice plates (Figure SK-19). The final configuration of sandwich keel Designs D1A and D1B is shown in Figures SK-20 to SK-22.

The subcontract with Sundstrand to develop insitu forming foams has been in place 4 months. Several restrictive clauses were identified in the Hercules neat resin "Non-Analysis" agreement. These clauses have been modified to Boeing's satisfaction and the agreement finalized. One gallon of neat resin will be shipped to Sundstrand the second week of June.

Sundstrand has identified several alternative resins for use in insitu foaming. These resins include a low viscosity epoxy and powder cyanate ester. Low viscosity resins may ease mixing of ingredients, while the powder resins are similar to the thermoplastic material form used in their current process.

Boeing is initiating a second subcontract with Sundstrand to study the manufacturability of keel gage sandwich structure. This study will consist of sandwich manufacturing trials including thicker facesheets, different thickness cores and sandwich with thickness-

tapered facesheets. A preliminary statement of work has been drafted and will be further refined following consultation with Sundstrand.

The study on the use of TTU for inspecting foam sandwich structure continued. A review was made of further efforts needed to complete the study, and a plan set up. No further analysis of the previous data set will be made. Instead, measurements will be taken on foam blocks to characterize properties of the Rohacell foam. The blocks have been cut in steps to allow propagation to be analyzed as a function of distance. Propagation speed and attenuation will be characterized as functions of frequency. This will allow the limits of TTU scanning to be defined, and procedures for scanning foam sandwiches to be set up in terms of frequency, sampling rate, and sample duration. Scans of panels with implanted defects will also be made and analyzed. Documentation of the study has begun.

Problems and Recommendations: No problems are currently foreseen and there are no recommended changes in plans or schedules at this time.

Near Term Plans: Work will continue in developing manufacturing plans for keel panel elements and installation. Most of the remaining work is with Family C concepts.

Boeing will confer with NASA resin experts and Sundstrand to determine the suitability of the Hercules and other alternative resins. Compatibility with the facesheets must be considered for any resin selected.

Boeing representatives will meet with Sundstrand to review and better define a second subcontract to investigate the manufacturability of keel type structure. A design build team including both Boeing and Sundstrand structures, materials, and manufacturing personnel will be formed to consider issues associated with the core material choice.

In the study to inspect foams, TTU measurements will be conducted on the stepped foam blocks and the defect panel, and the results will be analyzed for a propagation model. Test procedures will be developed for scanning foam panels. Efforts will also continue towards completion of the documentation.

4.2.3   Supporting Technology

Current Progress: A number of design drivers have been identified for the keel panels. The critical load case is a 2.5g symmetric maneuver which causes body bending and puts the keel in compression. This compression load is introduced into the forward end of the keel as a concentrated force, as the loads are forced around the large cutouts for the wing center section and wheel well. Typical aluminum designs carry these concentrated loads through two massive keel beams which are mechanically attached to the stiffened keel skin. The high splice loads are tempered somewhat in Designs D1, D2 and C2 by panelizing the loads into a thick laminate that replaces the relatively thin skin and large keel beams of the aluminum concept. The concentrated load is transferred rapidly from the keel beams (discrete or panelized) into the stiffened skin and then sheared out into the rest of the panel. The resulting compression and shear load

contours were shown in Figures 22-12 and 22-13 of Monthly Technical Progress Report #22 (February 1991). The figures also show the jump in loads in the area near the side panel cargo door opening.

Figure 25-16 is a schematic showing where specific design issues tend to be critical in the keel panel. The top drawing shows the skin of a Family C (i.e., skin/stringer) concept with discrete aluminum keel chords. The figure shows the important areas of load redistribution: the keel beam to skin joint, and the areas of high shear adjacent to the keel beam. Most of the skin is dominated by panel compression issues and minimum stiffness requirements. Minimum skin buckling tends to be critical in the areas of increased loads near the cargo door opening. The longitudinal and aft circumferential splice joints sometimes control the minimum skin thicknesses. Attaching discrete aluminum keel chords to a Gr/Ep skin presents the additional problems of thermal mismatch, which can add to the skin loads, and galvanic corrosion, which may require a fiberglass pad between keel beam and skin.

The bottom drawing of Figure 25-16 shows the critical design issues for a Family D (sandwich) skin . Note that minimum stiffness requirements are generally not critical in the sandwich structure which is more efficient in shear than the skin/stringers. In the area where the solid wedge transitions to core, the resulting shifts in the neutral axis cause significant kick loads. Other design issues are similar to those mentioned for the 'C' skin.
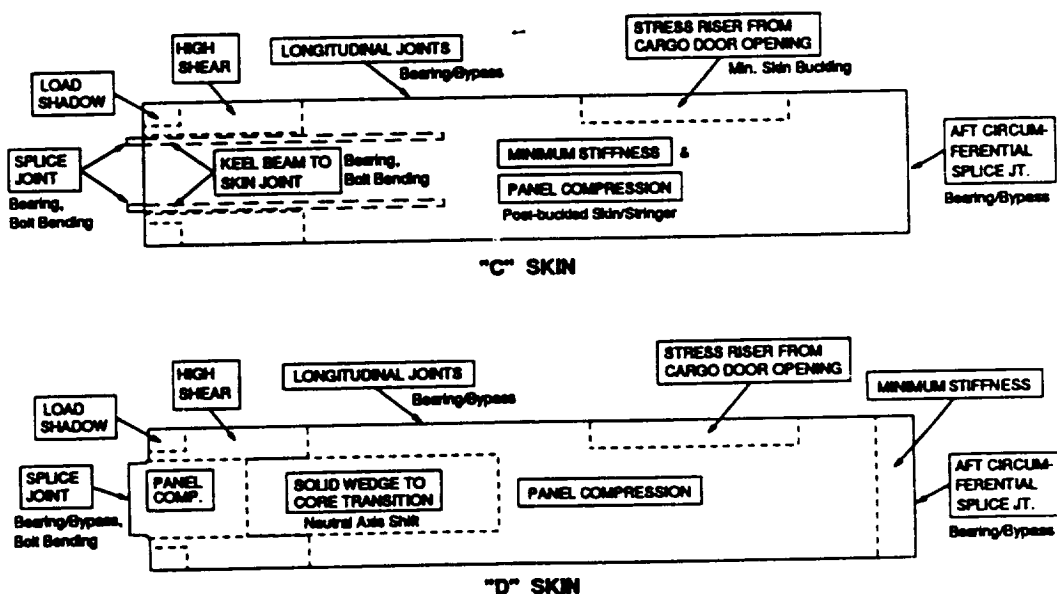
Figure 25-16: Critical Keel Panel Design Issues

In work to evaluate the effects of ply drops on compressive behavior, a test matrix was defined to further screen the effects of materials variables on ply drop compressive performance. Specimens for theses tests are currently being laid up. This set of tests will extend the evaluations reported in Monthly Technical Progress Report #24 (April 1991) to include the effects of varying resin content and dropped off-axis plies.

Work continued on the Drexel University (Awerbuch and Wang) subcontract to study the effect of loading function and environment on matrix damage growth in toughened composites. As discussed in the last monthly report, mechanical tests on the effects of temperature, loading rate, creep load history, and fatigue frequency were completed and documented. Detailed reports of these studies are available upon request. Some of the work will be summarized in technical papers which will appear in the appendix of future monthly reports.

The Drexel matrix splitting tests used double edge notched unidirectional specimens. Matrix splitting resistance was found to depend on material type. Figure 25-17 shows good analysis and test comparisons for each of the different material types studied. Splitting tests performed at room temperature were unaffected by the static loading rates and fatigue frequencies evaluated. Splitting results from static tests performed at 70°F and 180°F indicated little difference due to temperature. Some influence of temperature was evident in fatigue tests for each frequency studied (e.g., see Figure 25-18).
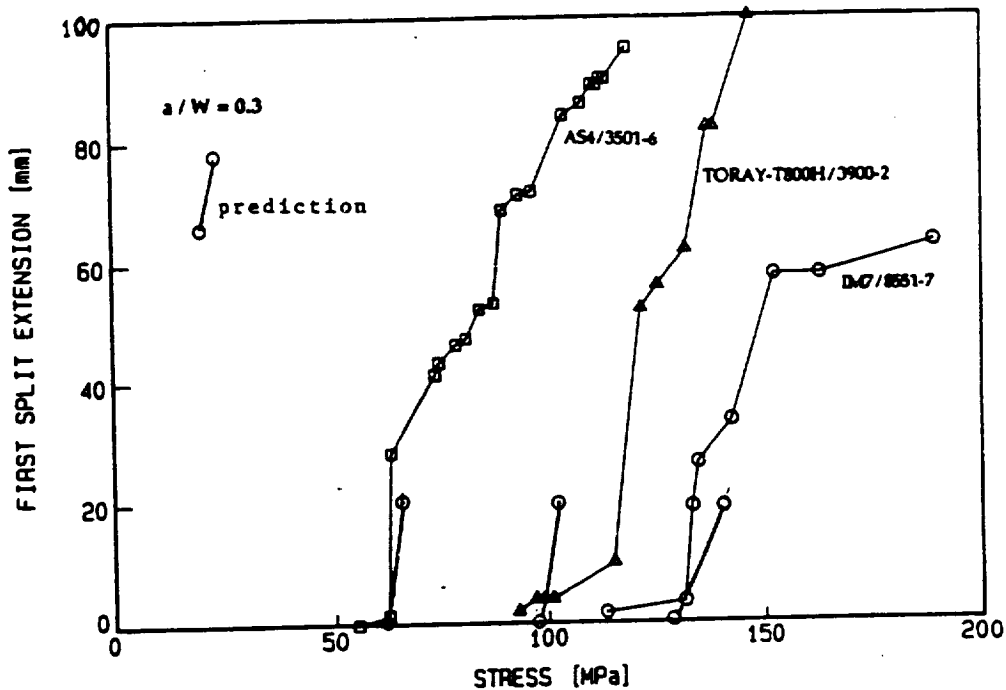
Figure 25-17: Comparison Between Predicted and Experimental Results of Matrix Splitting Growth in Coupons of Three Material Systems
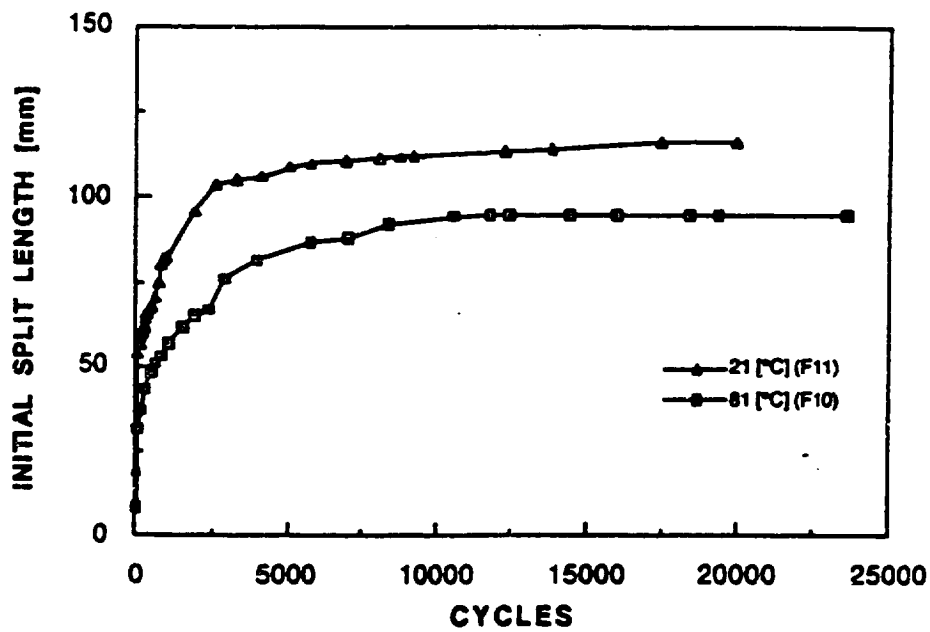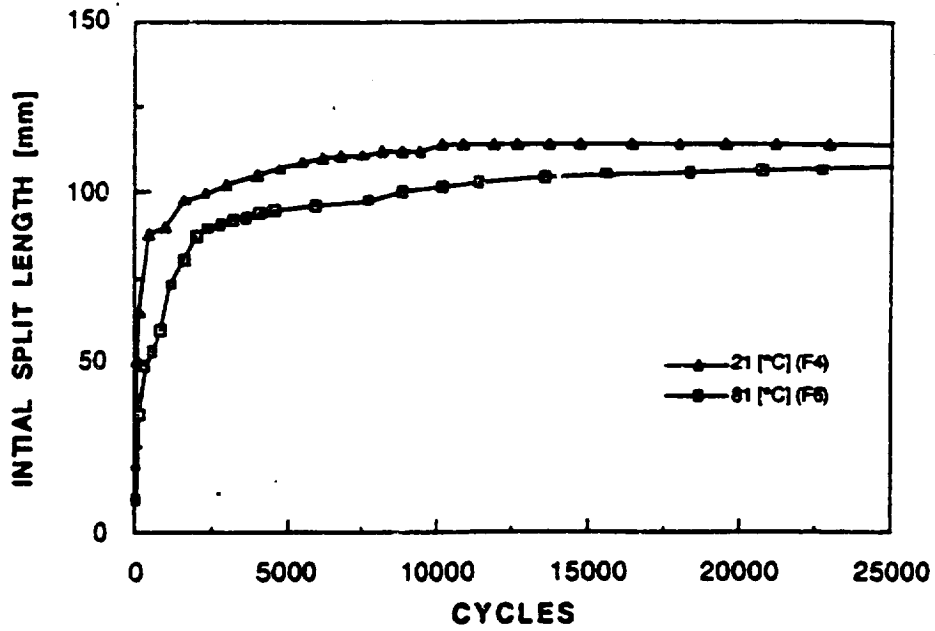
Figure 25-18: Effect of Temperature on Fatigue Growth of Matrix
Splitting: at 1 Hz (above); at 0.1 Hz (below).

Drexel tests for matrix splitting and mode I interlaminar crack growth (double cantilever beam, DCB, specimens) have indicated some influence of creep load history. All tests performed to date have been done in a room temperature environment. Creep loads held for up to 50 hours on DEN specimens have resulted in some matrix splitting, followed by a delay in additional growth until higher loads. Creep loads held for up to 50 hours on DCB specimens have resulted in no visual crack growth, followed by a delay in additional growth until higher loads. In each case, the change in behavior is on the order of 10%, which is close to the expected matrix stress relaxation for room temperature creep tests. Future tests will accelerate the effect of time with the help of elevated temperature creep. Creep load histories are crucial to the frame/skin bond which sustains pressure loads during flight.

Problems and Recommendations: No problems are currently foreseen and there are no recommended changes in plans or schedules at this time.

Near Term Plans: Additional design drivers may be identified as the Family C designs continue to be developed.

Fabrication of the ply-drop specimens will continue, in order to support the test matrix outlined above.

A limited effort will continue to evaluate the effect of creep loading history on interlaminar crack growth in toughened composites at Drexel University (Awerbuch and Wang). This will aid in the development of test and analysis methods for new work at Drexel supporting an evaluation of the frame/skin adhesive joint (see Section 4.4.2, Supporting Technologies for Frames and Attachment Details).

4.2.4 Mechanical Tests

Current Progress: Impact damage resistance DOE impacting is complete. All panels have had ultrasonic inspections performed to map out the extent of all impact damage states on each panel. Detailed time-of-flight pulse-echo inspections of individual damage sites have begun.

The stiffened panel warpage study continued with the delivery of an approximately 2' by 2' manufacturing demonstration panel to the test lab. This panel incorporates a curved skin, two stiffeners, and two frame elements. It will be measured for warpage using the shadow Moire technique.

Research studies on sandwich core materials continued at The University of Iowa (Lakes). A significant amount of work was documented in a Masters thesis for Kirsten Lynn Elms (Copies available upon request). In addition, work with metallic re-entrant foams used as model materials to evaluate the effects of a negative Poisson's ratio on mechanical performance was summarized in a technical paper. This paper is included in Appendix H for NASA's review. Please submit any recommended changes for this paper to the authors at University of Iowa within the next month.

Problems and Recommendations: No problems are currently foreseen and there are no recommended changes in plans or schedules at this time.

Near Term Plans: Data from detailed time-of-flight pulse-echo inspections will be interrogated using 3-dimensional imagery to better conceptualize the structural significance of the interconnecting delaminations and transverse cracks. Fiber failure studies will begin with the identification of candidate impact sites for deply.

The results of the current sandwich impact damage study will analyzed, taking into consideration the design-of-experiments test matrix. The conclusions and observations from this work will be used to scope further structural sandwich studies. The results of the current study will guide future coupon and structural test development. This work will consider and may be coupled with the research effort being performed at Sundstrand.

Warpage measurements for a curved, stiffened panel with frame elements will be collected and correlated with the various manufacturing details of the panel. The finite element models of the warpage panels will continue to be refined, including one which incorporates the attached frames.

Testing to examine the effect of several impact damage repair concepts are being considered. These tests would examine the effect of low cost, simple repairs on sublaminate stability.

Work will continue with damage resistant core materials at the University of Iowa (Lakes). A second subcontract will be issued to analyze and test foam materials fabricated by the Sundstrand subcontract.

4.3   Side Panels

The schedule for activities associated with window belt panels is shown in Figure 25-17. Work in this area is scheduled to re-start in the fall of 1991.

4.4   Frames and Attachment Details

The schedule for activities associated with frames and attachment details is shown in Figure 25-18. Work with the initial braided composite test matrix remains behind schedule. Fabrication tasks for this effort have been completed. Tests have started at the Mechanics of Materials Branch, NASA Langley.

4.4.1   Manufacturing Technology

Current Progress: Work by Boeing Helicopters (BH) continued on the coordination of manufacturing/test plans for braided materials selected for crown frame applications. Fabrication of braided/RTM panels to yield specimens for material characterization was completed at Fiber Innovations.

Figure 25-17: Side Panel Development and Test Verification
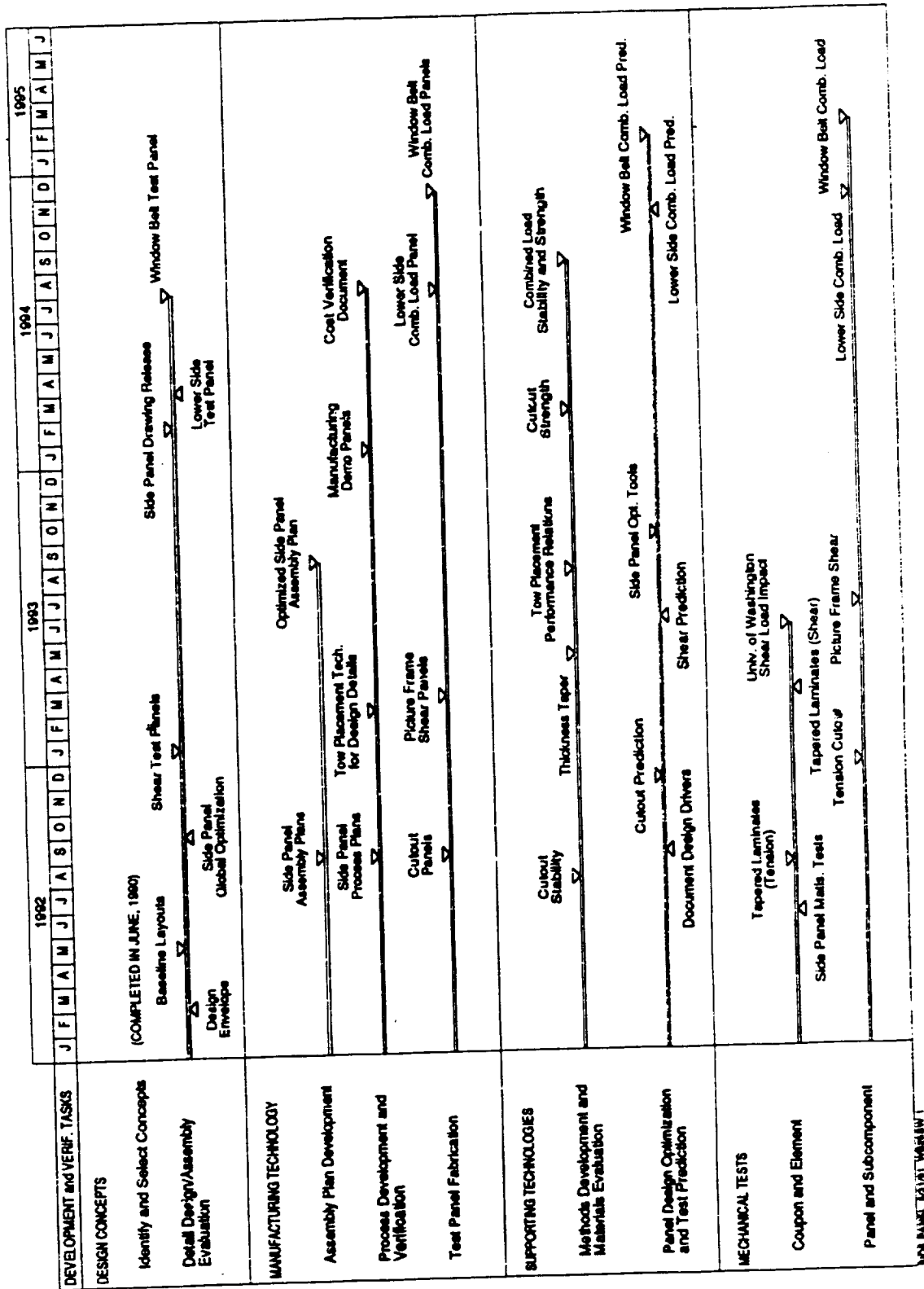
Figure 25-18: Frames and Attachment Details (Clips and Splices)
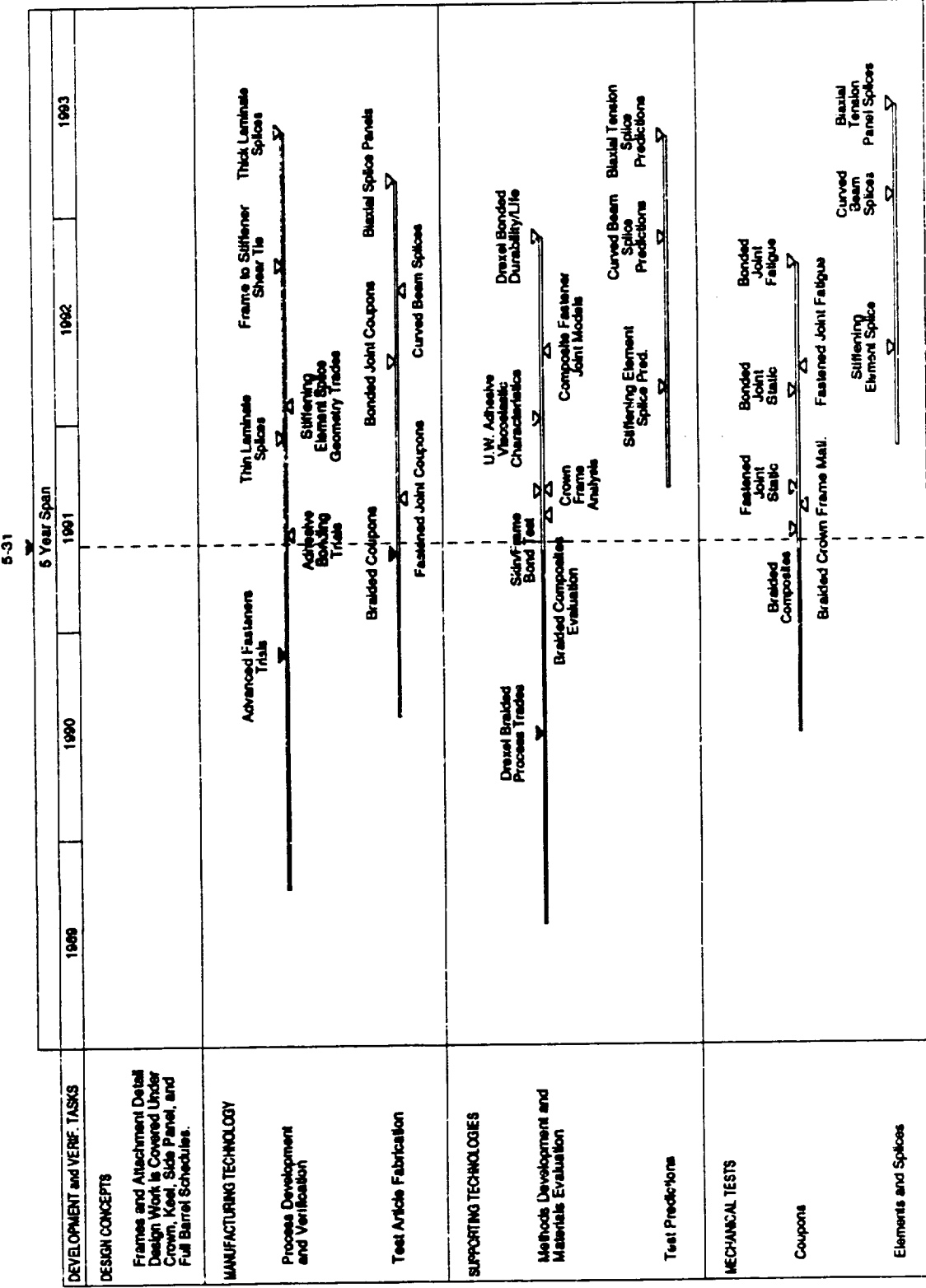
The RTM tool for 3' frames was finished and shipped to Fiber Innovations. This tooling is currently being tested for vacuum integrity and proper sealing. The design of the 8' RTM tool is still under review. A contract for the 8' tool was released and final drawing revisions will be based on the results of 3' frames that will be built in June.

The results of thermoplastic rivet lap-shear tests were sufficiently encouraging that Cherry were asked to demonstrate rivet installations at the NASA ATCAS Phase A Review held at Boeing on May 15-16. Cherry developed prototype portable riveting equipment which was demonstrated to an ATCAS team member during April. This equipment was used to successfully install rivets in CFRP plates at the review. The next step in the development of these rivets is the inclusion of representative circumferential frame web splice specimens in the BH splice test program.

Another potential application for thermoplastic rivets is considered to be the attachment of glass fiber reinforced plastic (GFRP) plates as repair patches for damaged carbon fiber reinforced plastic (CFRP) laminates in tension dominated structure. The GFRP material has very good tensile strength properties and the lower modulus for a patch material would pull less load into the repaired area. Past mechanically attached repairs of CFRP structures have utilized metal plates which have the effect of increasing the structural stiffness locally and, thereby increasing the load at the repair. This can lead to durability problems and failures in the mechanical attachment.

Problems and Recommendations: No problems are currently foreseen and there are no recommended changes in plans or schedules at this time.

Near Term Plans: All braided/RTM panels will be delivered to NASA Langley for specimen preparation. Eight 3' frames will be braided and resin transfer molded. Two frames will have variations of noodle types and cap preforms which will be used for frame/skin bond tests.

Future work utilizing thermoplastic rivets will be coordinated with mechanically fastened joint tests. The use of thermoplastic rivets in crown and keel panel repair concepts will also be considered.

4.4.2   Supporting Technology

Current Progress: All fabrication tasks were completed for the initial braided composite test matrix comparing two processes: (1) formation by subjecting graphite fiber preforms to a RTM process, and (2) consolidation of a commingled thermoplastic/graphite fiber preform. Specimens were shipped to NASA Langley for test preparation.

Work continued in planning Drexel University (Awerbuch and Wang) tests to evaluate the skin/frame adhesive bond. Basic characterization tests will include delamination crack growth with mode I (DCB) and II (ENF) specimens. In addition, skin/frame bond element tests will be performed using specimens cut from crown manufacturing demonstration panels. A preliminary configuration for the skin/frame bond test is shown schematically in Figure 25-19. The initial set of tests will screen different design and

manufacturing variables for the skin/frame bond detail (e.g., variations in the "noodle" insert used to fill a gap at the web/flange intersection).

Frame Geometry

5.4 in.

Skin Thickness = 0.096 in.

Pinned
Loading
Plates

2.7 in.

Mechanically Fastened
Attachment Plates

3 in.

Flange and Web
Thickness = 0.13 in.

12 in.

Note That Both the Frame and Skin Have a
Slight Curvature (122 in. radius) in the X-Direction
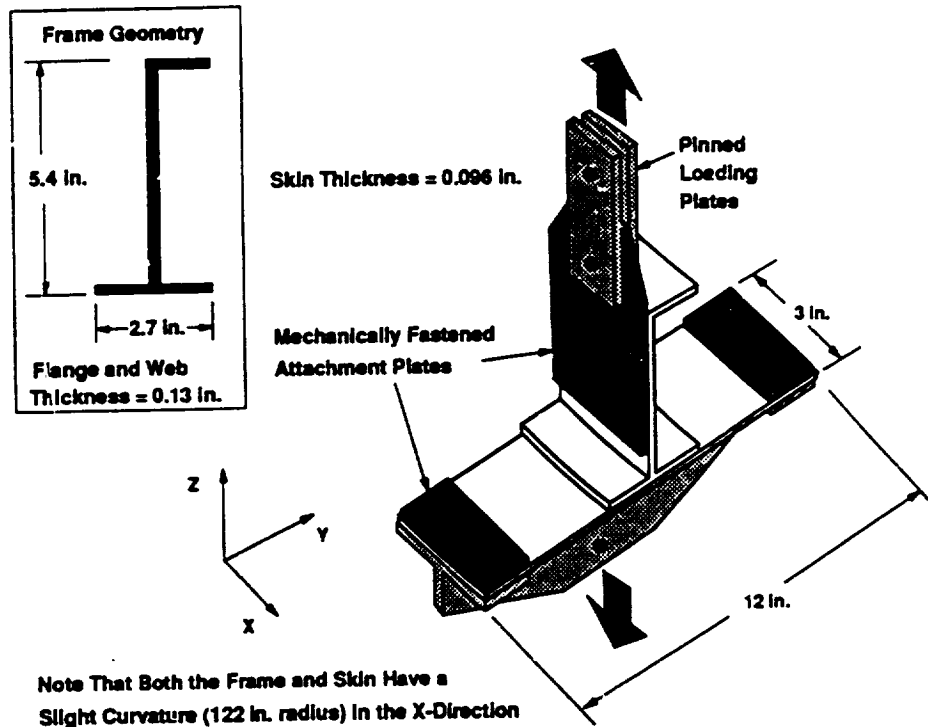
Figure 25-19: Preliminary Skin/Frame Bond Test Element Geometry

Problems and Recommendations: No problems are currently foreseen and there are no recommended changes in plans or schedules at this time.

Near Term Plans: In the University of Washington (Seferis) subcontract, work will continue on the viscoelastic characterization of 350°F curing film adhesives. Results giving the shift factors for creep, stress relaxation and DMA measurements on the Narmco 1515-3 adhesive are scheduled to be completed in time for the next monthly report.

Specimens will be fabricated for initial Drexel tests to screen skin/frame bond design and manufacturing variables. These tests will also enable Drexel to evaluate the test element geometry and material failure mechanisms. Test specimens will also be fabricated for mode I and II delamination crack growth of the skin/frame adhesive bond.

4.4.3 Mechanical Tests

Current Progress: Specimens were delivered to NASA Langley to start braided composite testing. Two sets of specimens will be tested: (a) crown material characterization (see Section 4.4.1) and (b) initial braided composite test matrix (see Section 4.4.2). Since more braided panels were fabricated for crown material

characterization than originally planned, some additional tests will be performed. These include:

- tension after impact

- transverse tension

- specimen width effect

- impact damage characterization

- additional fatigue (R = 10, -1).

Development of a bolted joint test plan required for the assembly of large, stiff cobonded structures continued at BH. Preliminary test specimen configurations have been developed to simulate the circumferential splice, longitudinal splice, and frame inner chord splice. The specimens have been configured to examine the joint component laminates under pure bearing, pure bypass, and interacting bearing and bypass loads. A preliminary test plan was presented at the NASA review in Seattle on May 15 and 16, 1991.

Problems and Recommendations: No problems are currently foreseen and there are no recommended changes in plans or schedules at this time.

Near Term Plans: Braided composite testing will start at NASA Langley, with a large portion of the tests scheduled to be completed during June, 1991.

Evaluation of methods for possible simplification of the circumferential joint will continue. Configurations for biaxial testing of specimens simulating the lor. dinal splice will be evaluated. Availability of crown panel and braided frame material for test specimens will also be assessed.

4.5 Full Barrel Studies

The schedule for activities associated with the full barrel section is shown in Figure 25-20. The only ongoing activity is consideration of the total barrel assembly issues as they relate to the design concept development.

4.6 Design Cost Model

The Phase A schedule for activities associated with the design cost model is shown in Figure 25-21. The Phase B schedule is shown in Figure 25-22. Applications of the model will be reported under the subheading of "Design Concepts" in association with local optimization of specific fuselage hardware elements and components. As discussed last month, a work statement and cost proposal was submitted to NASA Langley in response to the change order, Modification Number 13 to contract number NAS1-18889. Additional information on the subcontracts for this effort was assembled and sent to NASA contracts people per their request.

Figure 25-20: Full Barrel Studies (Including Metal Test Jig)

VERIFICATION TASKS	1992	1993	1994	1995

DESIGN CONCEPTS

Detail Design/Assembly Evaluation
- Design Envelope
- 360 Degree Concept Accept/Reject
- Final Global Cost and Weight Evaluation
- Lockheed Frame Optimization
- Attachment Detail Optimization
- Metal Test Jig Drawings
- Splice Optimization
- Full Barrel Cost Minimization
- Panel Drawing Updates

MANUFACTURING TECHNOLOGY

Assembly Plan Enhancement
- 360 Degree Evaluation
- Full Barrel Assembly Plans
- Test Jig Assembly Plan
- Optimized Full Barrel Assembly Plans

Process Verification and Test Article Fabrication
- Quadrant Frame Splice
- Upper Quadrant Long. Splices
- Lower Quadrant Long. Splices

SUPPORTING TECHNOLOGIES

Methods Enhancement and Materials Evaluation
- Composite Section 46 Internal Loads Model
- Tension Fracture Load Rate
- Test Jig Requirements
- Splice Optimization Tools
- F.E. of Full Barrel Test Jig
- Univ. of Iowa Sandwich Evaluation
- Dynamic Pressure Release

Splice Test Predictions
- Frame Splice Predictions
- Upper Quadrant Splice Pred.
- Lower Quadrant Splice Pred.

MECHANICAL TESTS

Splices
- Frame Splice
- Combined Load Upper Quadrant Splice
- Combined Load Lower Quadrant Splice

Metal Test Jig
- Fixture Fabrication
- Fixture Assembly
- Test Setup

FULL BARREL SECTION 3/3/91 PB/6W1

25-34

Figure 25-21: Cost Model Development
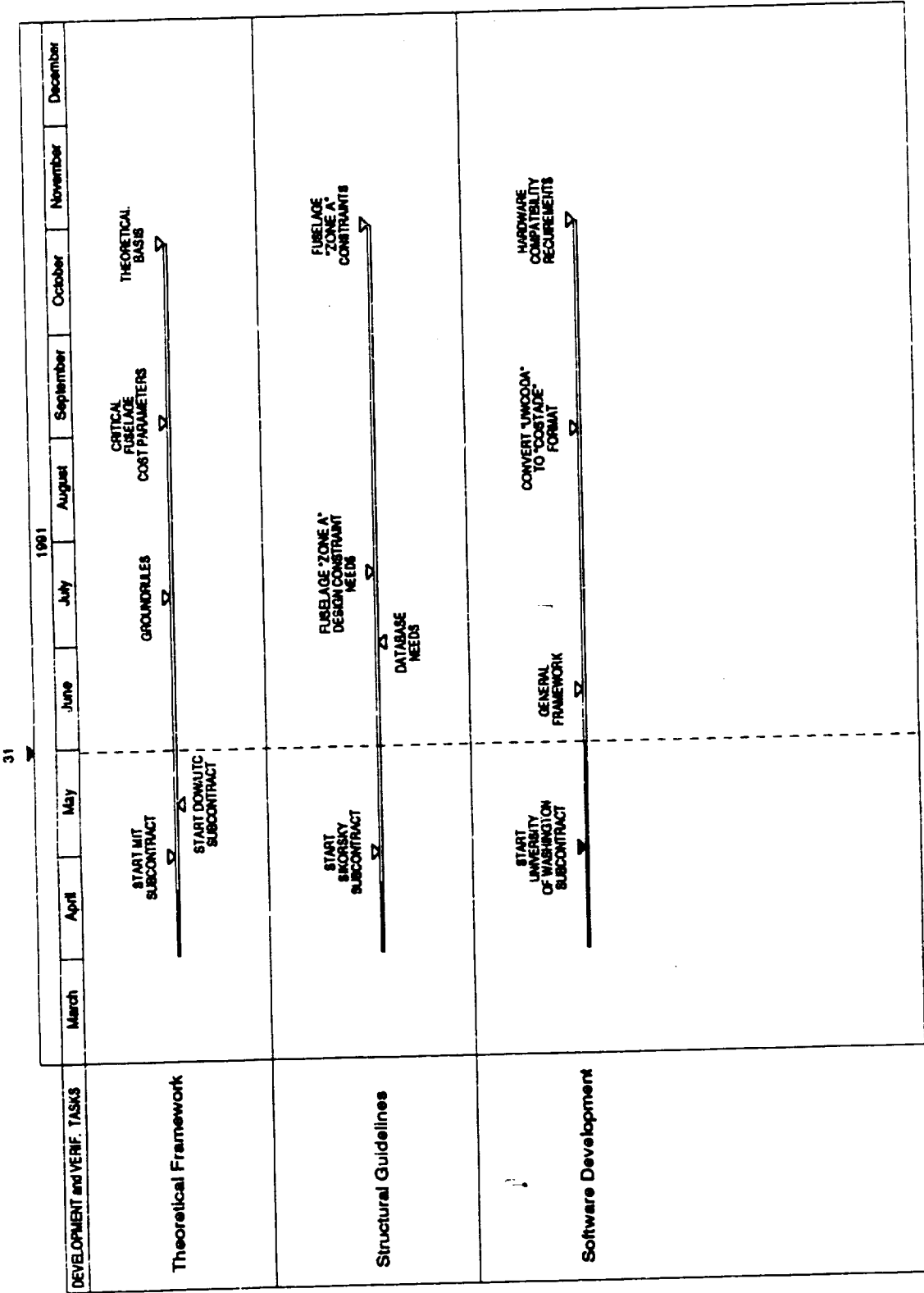
Figure 25-22: Cost Model Implementation (Sheet 1)
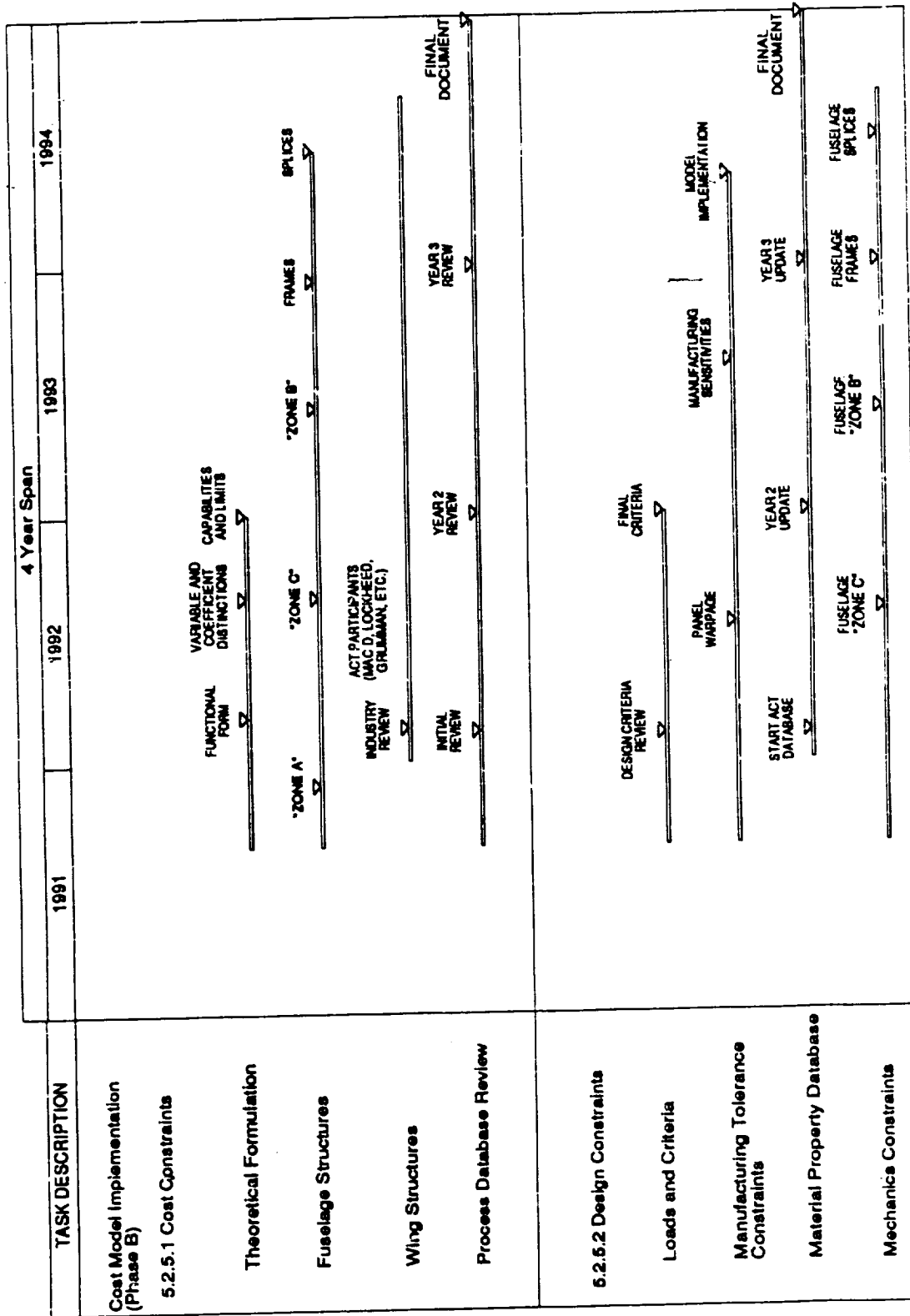
Figure 25-22: Cost Model Implementation (Sheet 2)

25-37
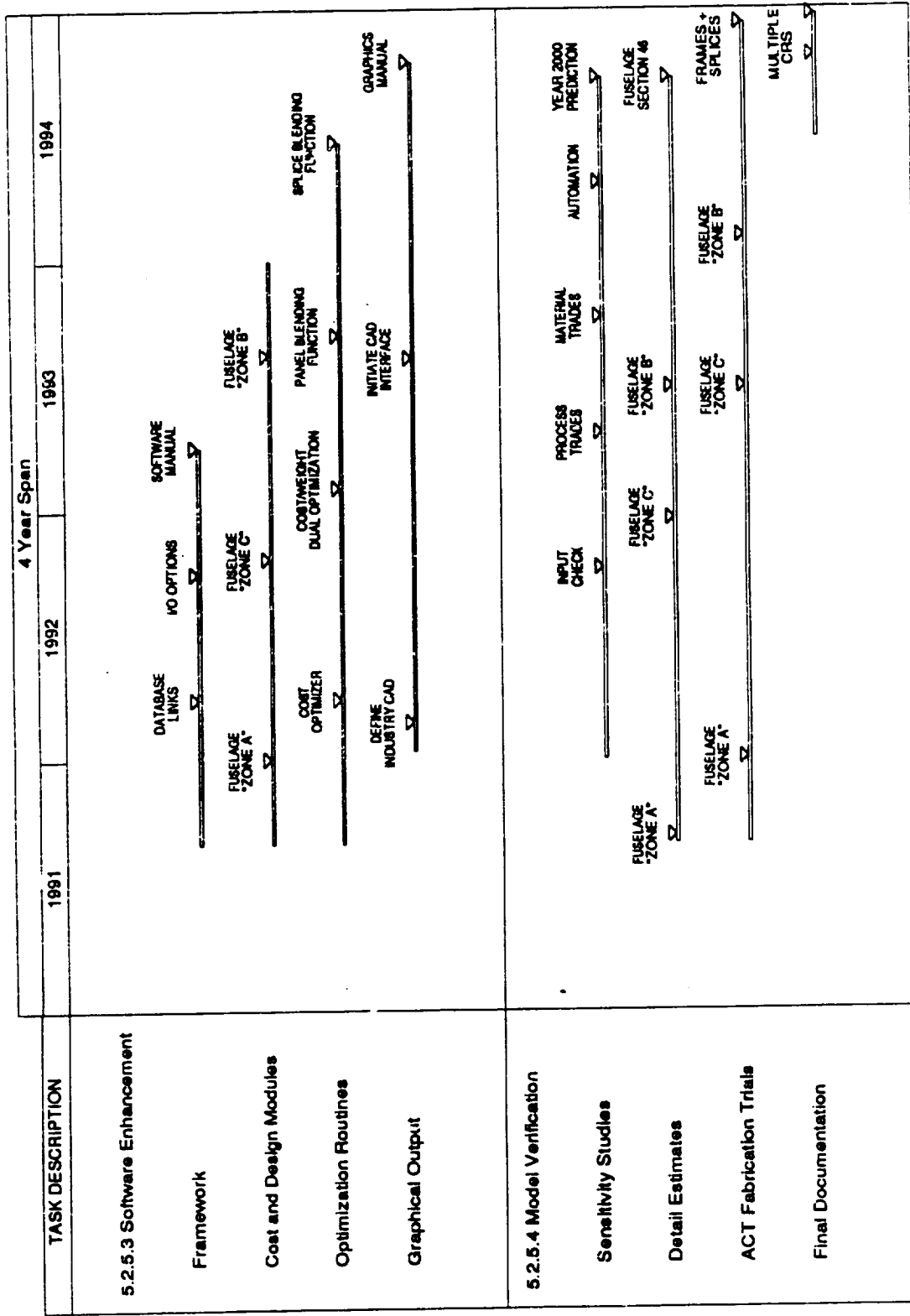
A meeting is being planned to coordinate design cost model subcontractor tasks and review progress to date. This meeting is tentatively planned for August. The specific date and location for the meeting will be chosen with help from NASA.

4.6.1 Theoretical Framework

Current Progress: Procurement efforts continued to arrange subcontracts with the Massachusetts Institute of Technology (MIT) and Dow/United Technologies (Dow/UT). Several issues have arisen which have made negotiations between Boeing and MIT difficult. Boeing Buyers are scheduled to visit MIT during the month of June. A proposal and cost statement was received from Dow/UT.

Work at Boeing started to review the cost modeling approach performed in support of local optimization for the crown. Insight for a theoretical basis for the cost model is expected to benefit from this review. Critical fuselage cost parameters for Family C crown structures were identified.

Work to establish a list of definitions for terms used in design cost modeling began. A list of terms will be documented prior to the August review with NASA and cost model subcontractors.

Problems and Recommendations: No problems are currently foreseen and there are no recommended changes in plans or schedules at this time.

Near Term Plans: Procurement efforts will continue to resolve problems in establishing a subcontract with MIT. The Dow/UT proposal will be reviewed and negotiations will continue towards establishing the subcontract.

Work at Boeing will continue to review the cost model used for crown local optimization. Additional definitions will be added to the list of cost modeling terms.

4.6.2 Design Constraints

Current Progress: Procurement efforts continued to arrange the Sikorsky subcontract. A proposal and detailed cost statement from Sikorsky is pending.

The proposed data abstraction form (Composites Information System, COINS) developed for the ACT program by Analytical Services Inc. is under review. Specifically, Boeing was asked to review the types of manufacturing data sought by a designer. In addition, mechanical properties useful for design sizing will be assessed for possible inclusion in the COINS database.

Problems and Recommendations: No problems are currently foreseen and there are no recommended changes in plans or schedules at this time.

Near Term Plans: Negotiations will continue towards a subcontract with Sikorsky.

Work to review capabilities of the COINS database will be completed. The review will be documented and sent to Analytical Services Inc.

4.6.3 Software Development

Current Progress: Work has been initiated at the University of Washington (Tuttle, Zabinsky) on subjects relating to the cost model. An initial meeting was held to discuss goals and directions. Work at the University of Washington will initially focus on the structural mechanics issues that have been identified as strong cost drivers in the fuselage crown quadrant. In addition, work to define techniques to optimize a large configured structure with respect to both structural mechanics and manufacturing constraints, referred to as the blending function, will be initiated.

Problems and Recommendations: No problems are currently foreseen and there are no recommended changes in plans or schedules at this time.

Near Term Plans: Work at the University of Washington will continue on both the mechanics issues and the blending function

APPENDIX A

DESIGN FAMILY PICTORIALS
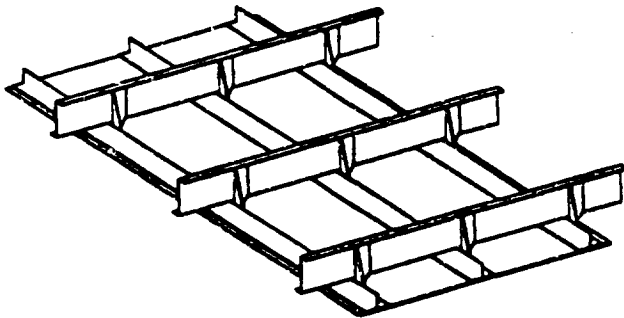
FAMILY A

Mechanically Fastened
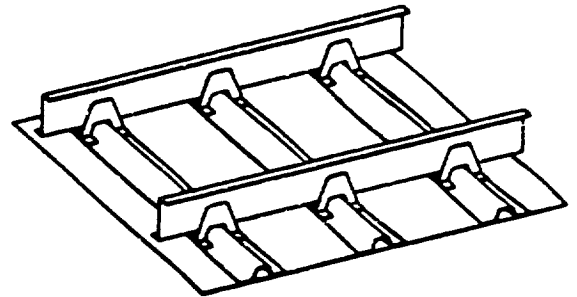
FAMILY B

Bonded Stiffeners
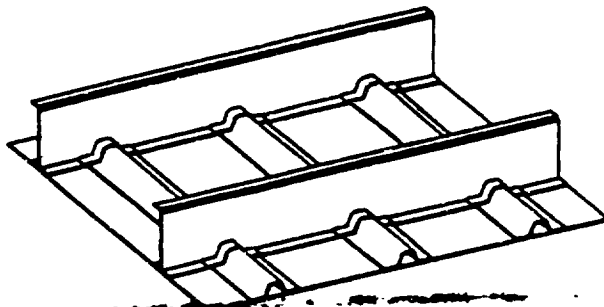
FAMILY C

Bonded Stiffeners
and Frames
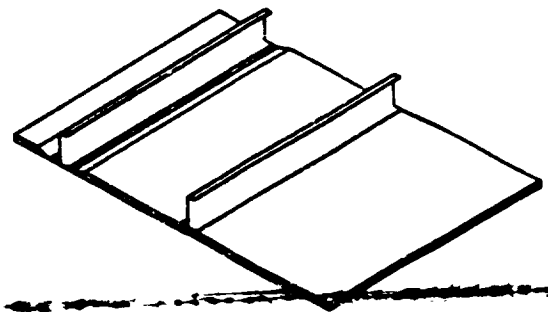
FAMILY D

Sandwich
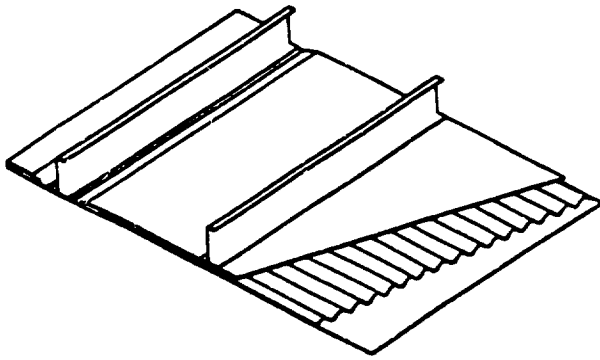
FAMILY E
Corrugated
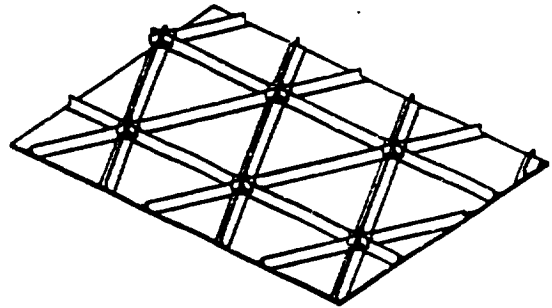
FAMILY F
Geodesic
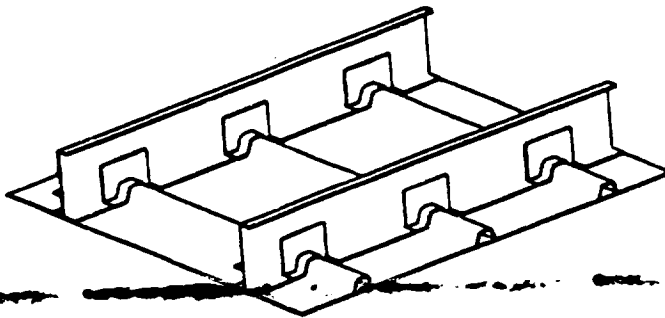
FAMILY G
Integrally Stiffened
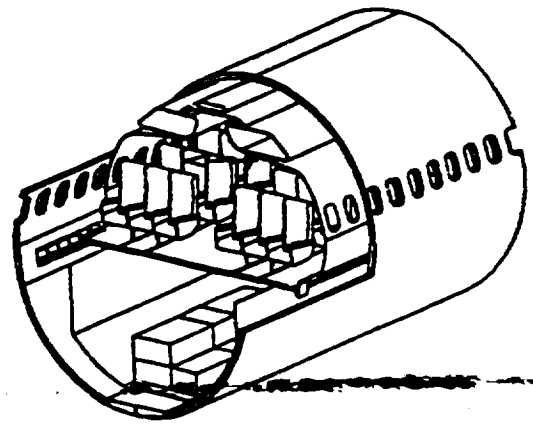
FAMILY H
Closed 360°

APPENDIX B

KEEL DESIGN D1 AND D2 INTERCOSTAL DRAWING

APPENDIX C

KEEL DESIGN D1 CARGO FLOOR FRAME DRAWING
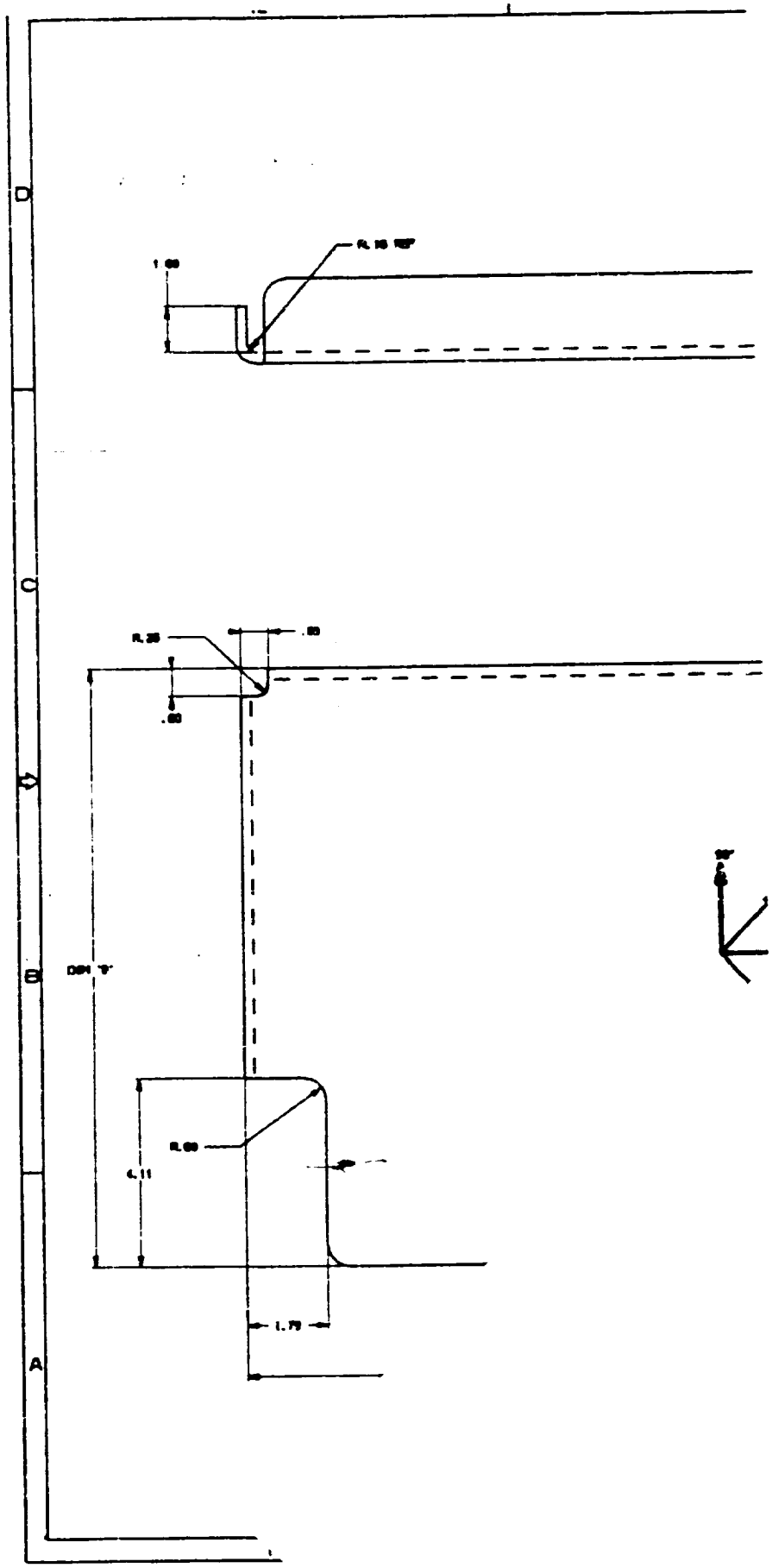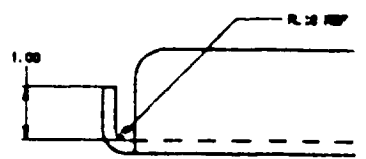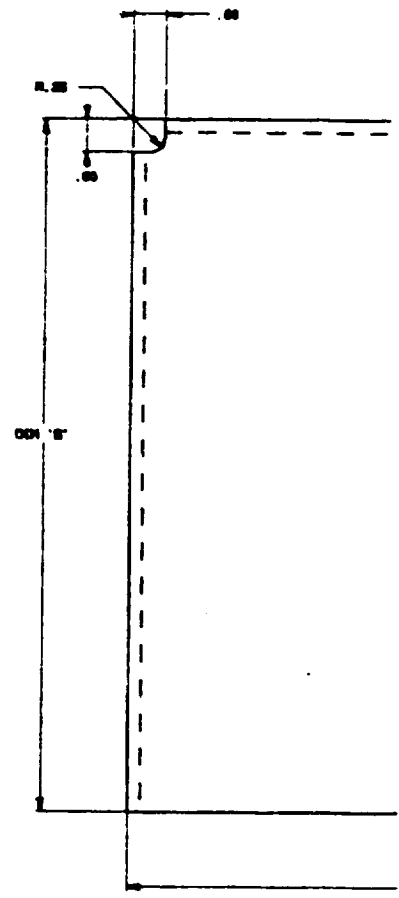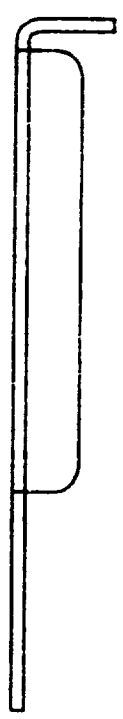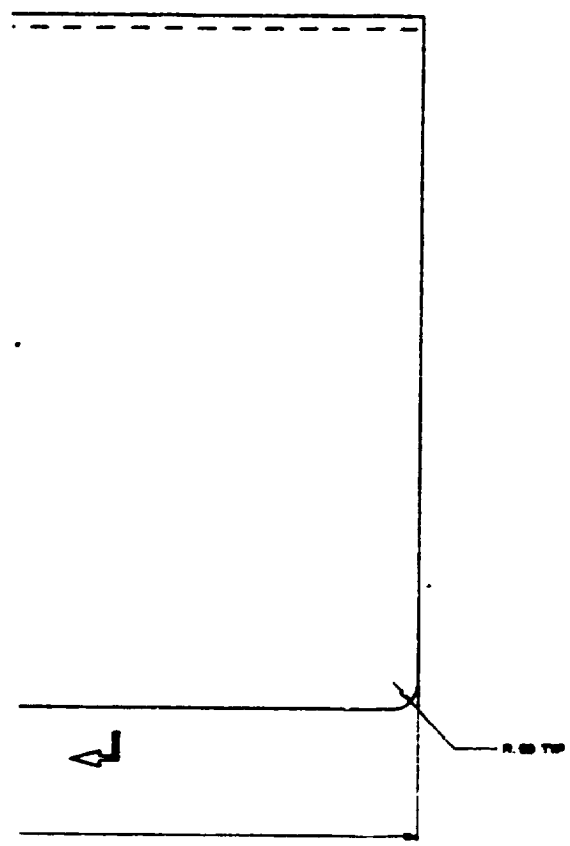
2
FOLDOUT FRAME

DIM "C"

R. 38 REF

1.00

SEE SH. 4

R. 38

.88

DIM "B"

R. 88 TYP

65C35562

3.

FOLDOUT FRAME

R. 18 REF

DIM "C"

— .88

1C7C8(-1 THRU -4)
2C7AM-13 & -14)
3C7CH-5 & -6)

90°
+45°
0°
-45°

R.38 TYP

DIM "A"
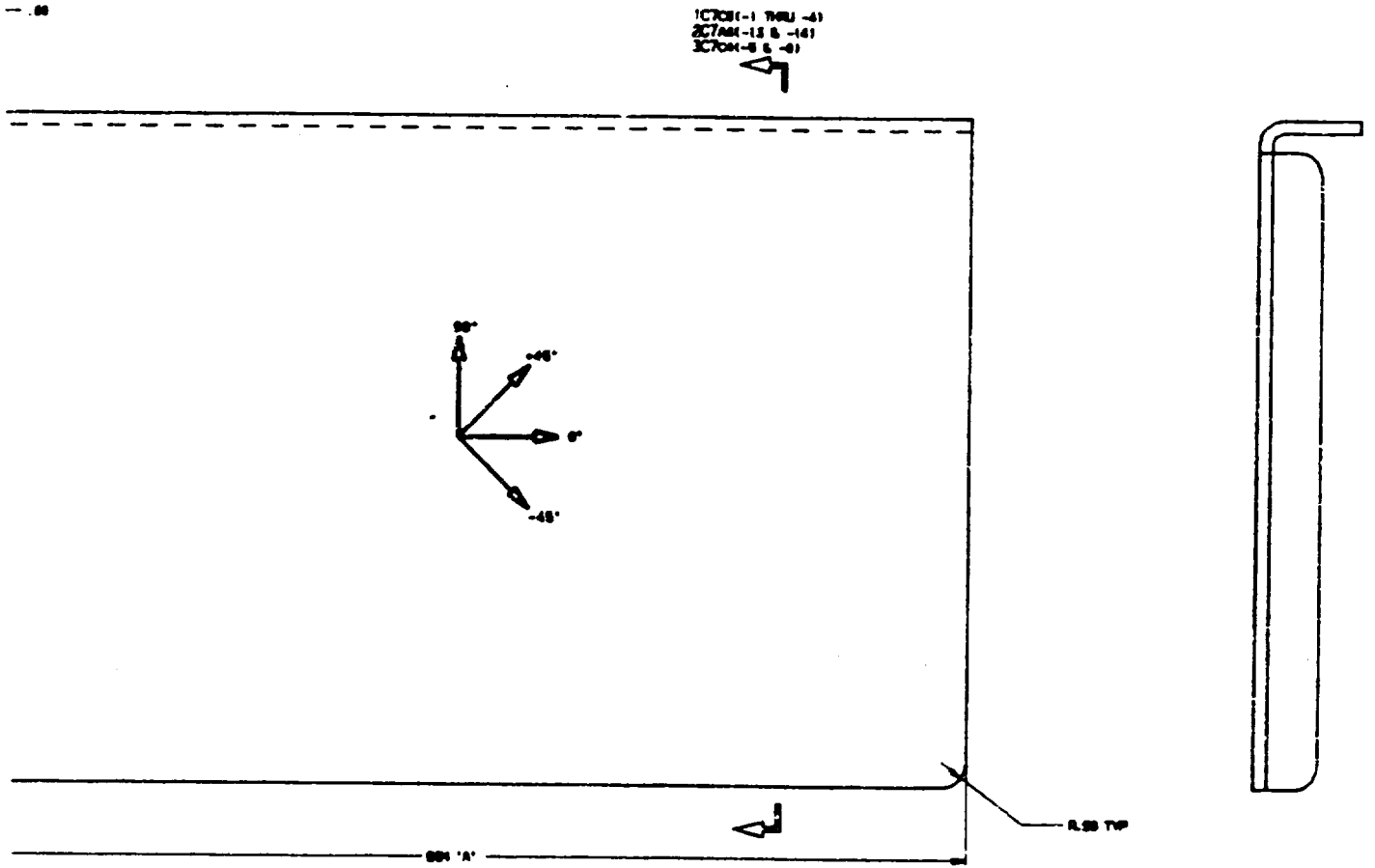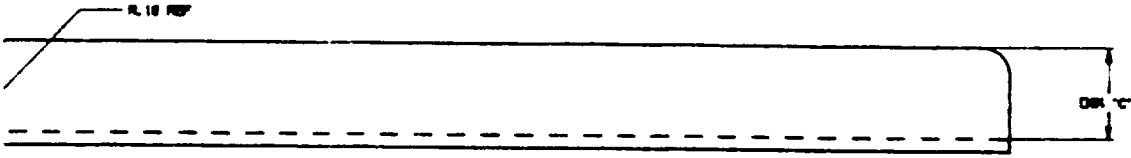
-1, OPP-2
-3, OPP-4
-5, OPP-6
-7, OPP-8
-13, OPP-14
INTERCOSTAL

4

FOLDOUT FRAME

IC7
-1 THRU -4
SCALE: NONE

2C7
-5 THRU -16
SCALE: NONE

65C35562

5.

FOLDOUT FRAME

TABLE I

PIN "D"	PART NO.	DIM "A"	DIM "B"	DIM "C"	MAT'L	PROCESS
DIE 1A	-1.GRP-2	16.72	9.50	1.35	STITCHED DRY UNI TAPE	RTM
DIE 1A	-3.GRP-4	28.82	11.00	1.70	STITCHED DRY UNI TAPE	RTM
DIE 1B	-5.GRP-6	16.72	9.00	1.03	THERMOPLASTIC SHEET	PREEFORM
DIE 1B	-7.GRP-8	28.82	12.00	1.03	THERMOPLASTIC SHEET	PREEFORM
DIE 2	-9.GRP-10	16.00	9.00	1.70	PREIMPREG. FABRIC BROADGOODS	PRESS CURE
DIE 2	-11.GRP-12	28.00	12.00	1.70	PREIMPREG. FABRIC BROADGOODS	PRESS CURE
DIE 2	-13.GRP-14	28.30	12.00	1.70	PREIMPREG. FABRIC BROADGOODS	PRESS CURE

2　　　　　　　　　　　1

6.

FOLDOUT FRAME

D

C

B

A

CTD

INTERCOSTAL BONDED KEEL
COST/WT TRADE STUDY
... "D" ...

J 81205 65C35562

DOUT FRAME

1B9
STIFFENER UNCURED
SCALE: NONE

STIFFENER ASSY DIAGRAM
SCALE: NONE

1B6
STIFFENER UNCURED
SCALE: NONE

3B4

1A9

.DOUT FRAME

| 81205 | 65C35561 | | A |

3.

FOLDOUT FRAME

1B3
FLOOR FRAME UNCURED
SCALE +ONE

1A8

2A3

1A7

1A3

4.

FOLDOUT FRAME

5.

FOLDOUT FRAME

BONDED ASSY -1
TYPICAL CARGO FLOOR FRAME

1A3

CTD

CARGO FLOOR FRAME-KEEL
COST/WT TRADE STUDY
FAM"D" - DES 1

J 81205 65C35561

APPENDIX D

KEEL DESIGN D2 FRAME DETAILS DRAWING
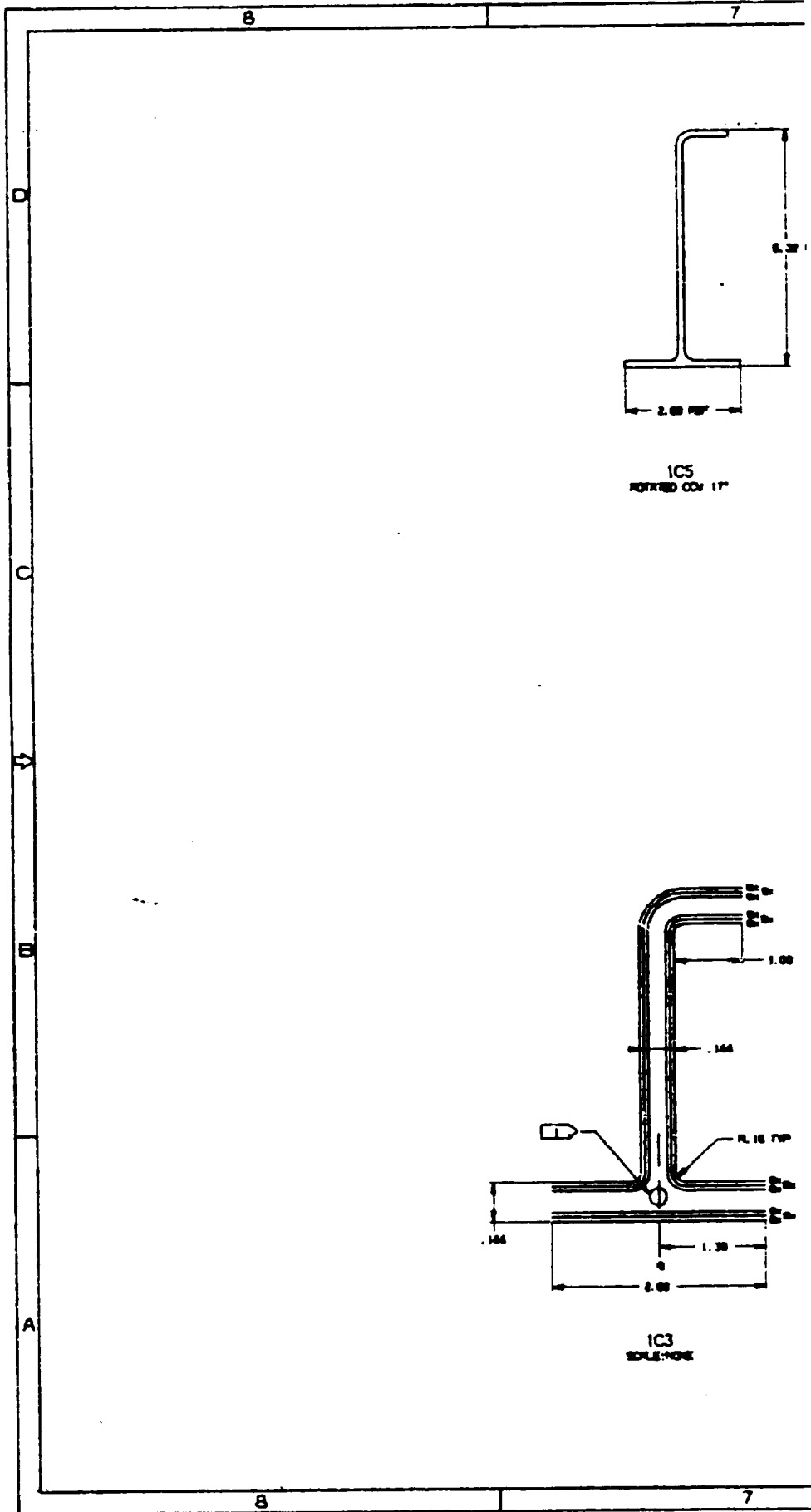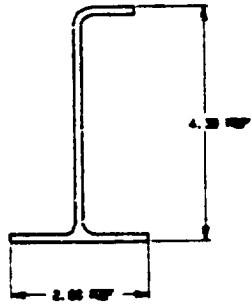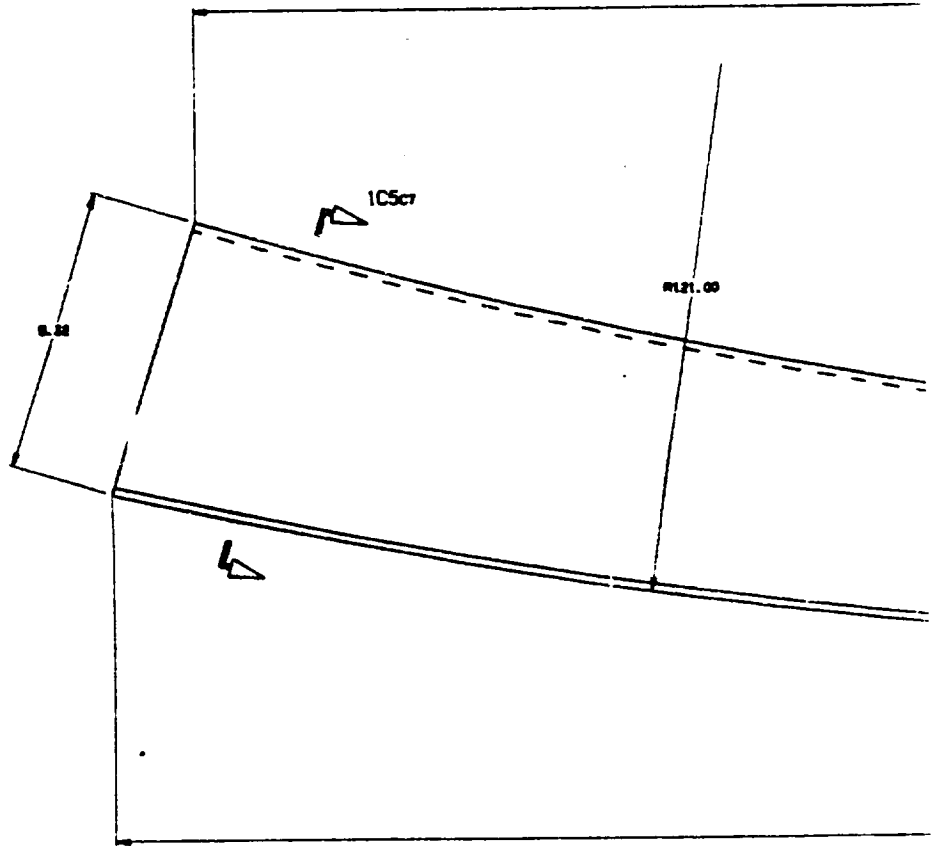
8

7

D

C

B

A

IC5
ROTATED CCW 17°

IC3
SCALE: NONE

2.00 REF

1.00

.144

R. 16 TYP

.144

1.38

2.00

8

7

FOLDOUT FRAME

4.39 REF

2.05 REF

2C3

1C5c7

R121.00

8.38

65C35566   1 A

3
FOLDOUT FRAME

DETAIL -1

FOLDOUT FRAME

1C3A7
2C3C8

CTD

FRAME DETAIL - KEEL
COST/WT TRADE STUDY
FAM 'D' - DES 2

APPENDIX E

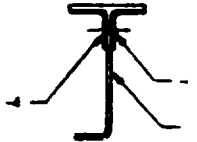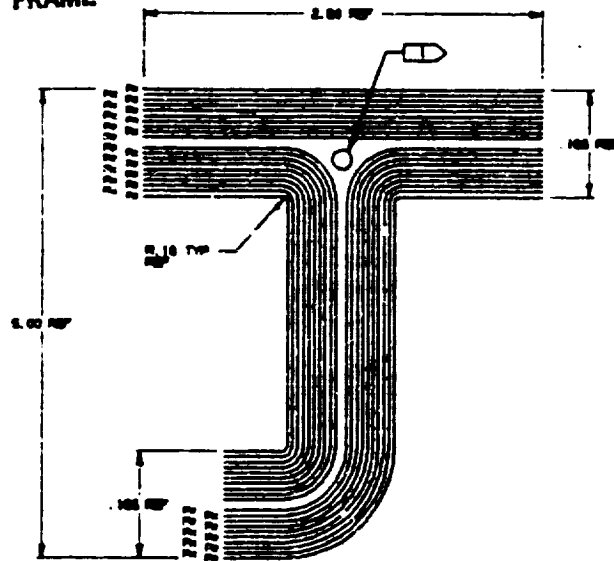# KEEL DESIGN D2 CARGO FLOOR DETAILS DRAWING

FOLDOUT FRAME
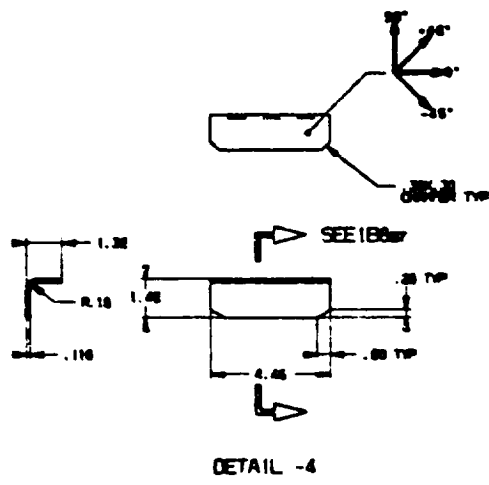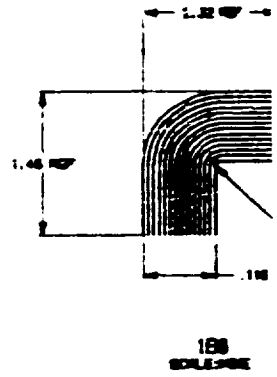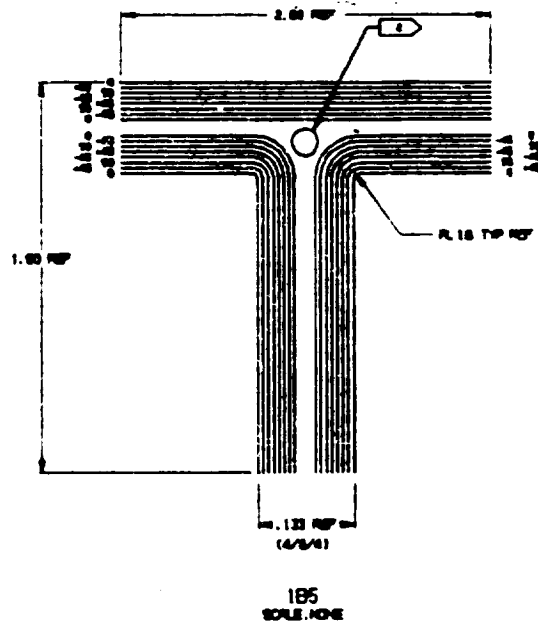
D

C

B
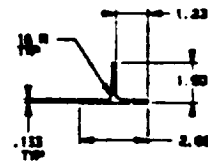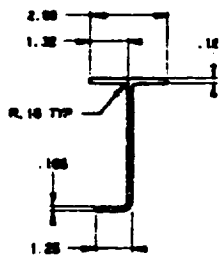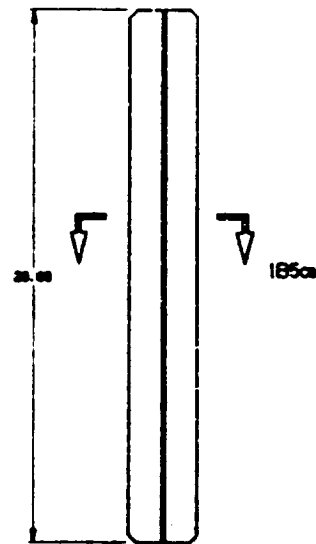
A

2

FOLDOUT FRAME

GSC.35565

3 .

FOLDOUT FRAME

FOL

104∞

CARGO FLOOR BEAM -1

182∞

STANCHION -2

4.

FOLDOUT FRAME

D

C

B

APPENDIX F

KEEL DESIGN C1 CARGO FLOOR DETAILS DRAWING

185
SCALE:NONE

186
SCALE:SIZE

DETAIL -4

2.

FOLDOUT FRAME

1B4
SCALE:NONE
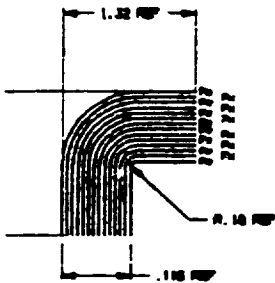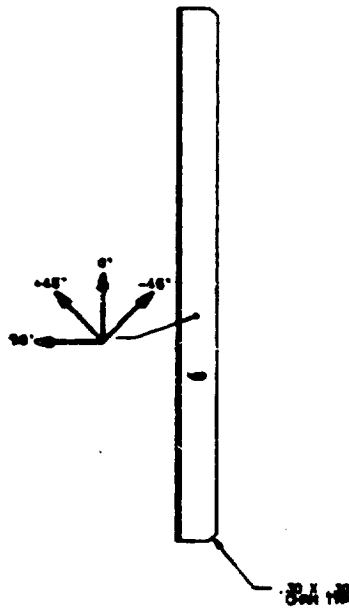
1B6
SCALE:NONE

STANCHION -2
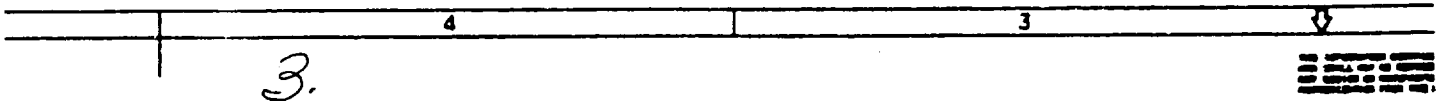
$3.$

FOLDOUT FRAME
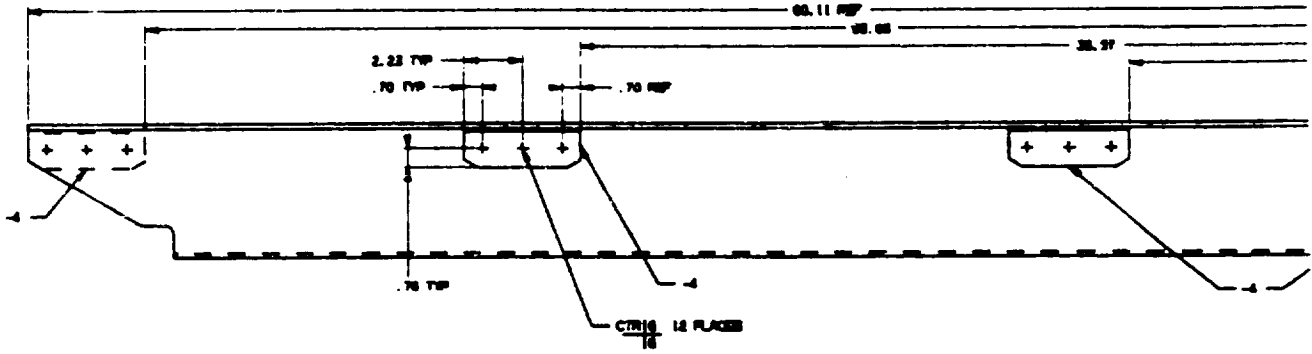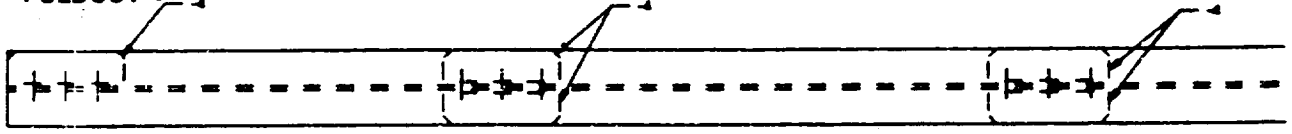
CARGO FLOOR BEAM ASSY-1

CARGO FLOOR BEAM -3

FOLDOUT FRAME
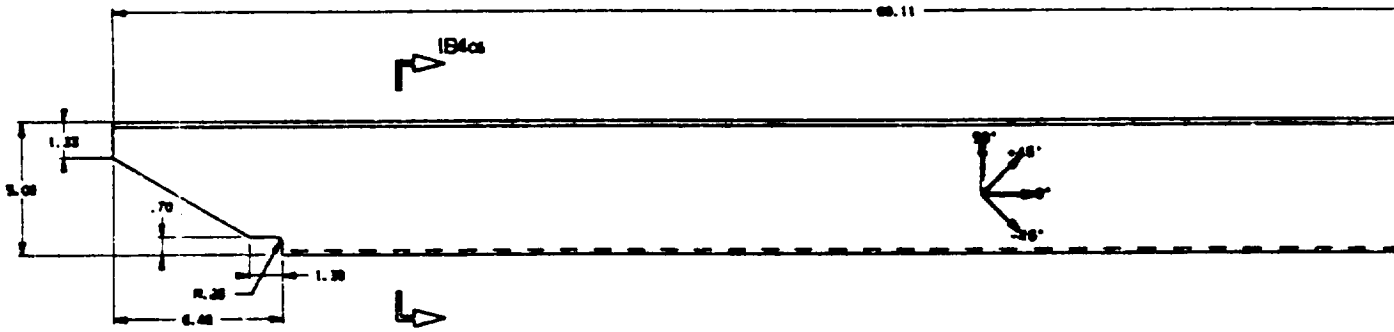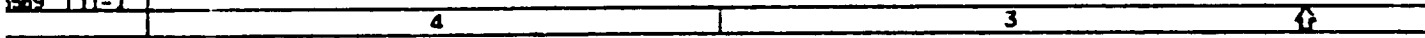
APPENDIX G

PICTORIAL OF ASSEMBLY OF KEEL DESIGNS D1A AND D1BD

PRE-CURED CHORD DETAILS
CO-BONDED TO SKIN

SEE SK-2

75.6"

KEEL PANEL

377"

FWD

ATCAS
CURED KEEL PANEL
SK-1

CARGO FLOORBEAM CHORD (18) PLS.

VARIABLE 21" TO 12.5"

1.3"

36.0"

10.5"

INTERCOSTAL CHORD (8) PLS.
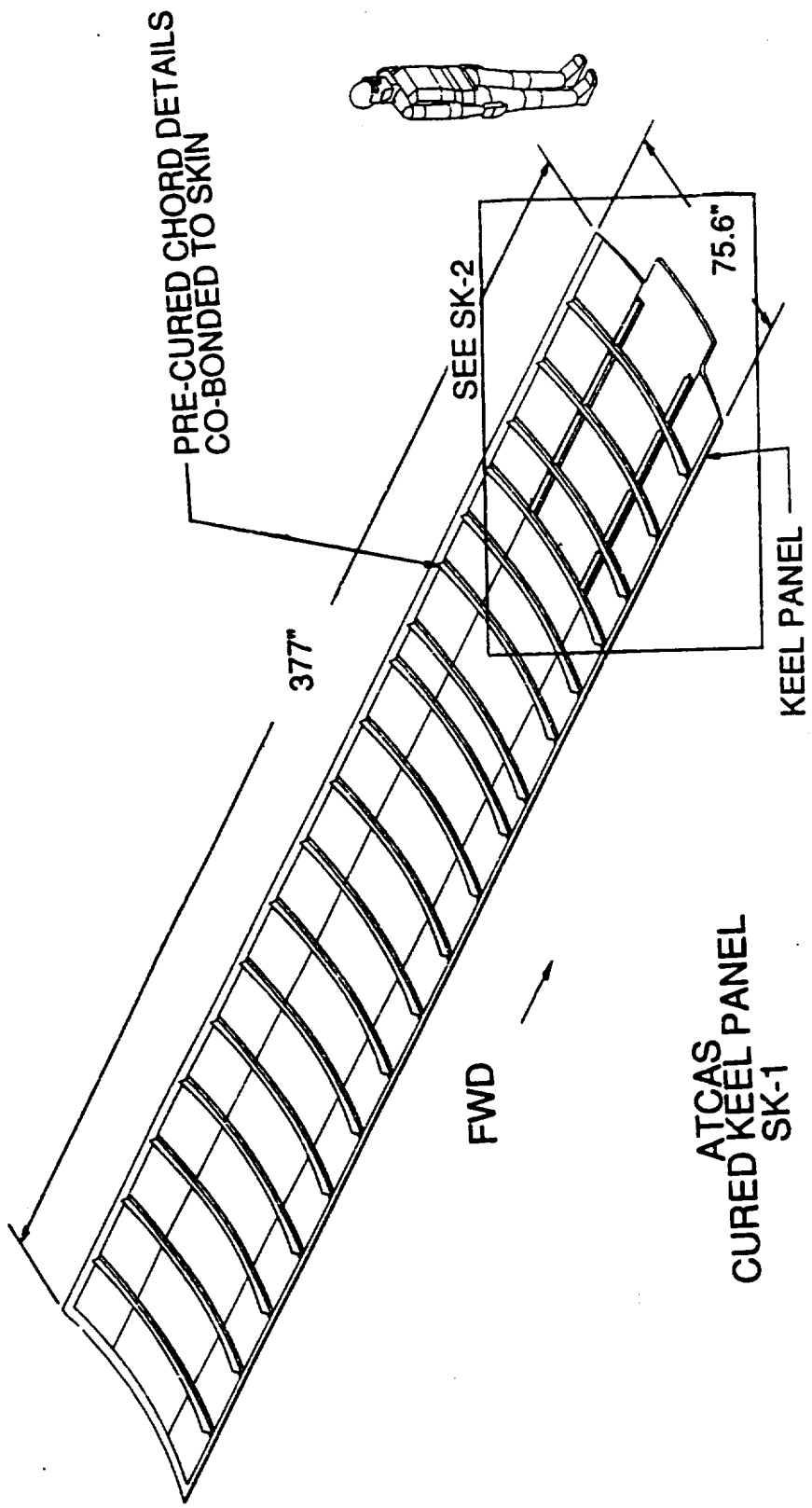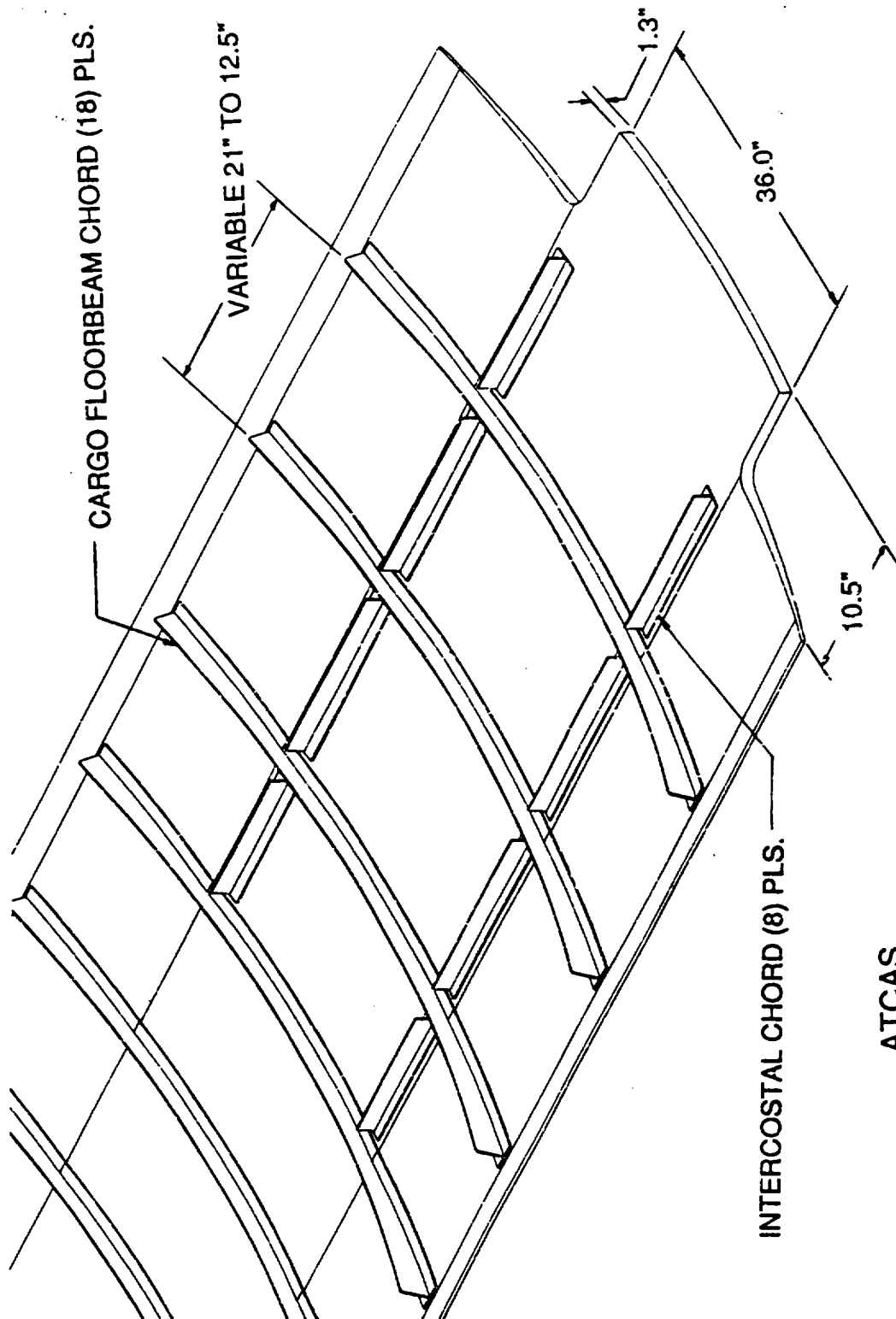
ATCAS
CURED KEEL PANEL
CLOSE-UP
SK-2

NOTE: SIDE PANELS ACTUALLY 118°
NOT AS SHOWN.

KEEL PANEL

SEE SK-4

ROBOTIC FASTENING SYSTEM

ATCAS
INSTALLATION OF
SIDE PANELS
SK-3

SIDE PANEL

LAP SPLICE
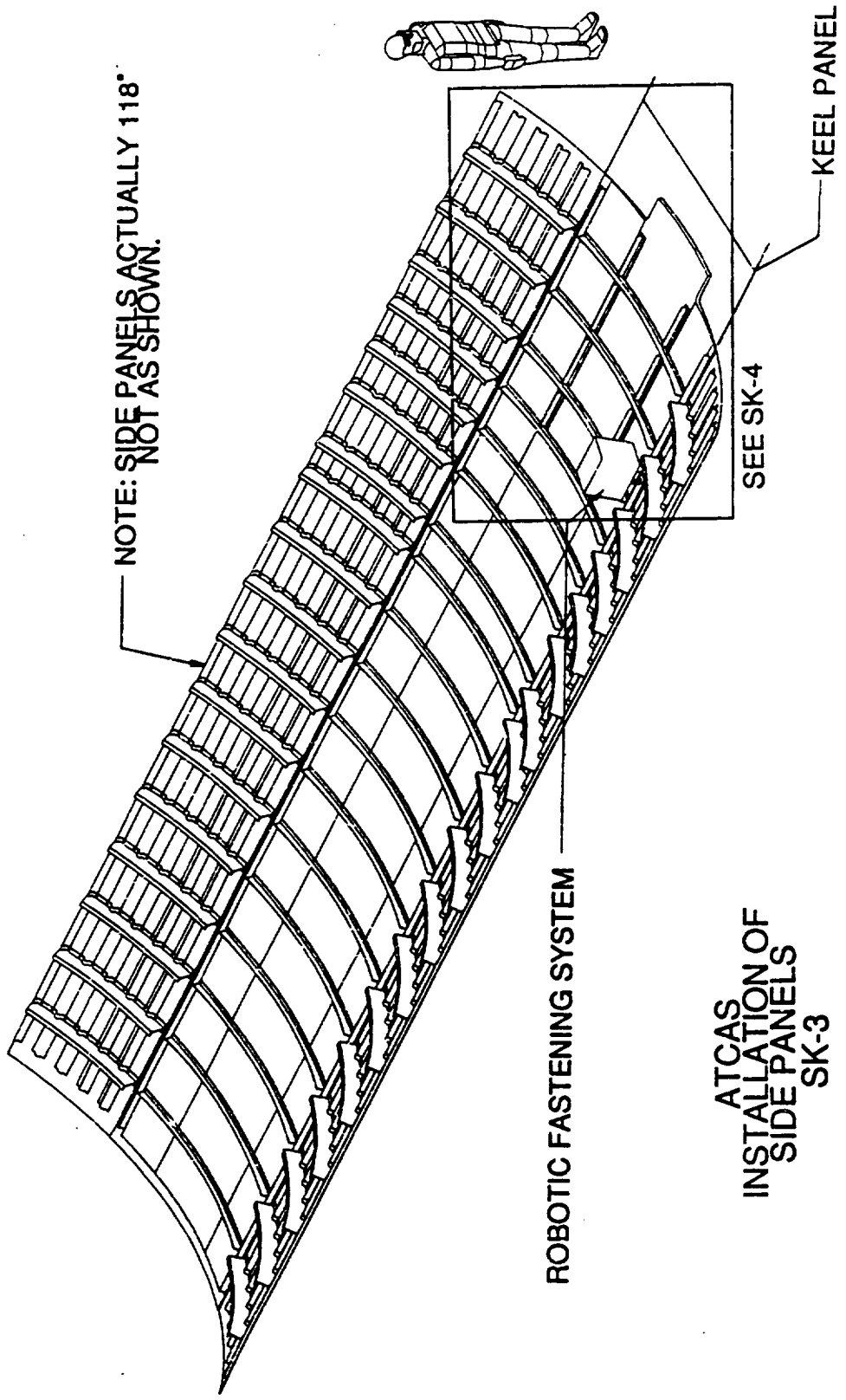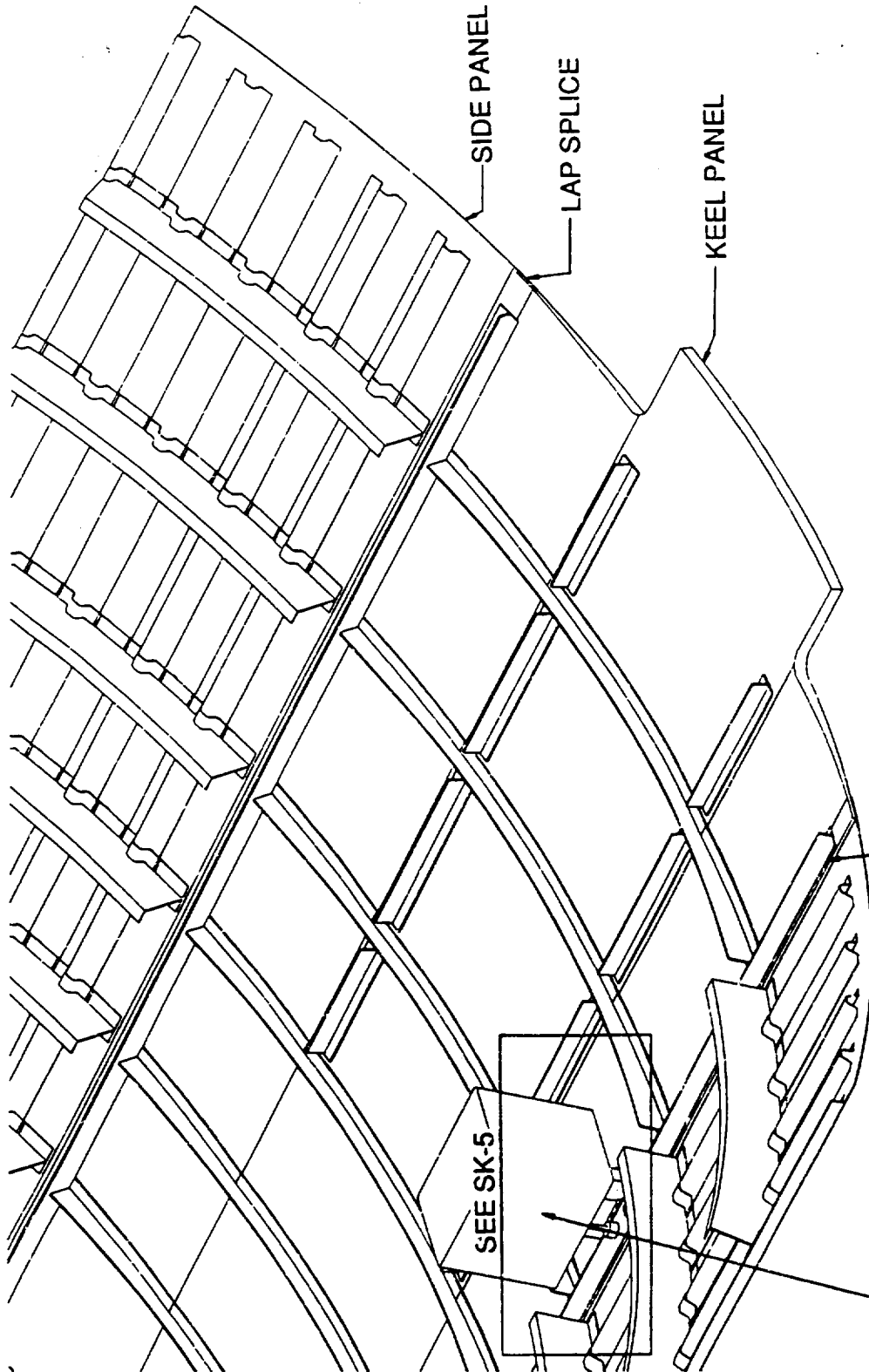
KEEL PANEL

ATCAS
INSTALLATION OF
SIDE PANELS
CLOSE-UP
SK-4

LONG. BLADE STRINGER

ROBOTIC FASTENING SYSTEM

SEE SK-5
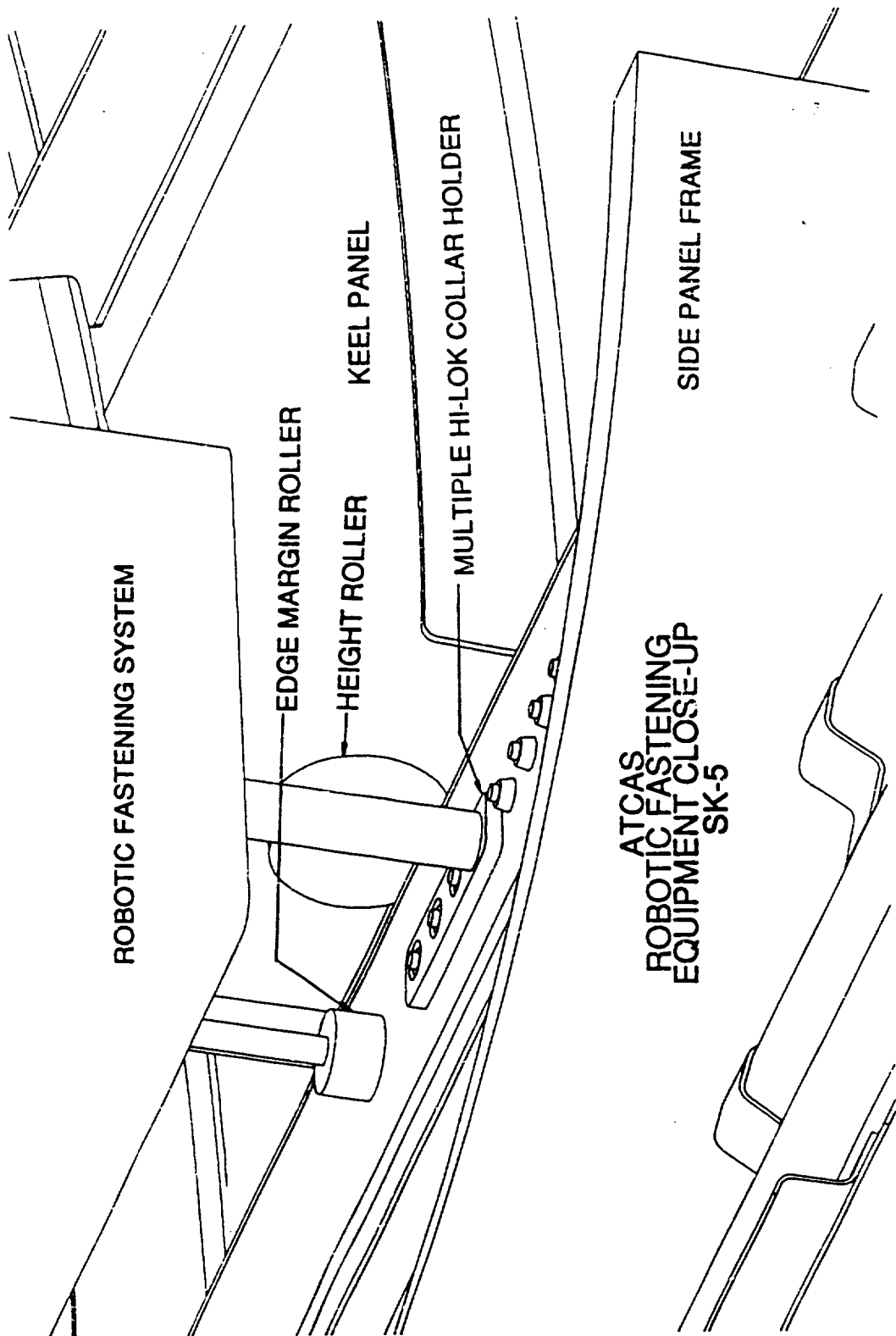
ROBOTIC FASTENING SYSTEM

EDGE MARGIN ROLLER

HEIGHT ROLLER

KEEL PANEL

MULTIPLE HI-LOK COLLAR HOLDER

SIDE PANEL FRAME

ATCAS
ROBOTIC FASTENING
EQUIPMENT CLOSE-UP
SK-5

25G-5

SIDE PANEL

SEE SK-7
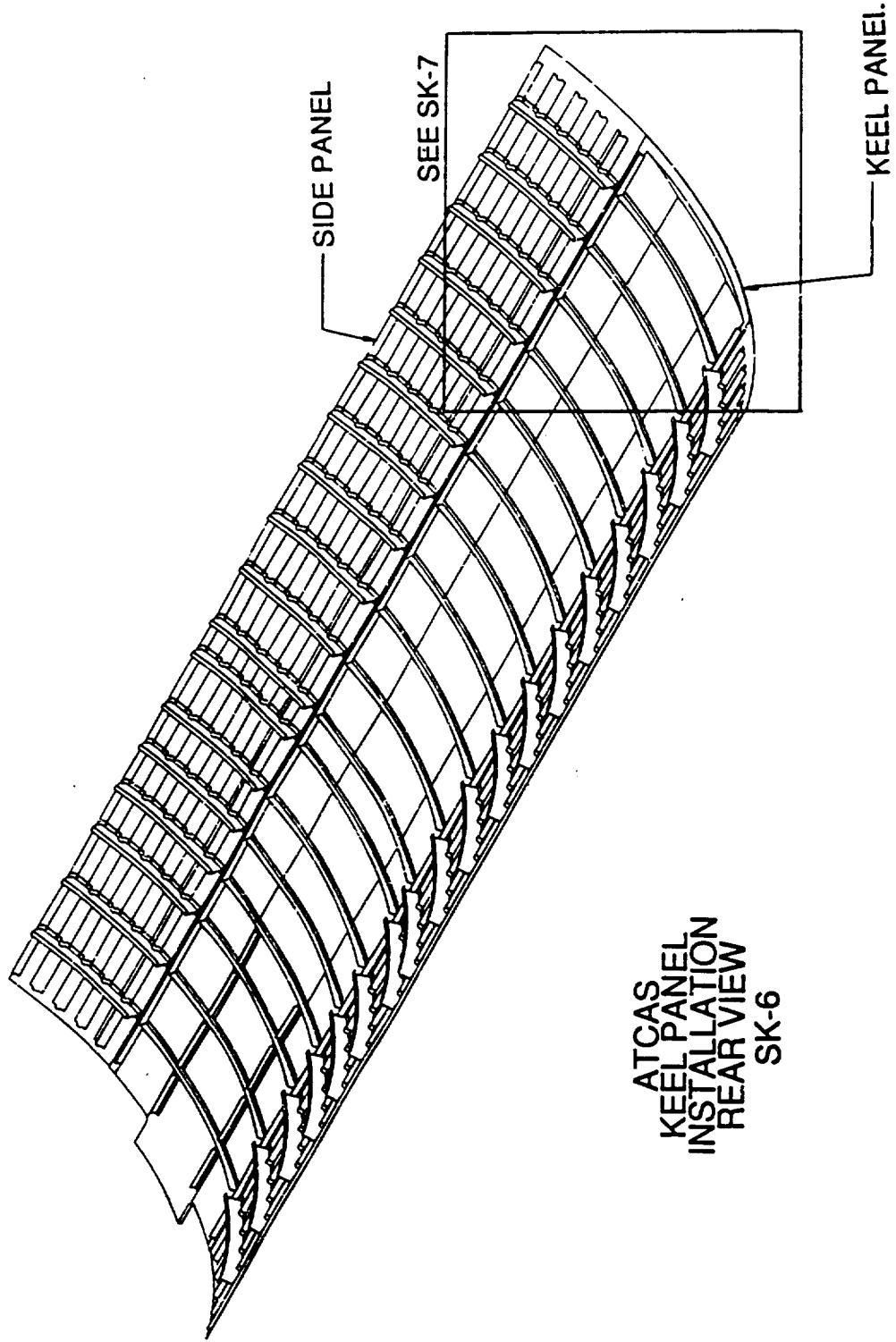
KEEL PANEL.

ATCAS
KEEL PANEL
INSTALLATION
REAR VIEW
SK-6

ATCAS
KEEL PANEL
INSTALLATION
REAR VIEW CLOSE-UP
SK-7

SIDE PANEL

LAP SPLICE

KEEL PANEL

CORE RAMP

25G-7
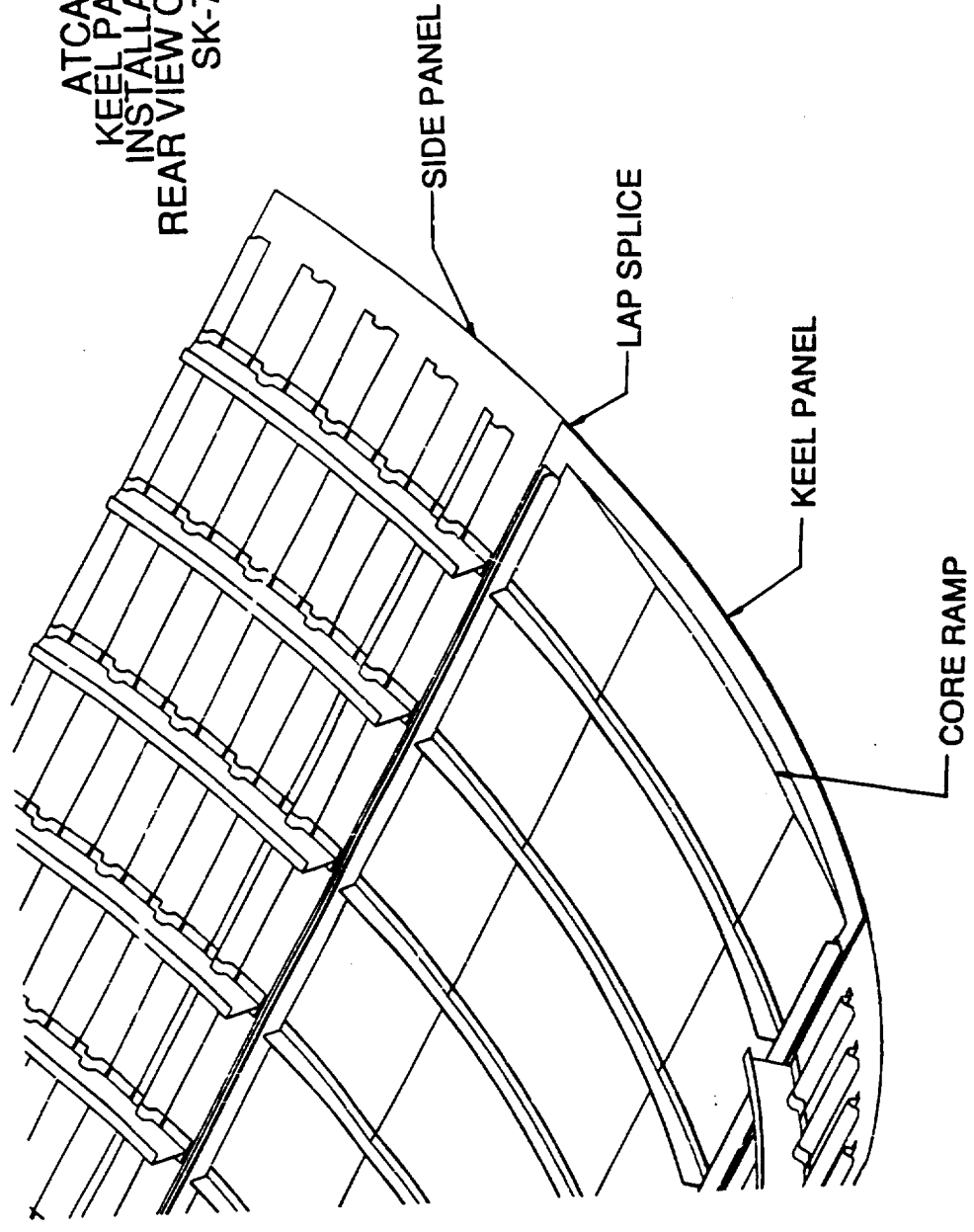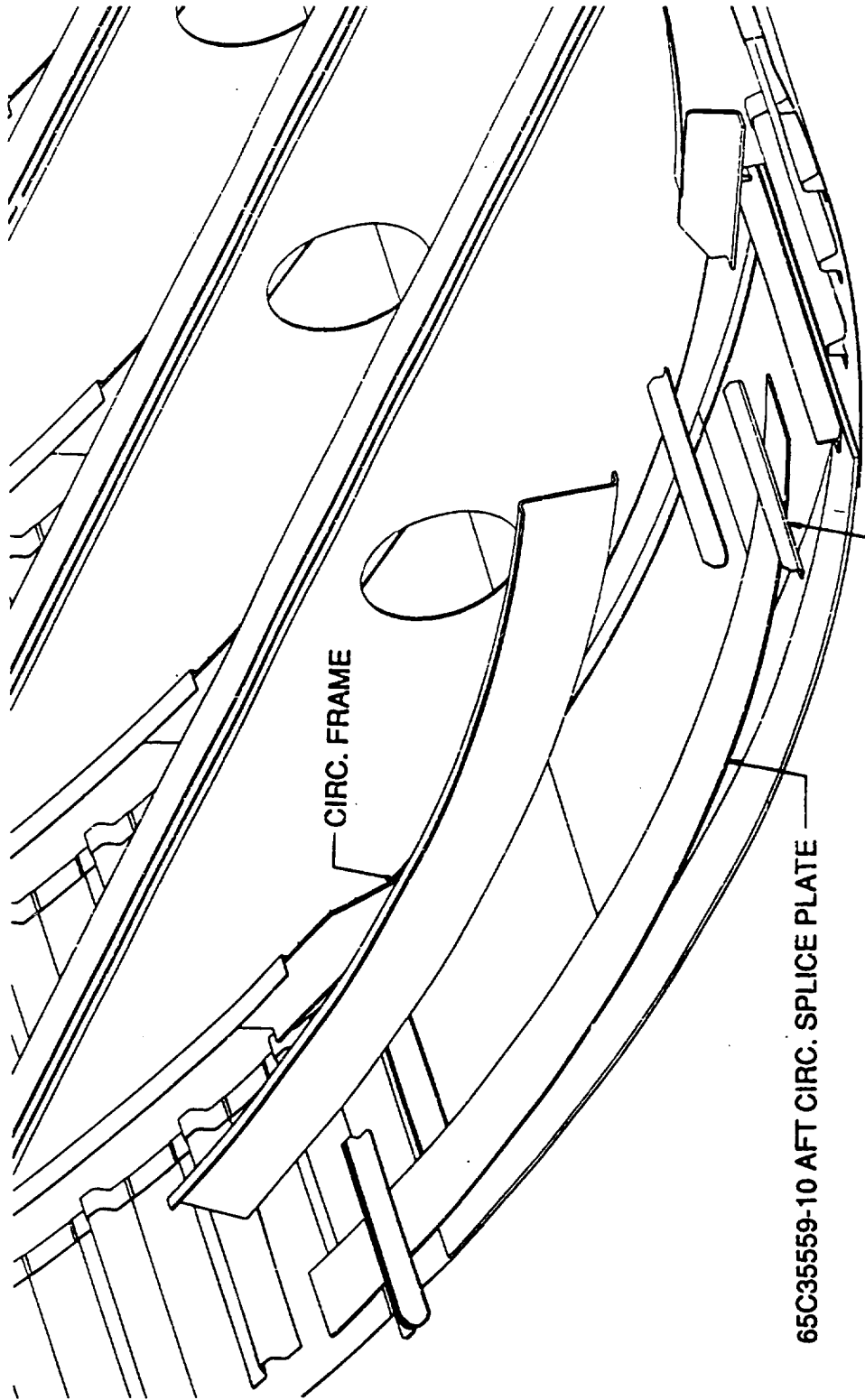
CIRC. FRAME

65C35559-7 AFT STRINGER SPLICE

65C35559-10 AFT CIRC. SPLICE PLATE

ATCAS
EXPLODED VIEW OF
AFT CIRC. SPLICE
DETAILS
SK-8

ATCAS
KEEL PANEL
INSTALLATION
SK-9

SIDE PANEL

ROBOTIC FASTENING SYSTEM
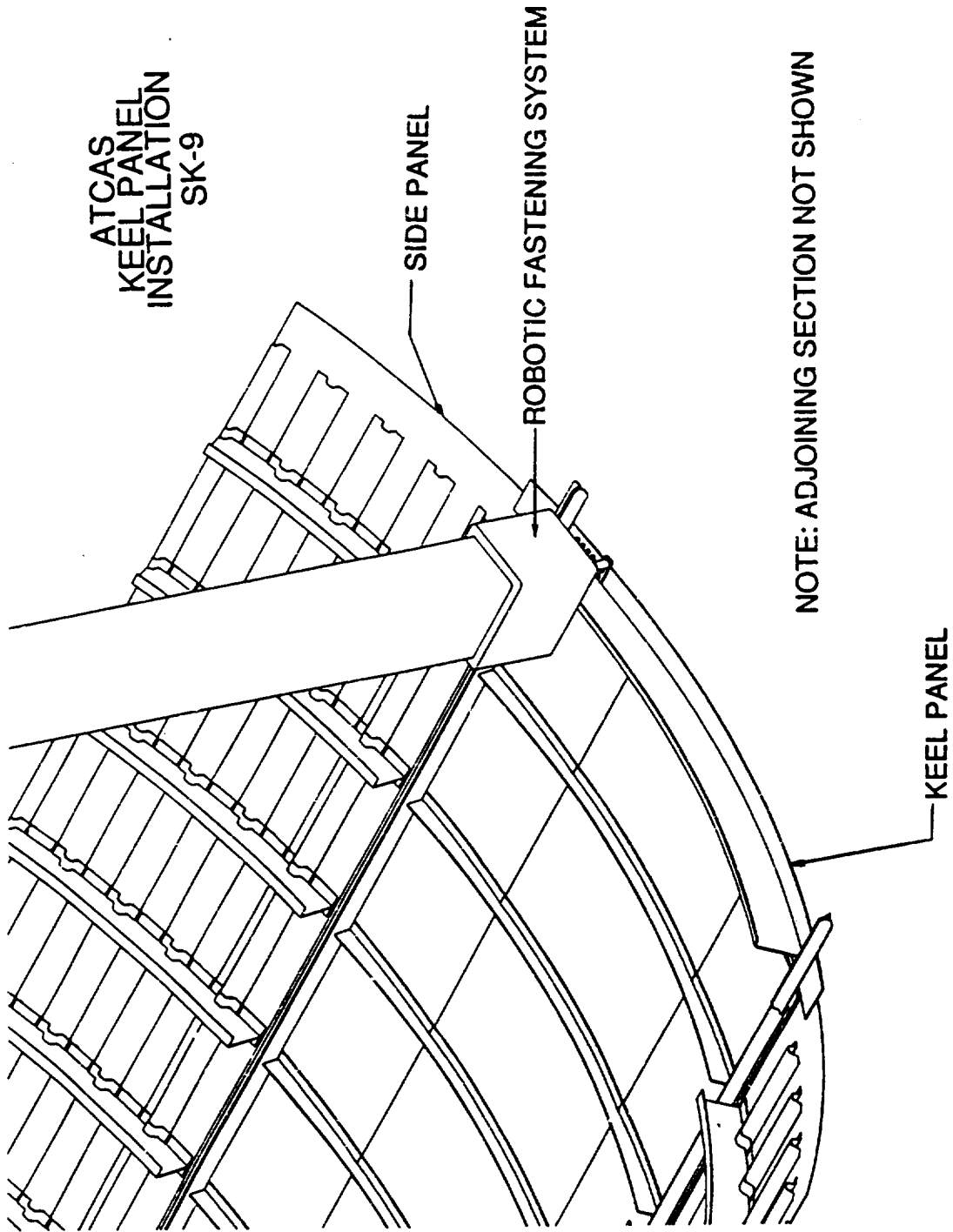
NOTE: ADJOINING SECTION NOT SHOWN

KEEL PANEL

25G-9

ATCAS
AFT CIRC.
INSTALLATION
COMPLETED SK-10

SIDE PANEL

KEEL PANEL
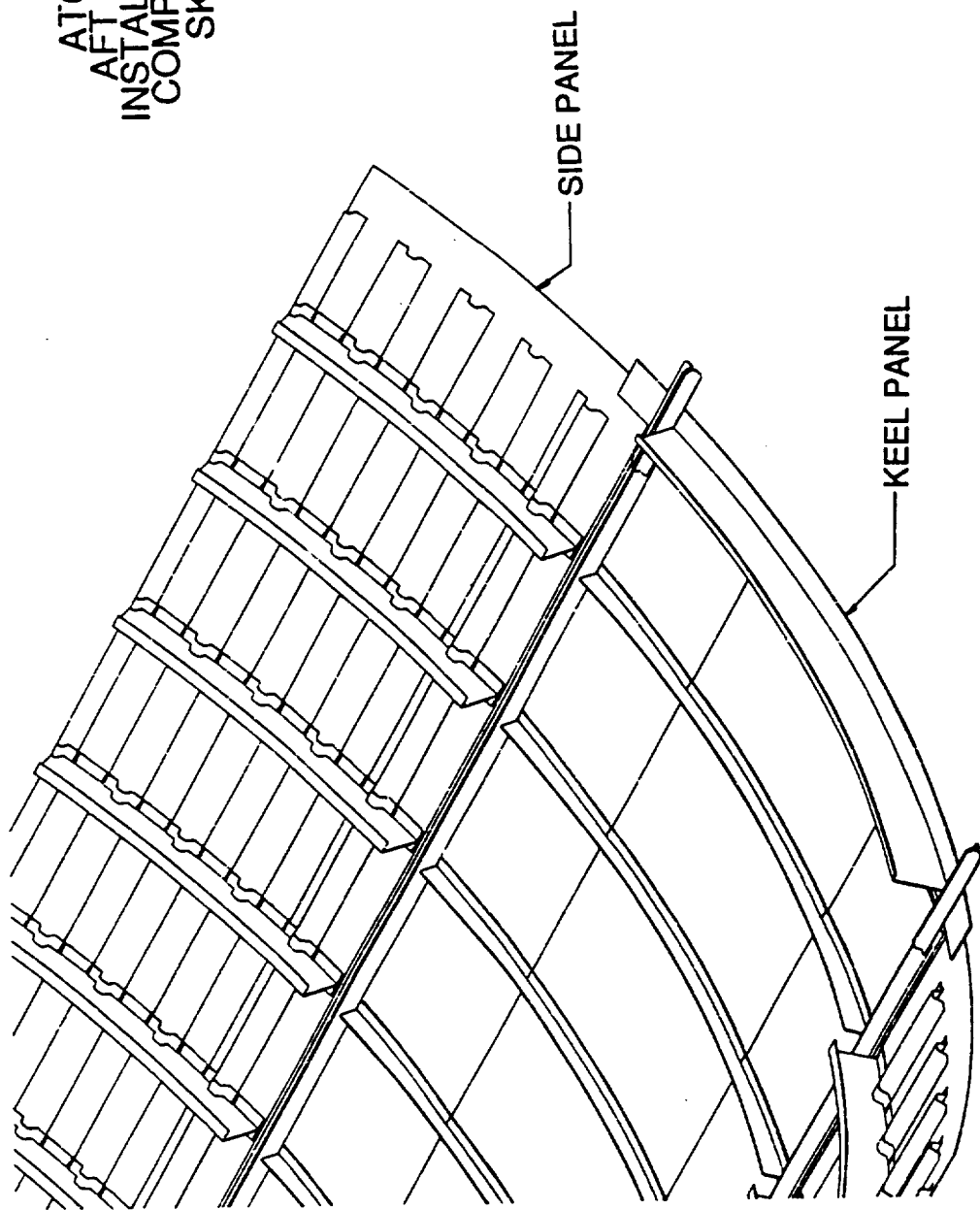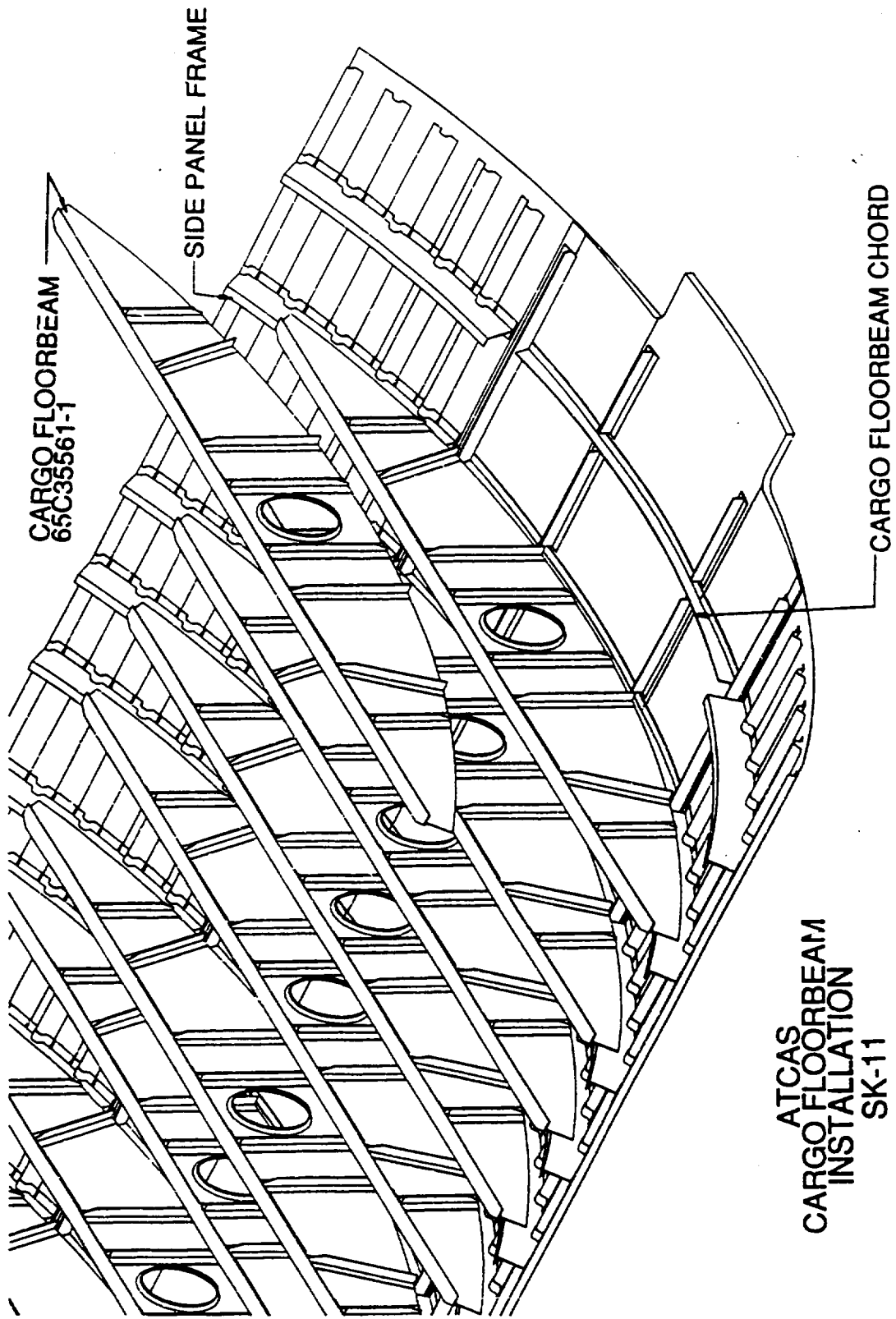
CARGO FLOORBEAM
65C35561-1

SIDE PANEL FRAME

CARGO FLOORBEAM CHORD

ATCAS
CARGO FLOORBEAM
INSTALLATION
SK-11

25G-11

SIDE PANEL

KEEL INTERCOSTAL
65C35562-4,-2,-8 OR -6

INTERCOSTAL CHORD

KEEL PANEL

ATCAS
KEEL INTERCOSTAL
INSTALLATION
SK-12

25G-12
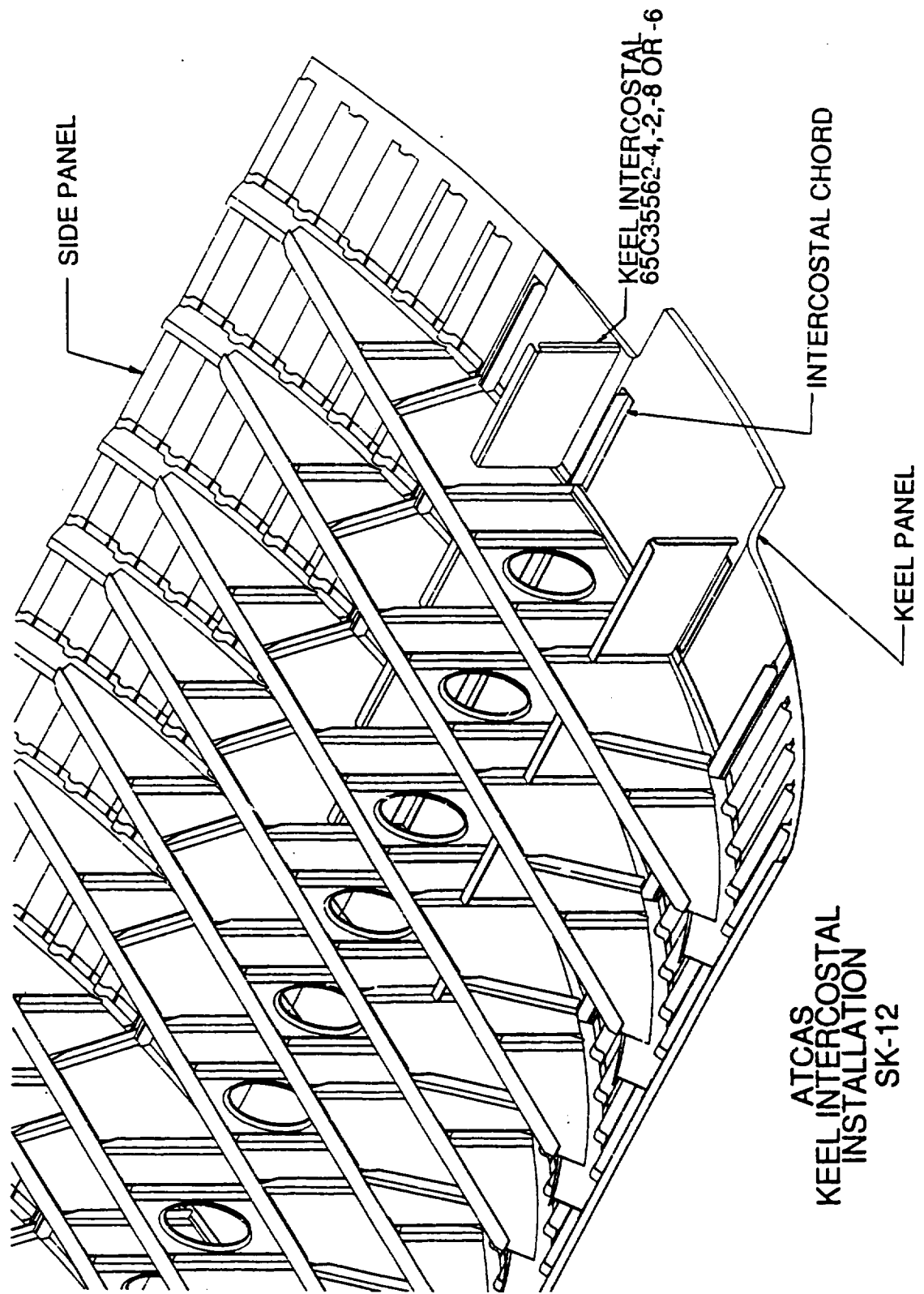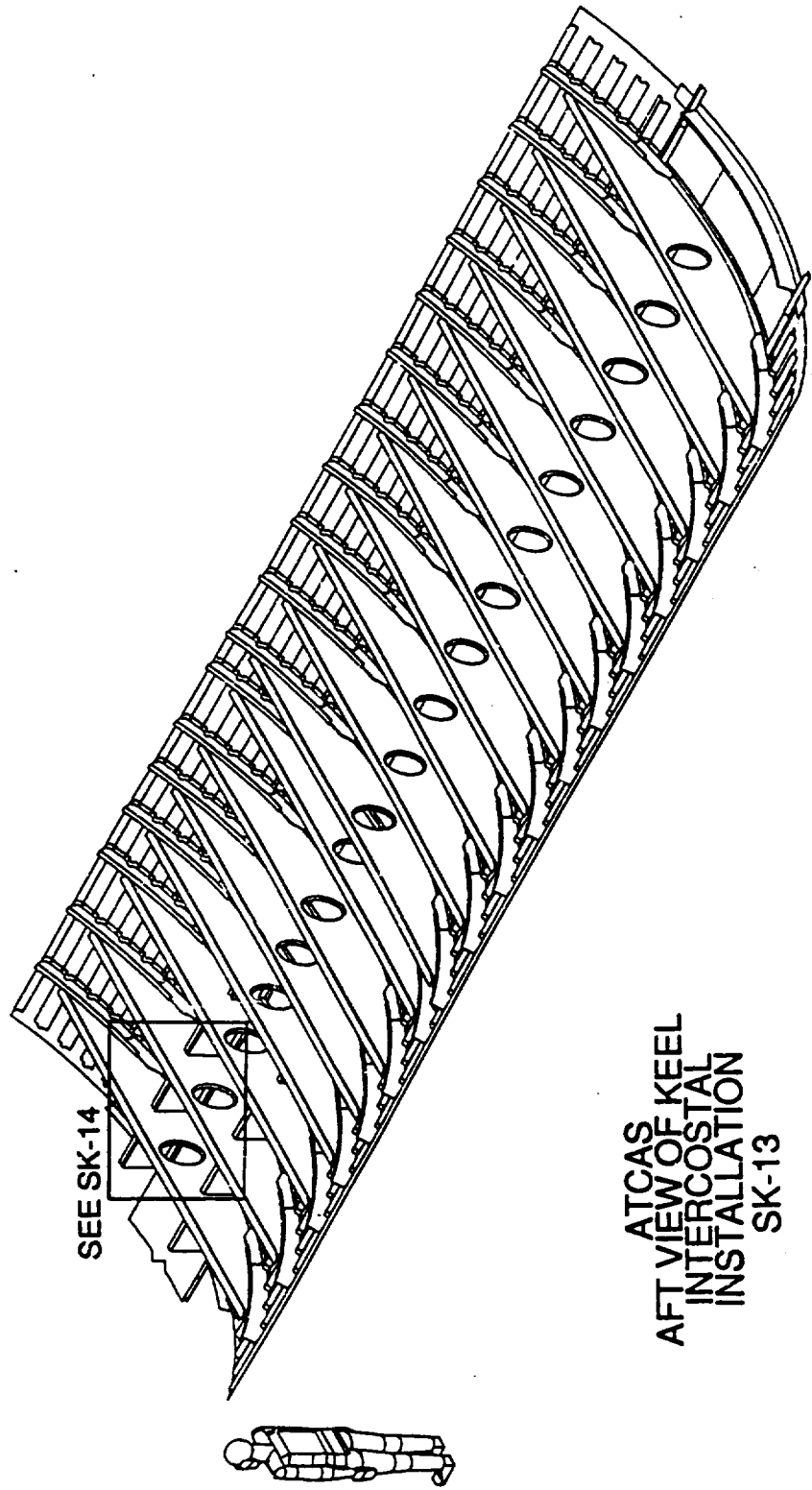
SEE SK-14

ATCAS
AFT VIEW OF KEEL
INTERCOSTAL
INSTALLATION
SK-13

25G-13

SPACER SHIM

KEEL INTERCOSTAL

NOTE: CARGO FLOORBEAM REMOVED
FOR VISUALIZATION
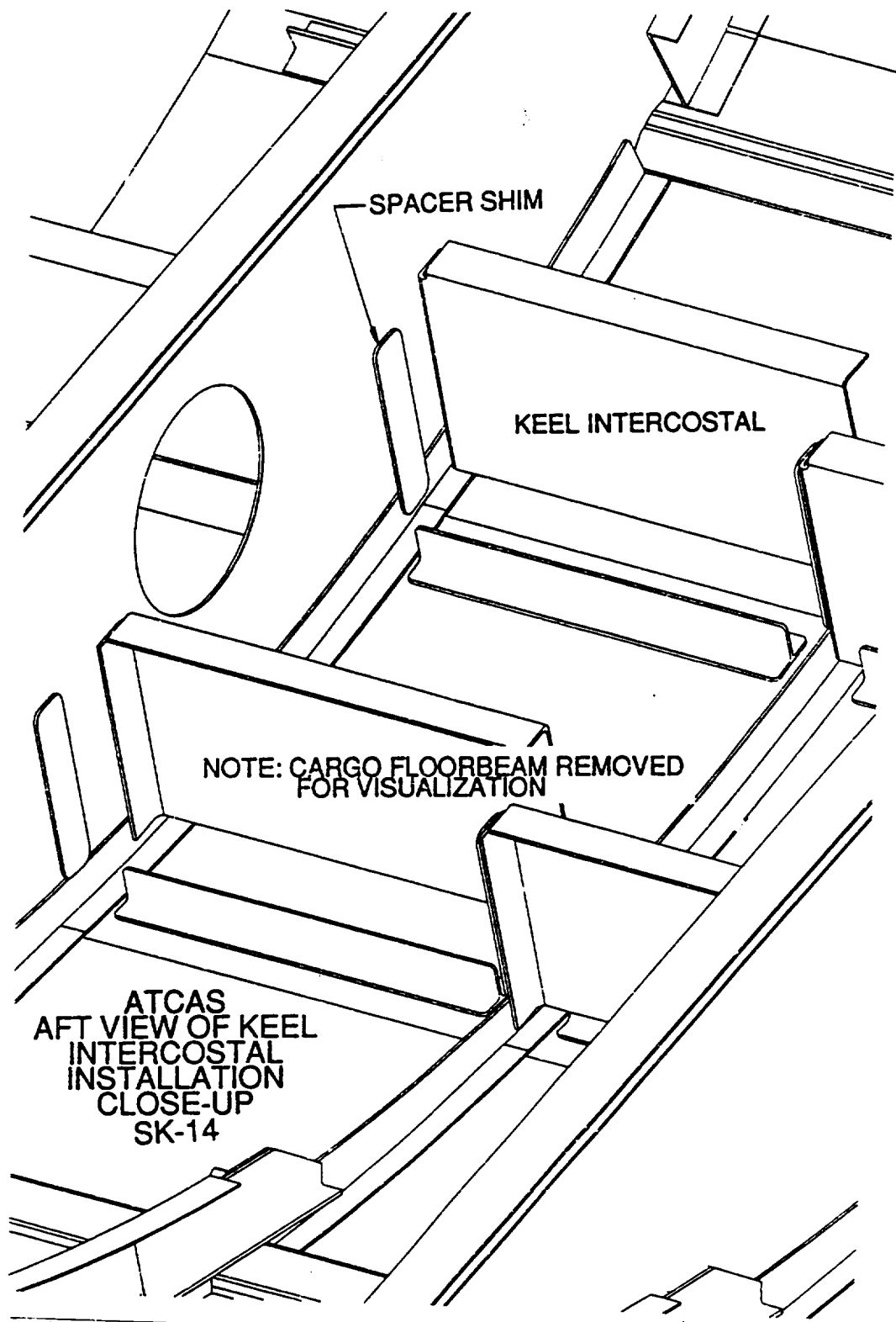
ATCAS
AFT VIEW OF KEEL
INTERCOSTAL
INSTALLATION
CLOSE-UP
SK-14

ATCAS
INSTALLATION OF
LONG. STRINGER
CLIP
SK-15

SEE SK-16

CARGO FLOORBEAM STIFFENER

STRINGER CLIP
65C35559-6 OR -5

ATCAS
INSTALLATION OF
LONG. STRINGER
CLIP CLOSE-UP
SK-16

KEEL PANEL

LONG. BLADE STRINGER

SIDE PANEL
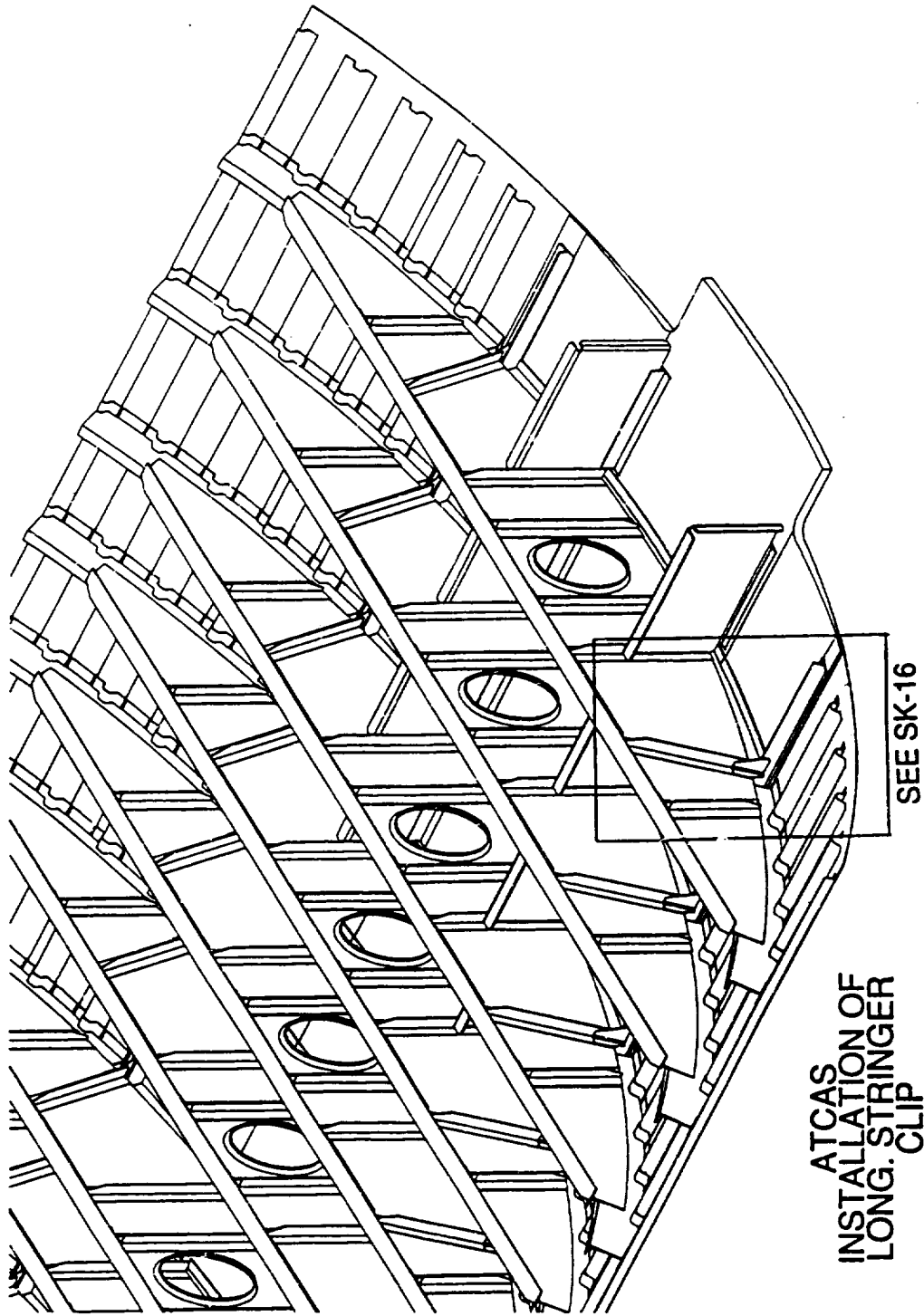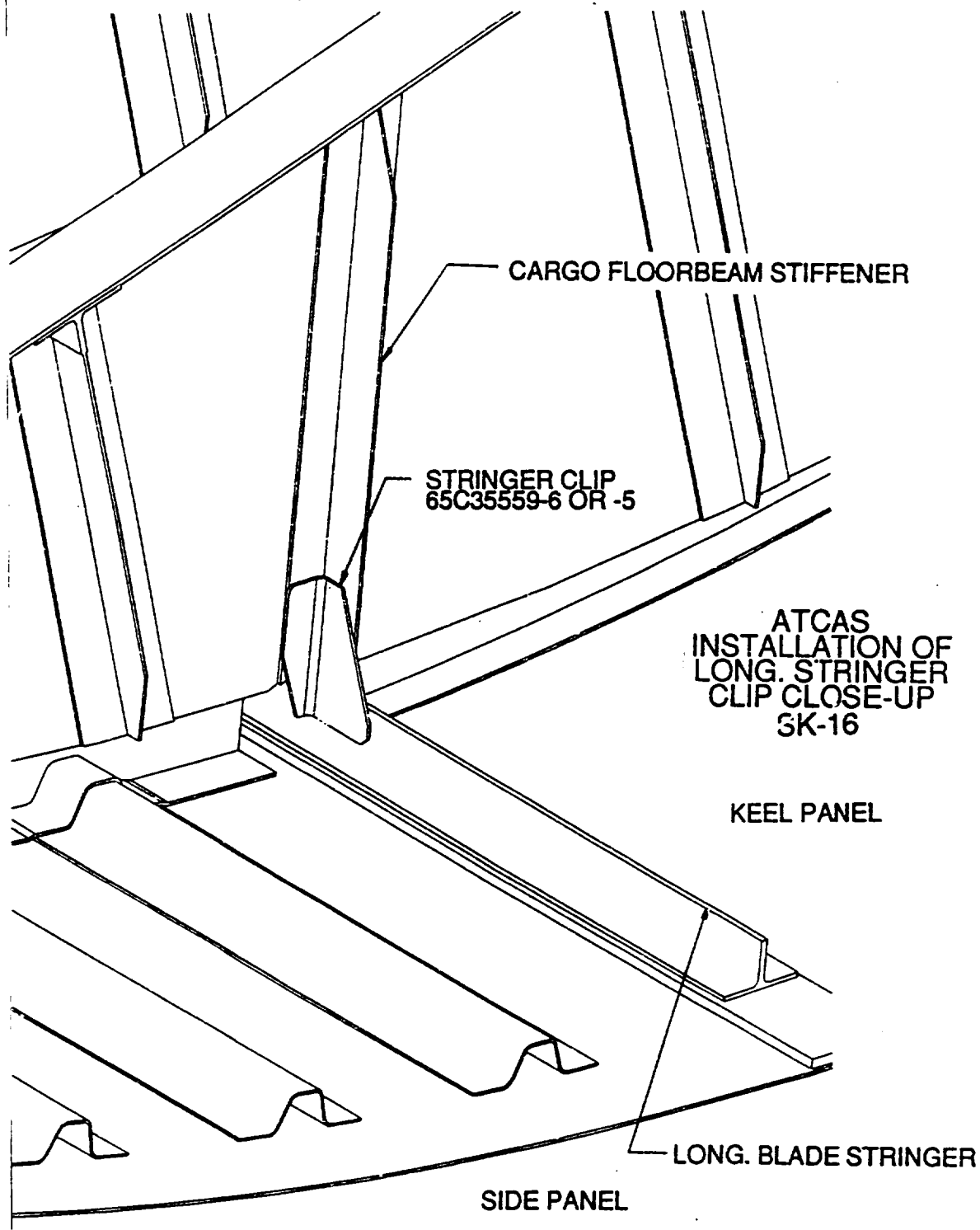
25G-16
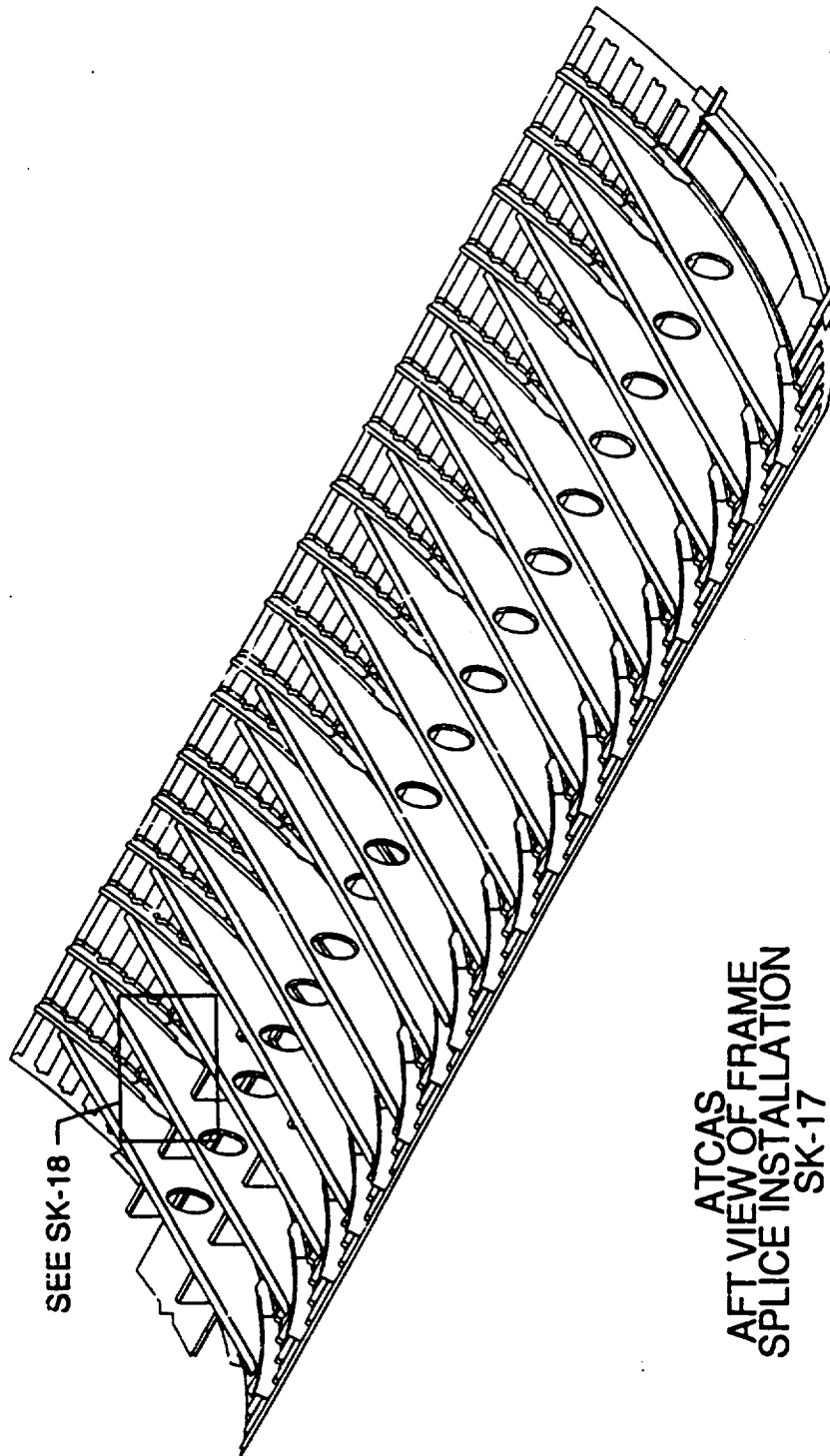
SEE SK-18

ATCAS
AFT VIEW OF FRAME
SPLICE INSTALLATION
SK-17

25G-17

SIDE FRAME

FRAME SPLICE
65C35559-3 OR -4

CARGO FLOORBEAM CHORD

ATCAS
AFT VIEW OF FRAME
SPLICE INSTALLATION
CLOSE-UP
SK-18

FRAME SHIM
65C35559-11

FWD BULKHEAD

TIA SPLICE PLATES
0.3" THICK EACH

1.3 MILLION LBS. OF
AXIAL COMPRESSIVE LOAD

KEEL GRAPHITE TAB
1.3" THICK

3 ROWS OF (33) 0.75"
TIA LOCKBOLTS
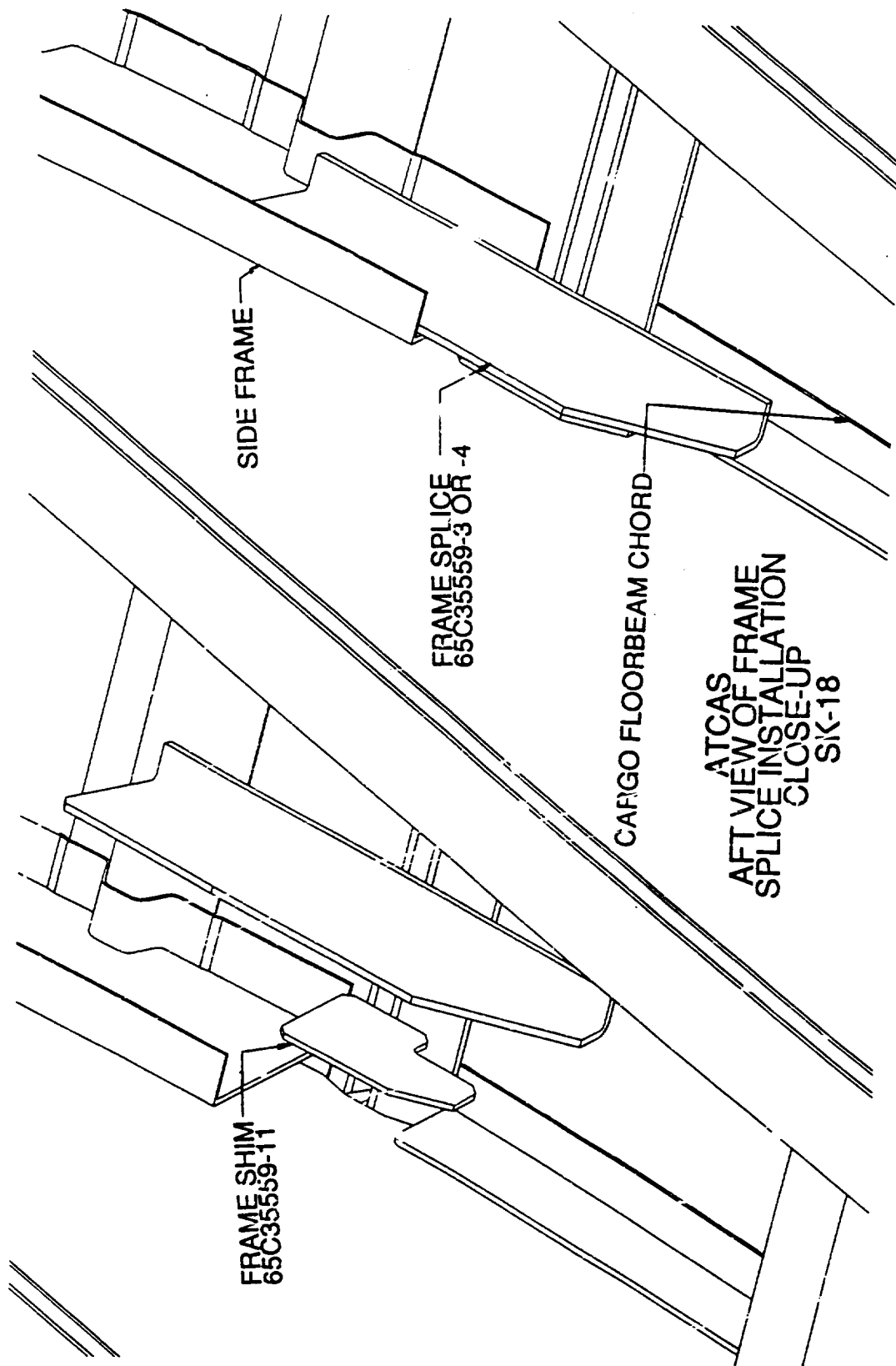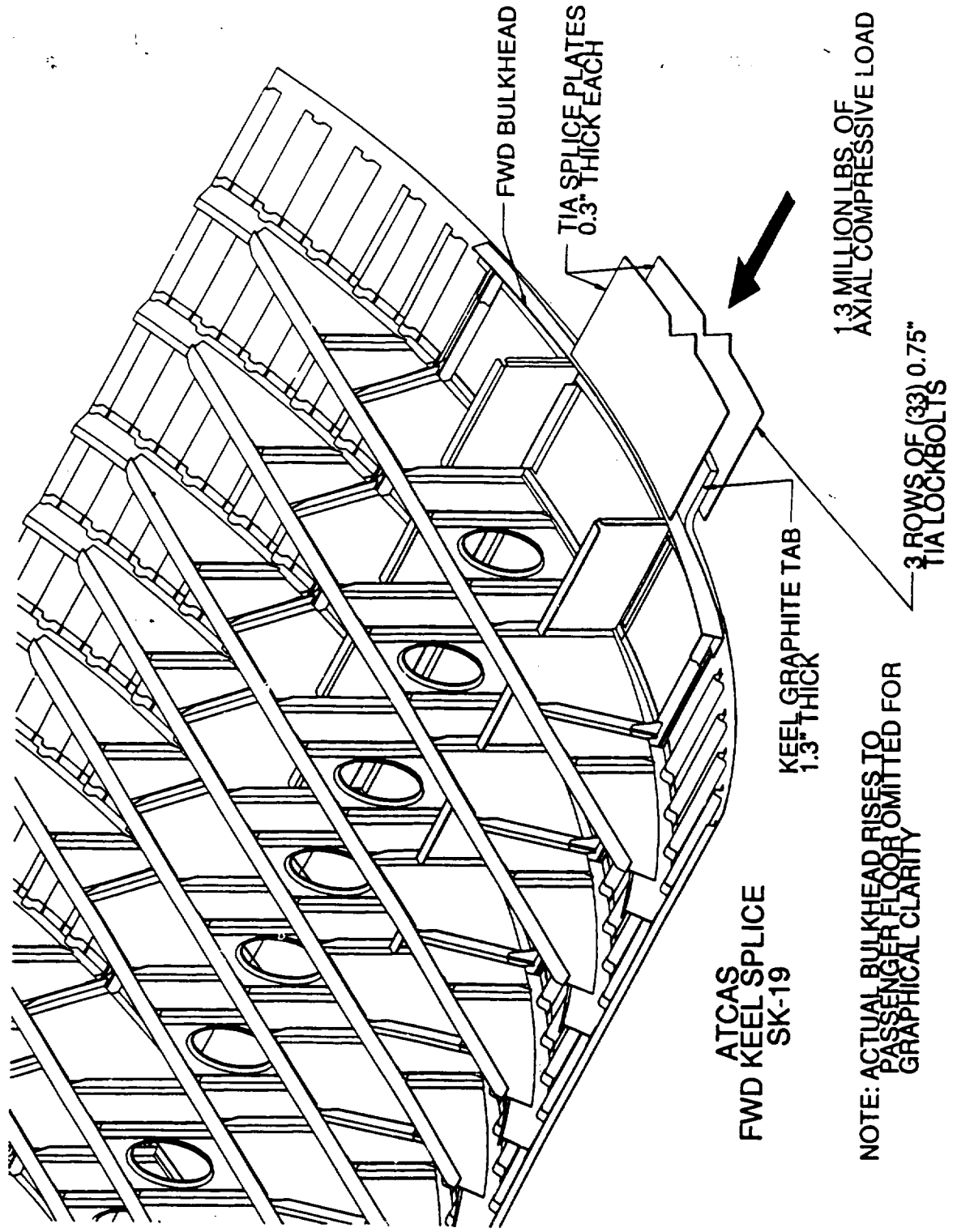
ATCAS
FWD KEEL SPLICE
SK-19

NOTE: ACTUAL BULKHEAD RISES TO
PASSENGER FLOOR OMITTED FOR
GRAPHICAL CLARITY

ATCAS
COMPLETED
INSTALLATION
FORWARD VIEW
SK-20

FWD
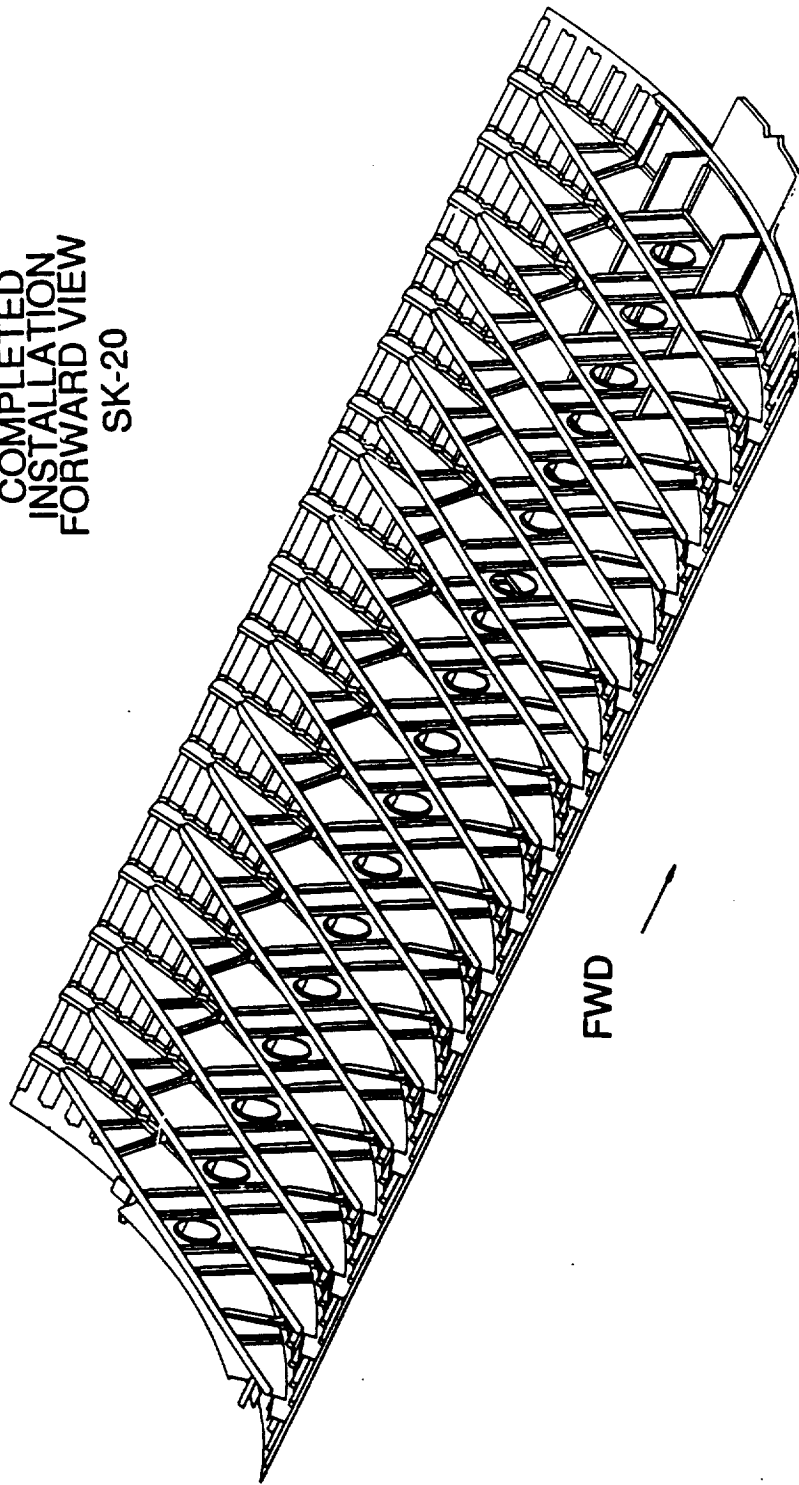
ATCAS
COMPLETED
INSTALLATION
AFT VIEW
SK-21

SEE SK-22

FWD

25G-21
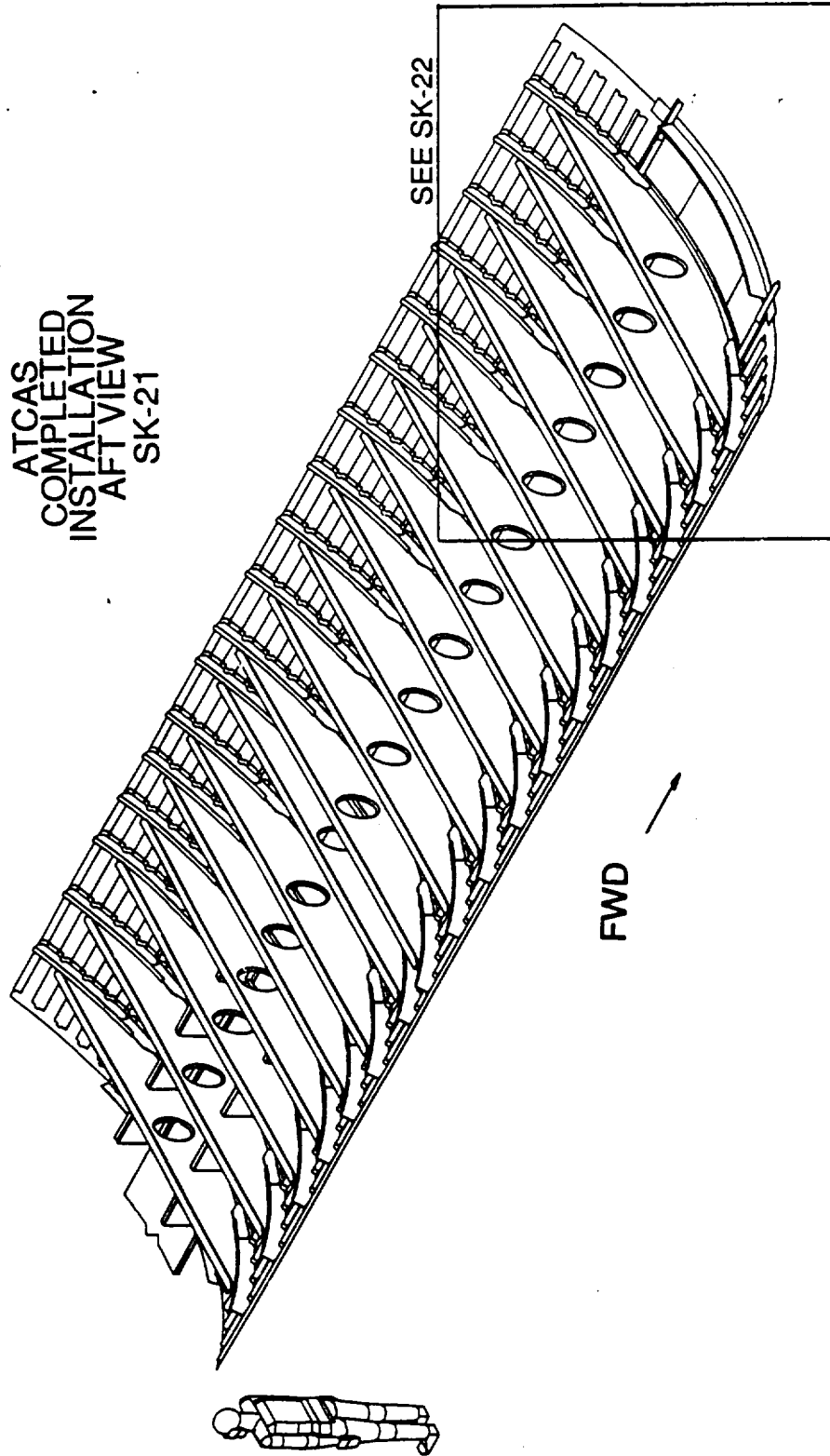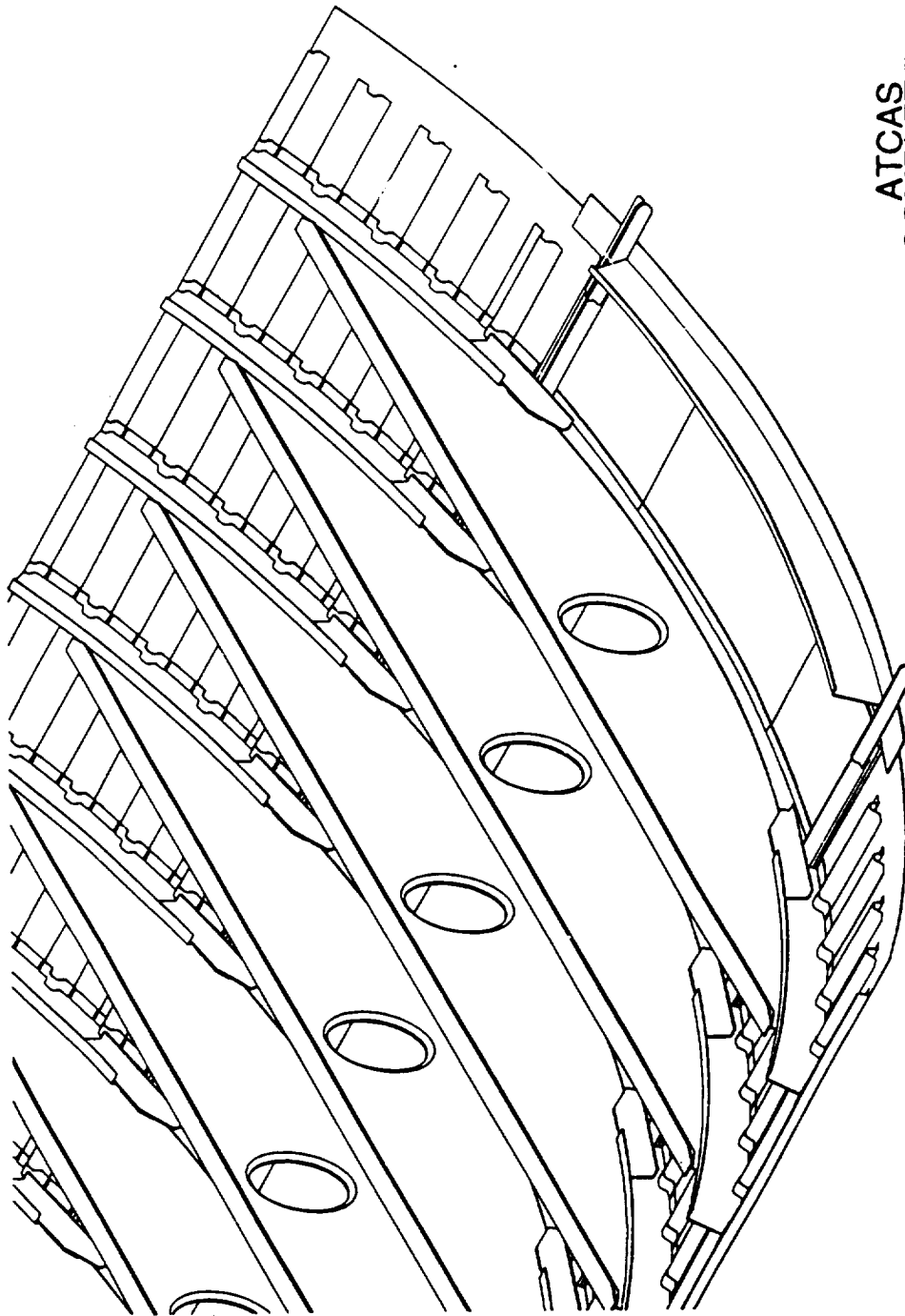
ATCAS
COMPLETED
INSTALLATION
AFT VIEW CLOSE-UP
SK-22

25G-22

C-2

APPENDIX H

REVIEW DRAFT OF:

"NONLINEAR PROPERTIES OF METALLIC CELLULAR MATERIALS WITH A NEGATIVE POISSON'S RATIO"

Nonlinear Properties of Metallic Cellular Materials with a Negative Poisson's Ratio

J.B. Choi*, M.S., Graduate Student

and

R.S. Lakes§, Ph.D., Professor

§Department of Mechanical Engineering
*§Department of Biomedical Engineering
§Center for Laser Science and Engineering
University of Iowa, Iowa City, IA 52242
Department of Biomedical Engineering
University of Iowa
Iowa City, Iowa 52242

May 23,1991

Abstract

Negative Poisson's ratio copper foam was prepared and characterized experimentally. The transformation into re-entrant foam was accomplished by applying sequential permanent compressions above the yield point to achieve a triaxial compression. The Poisson's ratio of the re-entrant foam depended on strain and attained a relative minimum at strains near zero. Poisson's ratio as small as -0.8 was achieved. The strain dependence of properties occurred over a narrower range of strain than in the polymer foams studied earlier. Annealing of the foam resulted in a slightly greater magnitude of negative Poisson's ratio and greater toughness at the expense of a decrease in the Young's modulus.

1. Introduction

Cellular solids are lightweight materials consisting of a network of solid ribs or plates. Man-made cellular solids have been widely utilized in the form of structural honeycombs (two dimensional cellular solids) in aircraft and in the form of foams (three dimensional cellular solids) for packing, cushioning, energy absorption applications, sandwich panel cores, structural purposes and thermal protection systems. Natural materials such as wood, cancellous bone, coral and leaves have a cellular structure. All these 'conventional' cellular materials have a convex cell shape and exhibit a positive Poisson's ratio. Recently, isotropic foam structures with negative Poisson's ratios have been fabricated by one of the authors[1]. The fabrication was achieved through a transformation of the cell structure from a convex polyhedral shape to a concave or "re-entrant" shape. Increase in some material properties such as flexural rigidity and plane strain fracture toughness was reported[1,2,3].

The range of Poisson's ratio for isotropic material is -1 to 0.5, as demonstrated by energy arguments[4]. Negative Poisson's ratios are rare but not unknown. Negative Poisson's ratios have been reported in single crystal pyrites[5] and in some rocks[6]. Synthetic anisotropic microstructures[7] were found to give such an effect. One of the authors[8] suggested that non-affine deformation kinematics are essential for the production of negative Poisson's ratios in isotropic materials. A recent study of polymeric re-entrant foams with negative Poisson's ratio[9] reported other enhanced material properties: an increase in the toughness, in the shear modulus and in the resilience in the sense of a wide range of linear stress-strain behavior. Conventional and re-entrant polymer foams also differ in their stress strain behavior and deformation

mechanism maps [9]. In copper foam an increase in the indentation resistance was demonstrated experimentally [10], which is consistent with theory[11].

Mechanical properties of a conventional foam material depend on the physical properties of the solid material making up the cell ribs, relative density (the ratio of the bulk density of the foam material to the density of the solid from which it is made), cell shape, cell size and loading conditions. The simplest and most comprehensive treatment of conventional foam properties is that of Gibson and Ashby [12], which includes extensive comparisons between analytical results and experiment. In re-entrant foam, relative density is increased and the cell size is reduced slightly by the transformation process; the cell *shape* is dramatically altered. Mechanical behavior of a re-entrant foam material differs from that of a conventional foam in ways not addressed by existing theoretical treatments; most of the difference is attributed to the change in cell shape.

In this study, the mechanical properties of both conventional and re-entrant copper foam materials are examined at small strain by optical methods and at larger strains by servohydraulic (MTS) machine tests.

2. Experimental procedures

2.1. Specimen preparation: optical study

A large block of copper foam (Astromet Corporation) with relative density between 0.08 and 0.1 was cut into smaller 18 x 18 x 36 mm blocks; another large block with relative density 0.04 was cut into 25 x 25 x 50 mm blocks. Bar shaped specimens were cut from these blocks using the procedure described below. The blocks were not perfectly uniform: specimens of relative density of 0.04, 0.08, 0.09, 0.1 had deviations of 12%, 6%, 5.5%, 5%, respectively in relative density.

Block specimens were cut with a high speed saw to minimize surface plastic deformation. The foam was then transformed into a re-entrant structure by applying small sequential increments (less than 2% strain) of plastic deformation in three orthogonal directions using a vise fitted with PMMA (Plexiglas®) end pieces to provide an even surface. The compressed foams were cut again into slender bars (approx. 7 by 7 by 30 mm) following the above cutting method. The lengths of the cell ribs were measured with a microscope in order to compare the cell size for each specimen.

The re-entrant foam specimens have irregular surfaces which were polished with graded abrasives (silicon carbide grits 120, 320, 600 and 1000), under water irrigation, in order to obtain a smooth surface for optical tests. The water irrigation served to minimize temperature increases due to friction and improved the surface finish. High grinding speed and low pressure were used to avoid plastic deformation of the surface. The finest polishing medium grains of 1000 mesh had a size of about 18 μm[13]. This provided sufficient smoothness to the surface so that the shadow moiré method could be applied to measure deformation.

2.2. Specimen preparation - MTS machine test

Rectangular specimens from a large block of initial relative density 0.08 ± 5% , were made with volumetric compression ratio of 1, 2.0, 2.5, 3.0, according to the ASTM standard for subsize specimens[14] for both tension and compression tests. The dimensions of the specimens were 6.4x6.4x25.4(mm) for tension, 19x19x9.5(mm) for compression; the compression specimens were made shorter to prevent buckling. These specimens were polished as described above.

Specimen ends were cast in dental grade polymethyl methacrylate(PMMA) which is much more rigid (E=3GPa) than the copper foam (E=200MPa). This procedure

avoided the machine grips crushing the ends. The mold for casting was threaded and was made of Teflon® and was sprayed with Teflon® lubricant to prevent adhesion of the polymerizing PMMA. The viscosity of the polymerizing PMMA was adjusted to minimize leakage from the mold and to be sufficiently low to mold adequate threads. The curing temperature of PMMA was about $80^{\circ}C$, too low to affect the material properties of the copper foam.

2.3 Annealing

The re-entrant copper foam has some cold work due to the tri-axial compressions, so an annealing process was used to evaluate the effects of cold work. The polished specimen was dried for two days in room conditions and heated under nitrogen purge at a temperature of $500^{\circ}C$ for 1hr[15] and cooled slowly under nitrogen to minimize oxidation.

2.4. Optical test - Shadow moiré

The moiré methods are based on fringe patterns arising from overlap between gratings consisting of straight parallel opaque bars. In the shadow moiré method, a Ronchi ruling is placed close to the specimen surface and is illuminated with collimated light. Overlap occurs between the ruling and its reflected (shadow) image, generating fringes which represent a contour map of the deformed surface. The displacement δ of the surface perpendicular to itself is given by [16].

$$\delta = Np/(\tan\alpha + \tan\beta)$$

(1)

where N is the fringe order, p is the pitch of the grating, α is angle of the incident light and β is the viewing angle with respect to the normal to the grating.

Specimens of initial relative densities of 0.08, 0.09 and 0.1 were used, however conventional foam of initial relative density of 0.04 is was not used in the optical test because of the poor fringe pattern due to the large cell size.

Bending experiments were performed by applying known weights to an aluminum arm cemented to the top end of a vertically oriented copper foam specimen; the lower end was clamped. The aluminum arm was sufficiently long that specimen strain due to bending substantially exceeded compressional strain, approximating 'pure' bending. The Young's modulus E and Poisson's ratio ν were extracted from the displacement field by first using simple beam theory to obtain an approximate value for E from the end deflection δ:

$$\delta = ML^2/2EI \qquad\qquad (2)$$

where M is the bending moment, L is length, and I is the area moment of inertia. Then the three dimensional solution was used to infer ν and obtain a corrected value for E:

$$\delta = ML^2 (z^2 + vx^2 - vy^2)/2EI \qquad\qquad (3)$$

in which z is a longitudinal coordinate along the length of the bar, x is a lateral coordinate, and y is a transverse coordinate. The correction to E was small in all cases. Positive Poisson's ratios give rise to hyperbolic fringe contours, and negative Poisson's ratios give rise to elliptic contours. In either case the Poisson's ratio was found from the observed shape of the contours.

In this experiment, the grating was located a small distance, within a millimeter, away from the specimen, parallel to the surface and oriented so that no fringe pattern occurred. Light from a mercury vapor lamp was collimated by a lens and directed upon the grating at an angle 48° from the normal to the grating plane; the viewing angle was

19°. A 300 line/inch (11.8 line/mm) grating was used for determining the elastic modulus and a 1000 line/inch (39.4 line/mm) grating for obtaining the Poisson's ratio, since the latter was too sensitive for ready determination of fringe order at the specimen end. For Poisson's ratio determination, the grating was tilted so that the center of the fringe pattern appeared near the center of the bar. Measurements were performed at a specimen surface strain of 0.05% to 0.1%. Theoretical contour lines based on equation (3) were prepared for a variety of Poisson's ratio were drawn with an Apollo computer using 'Promatlab' graphics software to facilitate the analysis of the observed fringe patterns appearing on the specimen surface.

2.5. MTS machine test

A servohydraulic testing machine (MTS corp) with a 2.5 kN load cell was used to apply loads for the characterization of nonlinear properties of the foams. All the experiments were performed at equal strain rates of 0.006 sec^{-1}. To determine lateral deformation for the purpose of determining Poisson's ratio, dial gages (No. 25-109, Starrett company, resolution 1.2 μm, range 0.38 mm)were applied to each lateral surface near the center portion of the specimen. A flat tip was used in contact with the specimen in the case of lateral bulging, while a round one was used to evaluate lateral contraction. A universal joint was used in the tension test and a small ball socket joint was used in the compression test to assure alignment. In compression tests, Teflon tape was used between the specimen and the loading surface to minimize the friction force on the contact surfaces.

3. Results and Discussion

In the conventional copper foam, the moiré fringe patterns were observed to bə hyperbolas corresponding to a positive Poisson's ratio. Accuracy in the Poisson's ratio determination was limited to ±0.1 by uncertainty (about ±5%) in measuring the slope of the asymptote. For homogeneous materials, accuracy could be improved by increasing the strain hence the fringe density; however in these materials the fringes became blurred beyond a certain strain[17]. In the re-entrant copper foams, the moiré fringes had elliptical contours corresponding to a negative Poisson's ratio. It was possible to achieve better accuracy in this case as a result of the different fringe shape and the greater compliance of the transformed material.

Fig. 1 and 2 show optically determined Poisson's ratio at small strain as it depends on the initial and final relative densities. The Poisson's ratio of conventional foam with initial relative density of 0.09 is 0.2 ±0.1. In the re-entrant foam, the smallest Poisson's ratio observed was -0.8 ±0.05 at a strain of 0.1%; the permanent volumetric compression ratio was 2.13 and the initial relative density was 0.1.

The negative Poisson's ratio of re-entrant foam attains a minimum for an optimal value of permanent volumetric compression ratio; the optimal compression is smaller for higher values of initial relative density, as shown in Fig. 1. For copper foam with initial relative density of 0.04 the optimal compression ratio, 3.6, is comparable to that of the polymer foams, 3.3 to 3.7, which have a similar relative density of 0.03. This correspondence between two different materials suggests a geometrical cause associated with the cell structure. For example, the optimum volumetric compression ratio arises in part from the fact that too much compression causes the ribs to come in contact, which hinders the unfolding which gives rise to the negative Poisson's ratio. In such a simple view, one would expect the optimum to occur for a particular final relative

density (determined as the product of the initial relative density and the volumetric compression ratio). Fig. 2, however, shows the optimum to depend on both the initial and final relative densities, so the above interpretation is incomplete.

The elastic modulus decreases monotonically with permanent volumetric compression as shown in Fig. 3, so that re-entrant copper foam is less stiff than the conventional foam from which it was derived. Polymer foams behaved similarly, except that for sufficiently large permanent volumetric compression, the stiffness began to increase again.

The effect of annealing on the stress-strain relationships for foams with volumetric compression ratios of 1, 2.0, 2.5, 3.0 is shown in Fig. 4. In tension, most of the specimens failed near the cast polymer end piece due to stress concentration; the end points on the tensile side of the graphs represent this fracture. In compression, the tests were terminated at the beginning of unstable compression due to buckling. The conventional foam has some strain-hardening tendency, but the re-entrant foam does not exhibit this effect, thus, the latter can be modeled as a elastic-perfectly plastic material. In both tension and compression, the conventional and re-entrant foams exhibit a rather long plateau above the proportional limit. This behavior is attributed to the plastic hinge formation of cell ribs which occurs when the moment exerted on the cell ribs exceed the fully plastic moment. By contrast, the fracture behavior of both conventional and re-entrant copper foam in tension was brittle-like: failure occurred abruptly without necking or drawing. The foams were brittle even though the solid copper from which the foam was made is ductile; such behavior has been observed in other foams and has been analyzed in view of the alignment of cell ribs which occurs under tension [12].

As for the compressive properties, errors can arise due to the effect of friction with the loading surface combined with the Poisson effect. An apparent yield stress $\sigma_{y,app}$ can be expressed [18] in terms of the true yield stress for a specimen with a ratio of 2:1 in width to height as $\sigma_{y,app} = \sigma_{y,true}(1+m)$, where m is the friction coefficient. Since m is less than 0.1 for copper and Teflon, the maximum experimental deviation through the whole load history due to the friction force is within 10%.

For the conventional copper foams the properties in tension and compression are similar, as seen in Fig. 4. Young's modulus and the ultimate strength are lower by about 33% and 25%, respectively, for annealed material. The inset graph shows that the foams are nonlinear even for strains below 1%; by contrast to the polymer foams studied earlier. The difference arises from the yield of the ribs in copper foam at small strain. The re-entrant specimens as shown in Fig. 4 show very dissimilar properties in tension and compression. Increase in the permanent volumetric compression ratio results in reduced tensile stiffness and increased compressive stiffness, as seen in Fig. 5 which shows the effective Young's modulus at 0.5% strain as it depends upon permanent volumetric compression ratio. As for ultimate strength, it is reduced by about 15% in both tension and compression by the annealing process.

The experiments disclosed that the toughness, defined as the energy per unit volume to fracture, of the re-entrant foam compared to that of conventional foam, increased by factors of 1.4, 1.5, 1.7 with increases of volumetric compression ratio of 2.0, 2.5, 3.0, respectively. Annealing effects can further increase the toughness. This effect was most evident at a volumetric compression ratio of 2.0, as shown in Fig. 6. However, the annealed re-entrant foams at a volumetric compression ratio of 2.5 did not show as much increase, and the toughness actually decreased in the foam at a volumetric compression ratio of 3.0. In case of an elastomeric foam such as polyurethane foam, the

experimental results showed increases by factors of 1.7, 2.1, 2.3, 2.6, 3.2 in the toughness of the re-entrant foam compared to that of the conventional foam, at volumetric compression ratios of 2.0, 2.6, 3.2, 3.7, 4.2, respectively[9]. Elastomeric foam (which can be deformed at large strain)exhibited a somewhat greater toughness increase with re-entrant transformation in comparison to copper foam (which is elasto-plastic).

The Poisson's ratio of the conventional foam shows highly nonlinear dependence upon the strain, as shown in Fig. 7. The Poisson's ratios of the conventional copper foam are near 0.35 for small strain and approach 0.5 in tension and 0 in compression; similar behavior was observed in conventional polymer foam [9]. This approach of Poisson's ratio to zero at large strain in compression also agrees with other results: Poisson's ratio for the plastic compression of foam material was typically 0.03-0.05[19,20] and Poisson's ratio beyond the yield point was 0.04 [21] in compression.

As for small-strain behavior of conventional foam, a strong dependence of Poisson's ratio on the bulk density at a strain of not more than 0.5% was suggested [22]. Other authors showed a constant Poisson's ratio of 0.33 [12,23,24] or 0.23 [25] independent of relative density. Even though the cell morphology changes with the relative density [25] any effect may be difficult to extract from the considerable scatter in experimental values for Poisson's ratio [12]. The density changes in the re-entrant foam are accompanied by cell shape changes, so the above considerations are not applicable.

Annealed specimens gave a slightly better negative effect in the Poisson's ratio (Fig. 7,8,9) at the expense of a decrease in the Young's modulus for each volumetric compression ratio. The lowest Poisson's ratio obtained in this mechanical testing (MTS) experiment was -0.49 at a strain of 0.2% as indicated in Fig. 8. In comparison, a

Poisson's ratio of -0.6±0.05 was determined optically at a strain of 0.1% for specimens having the same initial relative density of 0.08 and the same volumetric compression ratio of 2.5. A minimum Poisson's ratio of -0.8±0.05 was determined optically at a strain of 0.1% for a different specimen as described above. Friis et. al. [3] obtained a minimum Poisson's ratio of -0.39 at a compressive strain of 0.013 in mechanical tests on copper foam with a permanent volumetric compression ratio of 2.0 and a relative density of 0.053. The difference may be attributed to the highly nonlinear behavior of the metal foam as indicated by the cusp in Poisson's ratio vs strain. This contrasts with the polymeric foam which exhibited a smoother dependence of Poisson's ratio upon strain and which exhibited a broader minimum in Poisson's ratio vs strain, in comparison with the metal foams. The difference in behavior between the metal and polymer foams is attributed to the fact that the ribs of the copper foam can yield and form plastic hinges at relatively small strain, in contrast to the polymer which is an elastomer. The nonlinearities in compression are attributed in part to regions of contact between cell ribs in the re-entrant foam; no such contacts occur in the conventional foam (Fig. 10).

4. Conclusions

1.   The Poisson's ratio of both conventional and re-entrant foam depends on strain. Poisson's ratio of re-entrant foam attains a relative minimum as small as -0.8 for zero strain.

2.   Optimum permanent compression to achieve the best negative Poisson's ratio depends on the initial foam relative density: higher density foam requires less compression for transformation. This optimum appears to have a purely geometrical origin, since the same value was observed for metal and polymer foam of the same relative density.

3.   The re-entrant copper foam in compression does not exhibit strain hardening.

4.   The toughness of the re-entrant foam increases with volumetric compression ratio and annealing effects further increase the toughness.

Acknowledgment

5. References

1. R. S. Lakes, Science, 235 (1987) 1038

2. R. S. Lakes, Science, 238 (1987) 551

3. E. A. Friis, R. S. Lakes and J. B. Park, J. Mat. Sci., 23 (1988) 4406

4. Y. C. Fung, "Foundation of Solid Mechanics" (Prentice-Hall Englewood, NJ, (1968) p.353

5. A. E. H. Love, in "A Treatise on the Mathematical Theory of Elasticity" (Dover Pub., NY, 1944) p.163

6. O. G. Ingles, I. K. Lee, R. C. Neil, Rock Mechanics, 5 (1973) 203

7. K. E. Evans, B. Caddock, J. Phys. D: Appl. Phys., 22 (1989) 1883

8. R. S. Lakes, J. Mat. Sci.,26 (1991) 2287

9. J. B. Choi, R. S. Lakes, J. Mat. Sci., submitted

10. K. Elms and R. S. Lakes, in preparation

11. S. P. Timoshenko and J. N. Goodier, "Theory of Elasticity" (McGraw-Hill, NY, 1969)

12. L. J. Gibson, M. F. Ashby, "Cellular Solids" (Pergamon Press, 1988)

13. L. E. Samuels, in "Metallographic Polishing by Mechanical Methods" (American Society for Metals,1982) p 80-81

14. "Annual Book of ASTM Standards" (Designation:E8-85b,1986)

15. "Metal Handbook, Heat treating,cleaning & Finishing" (American Society for Metals) p 285

16. A. S. Kobayashi, in "Manual of Engineering Stress Analysis" (Prentice Hall, 1978) p 62-63

17. C. P. Chen and R. S. Lakes, "Holographic study of conventional and negative Poisson's ratio metallic foams: elasticity, yield, and micro-deformation",
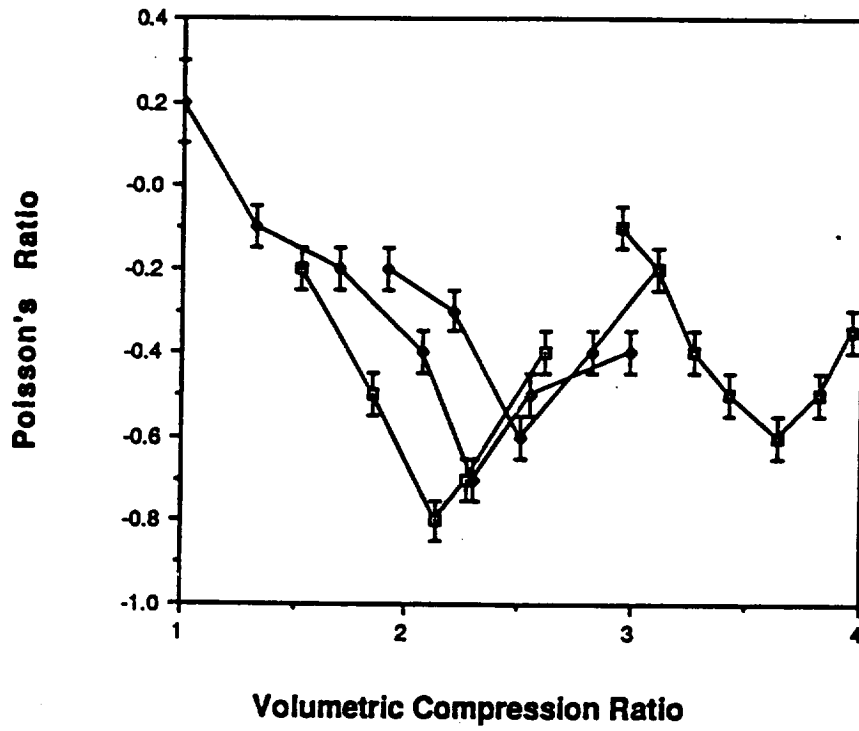
J. Materials Science, in press.

18. R. Hill, in "The Mathematical Theory of Plasticity" (Oxford University Press,1983) p 236

19. M. C. Shaw and T. Sata, Int. J. Mech. Sci., 8 (1966) 469

20. J. A. Rinde, J. Appl. Polym. Sci., 14 (1970) 1913

21. M. Wilsea, K. L. Johnson and M. F. Ashby, Int. J. Mech. Sci., 17 (1975) 457

22. A. G. Dement'ev, P. I. Seliverstov and O. G. Tarakanov, Mekhan. Polim., No. 1 (1973) 45

23. A. N. Gent and A. G. Thomas, Rubb. Chem. Tech., 36 (1963) 597

24. J. M. Lederman, J. Appl. Polim. Sci., 15 (1971) 693

25. A. McIntyre, G. E. Anderton, Polimer 20 (1979) 247
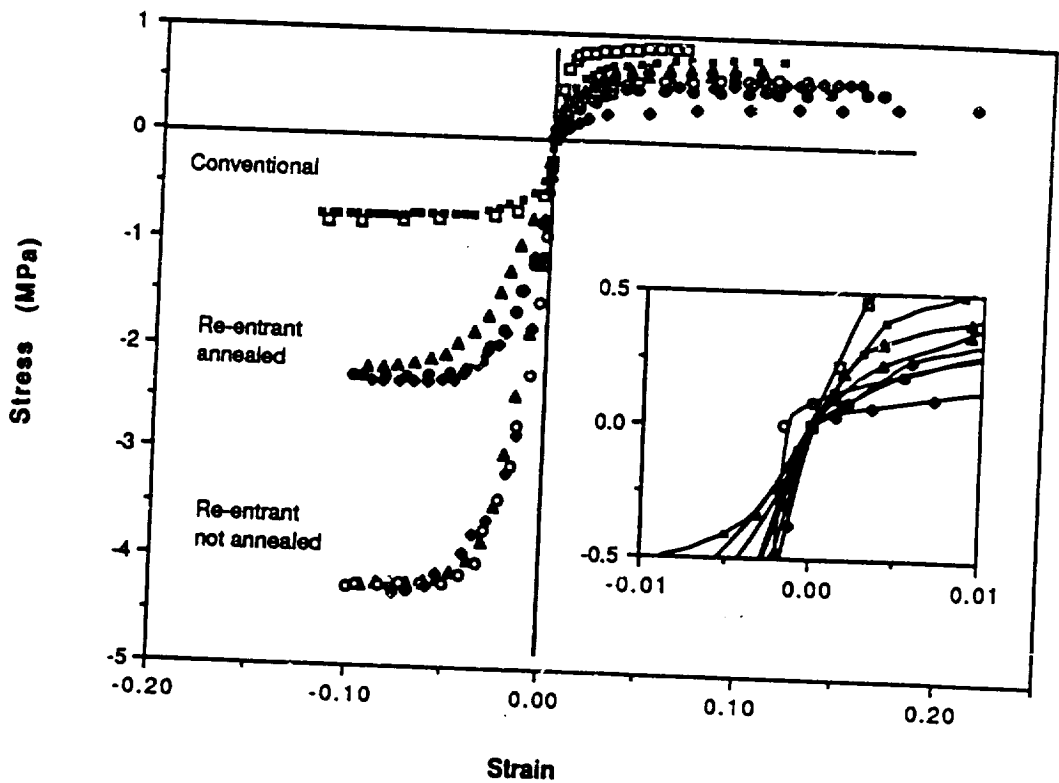
List of Figures

Fig. 1   Poisson's ratio vs volumetric compression ratio, Initial relative density; ▣ ,0.1; ◊,0.09; ♦ ,0.08; ▫ ,0.04

Fig. 2   Poisson's ratio vs final relative density; Initial relative density;   ▣ ,0.1; ♦,0.09; ▣ ,0.08; ▫ ,0.04

Fig. 3   Young's modulus as it depends upon initial relative density and upon volumetric compression ratio; Initial relative density; ▣ ,0.1; ▫ ,0.09; ♦ ,0.08; ○ ,0.04

Fig. 4   Stress- strain relationships for conventional and re-entrant foams. Initial relative density: 0.08.   Solid symbols: annealed. Open symbols: not annealed.

▫   Squares: conventional foam, volumetric compression 1.

△   Triangles: re-entrant foam, volumetric compression 2.0.

○   Circles: re-entrant foam, volumetric compression 2.5.

◊   Diamonds: re-entrant foam, volumetric compression 2.0.

Fig. 5   Young's modulus vs permanent volumetric compression ratio for annealed and non annealed copper foam at a strain of 0.5%; ◊ ,non-annealed; ♦ ,annealed

Fig. 6 Toughness vs permanent volumetric compression of the conventional and re-entrant copper foams: ▫ , non-annealed; ♦ , annealed

Fig. 7   Poisson's ratio vs longitudinal strain for copper foam, initial relative density: 0.08. Solid ♦, conventional foam; ○, re-entrant foam, not annealed, volumetric compression ratio of 2.0

Fig. 8   Poisson's ratio vs longitudinal strain for volumetric compression ratio of 2.5, Initial relative density: 0.08; ○ ,non-annealed; ● ,annealed; ▫ ,optical result
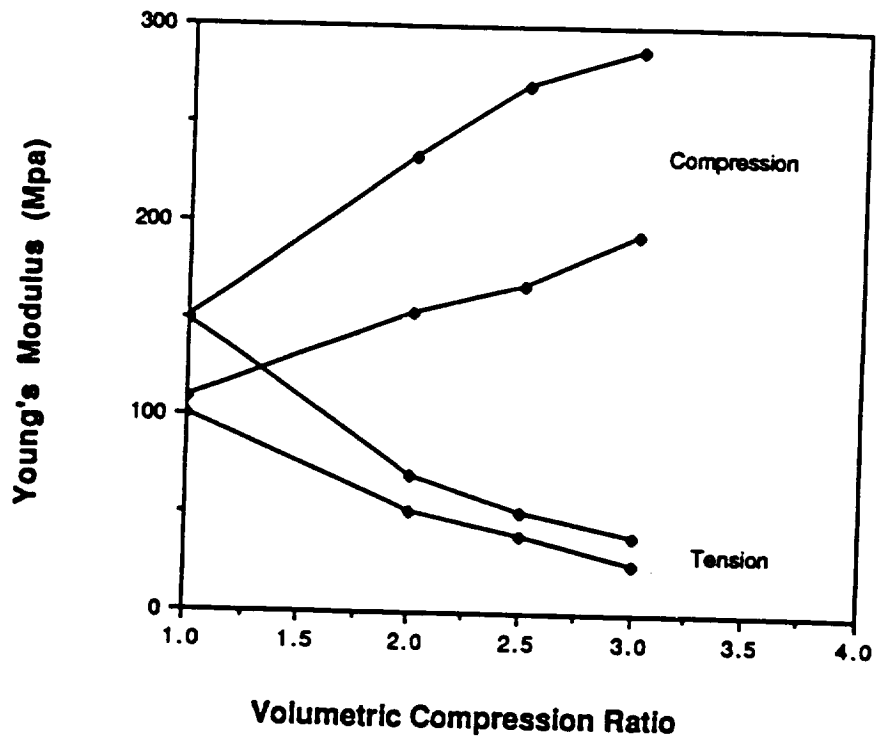
Fig. 9   Poisson's ratio vs longitudinal strain for volumetric compression ratio of 3.0, Initial relative density: 0.08; o ,non-annealed; • ,annealed
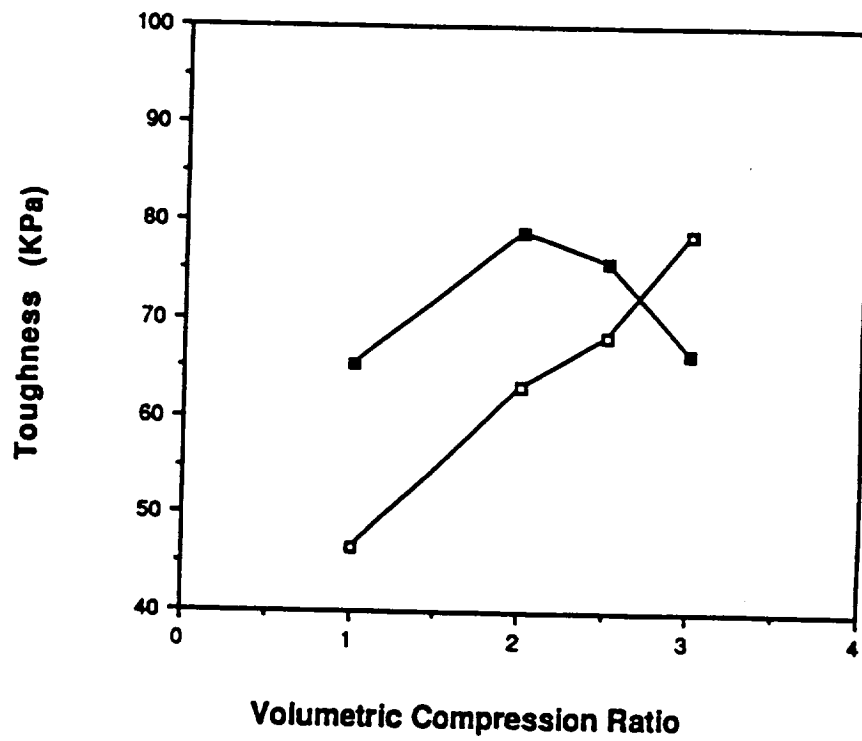
Fig. 10   Scanning electron micrographs of conventional copper foam (top), relative density 0.08; re-entrant copper foam (bottom) initial relative density 0.03, volumetric compression ratio 2.5.
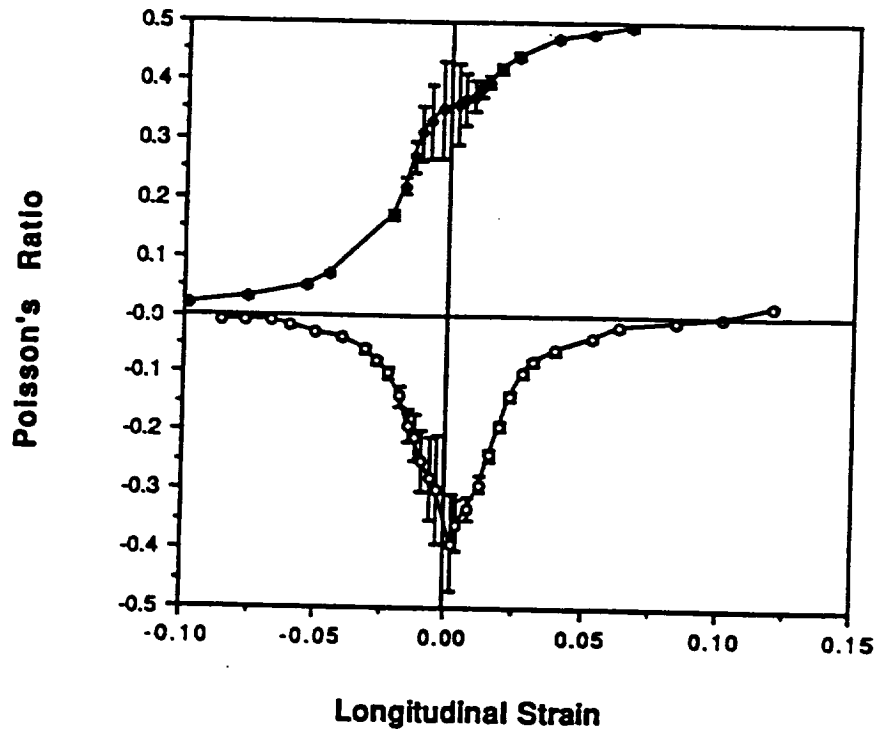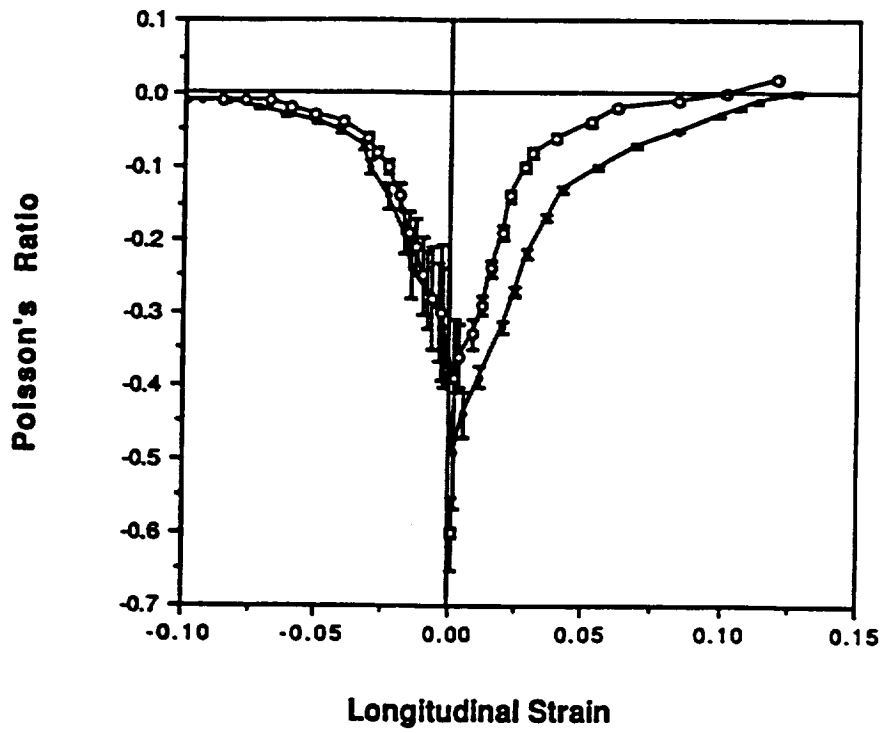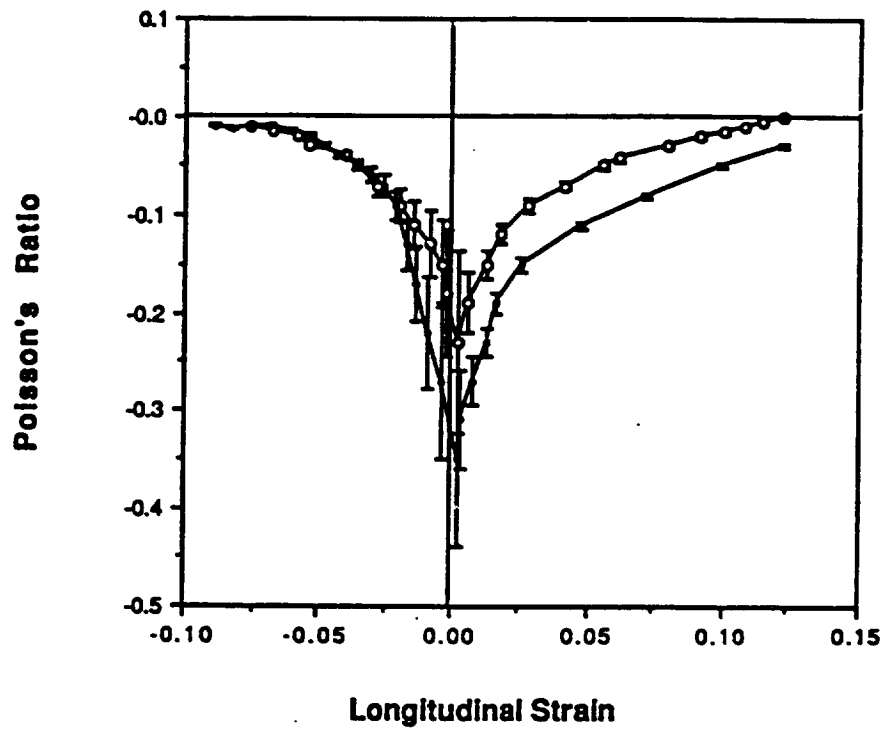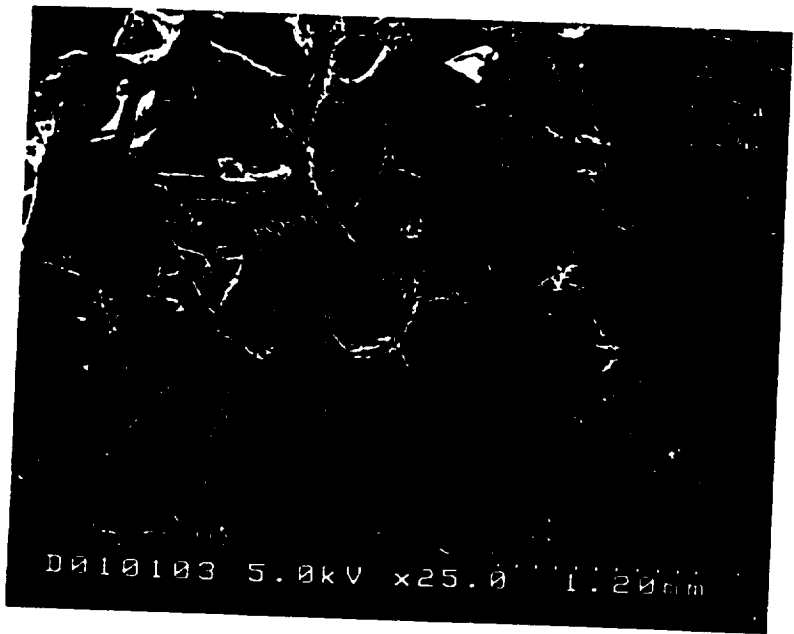
Volumetric Compression Ratio

Young's Modulus (Mpa) vs **Volumetric Compression Ratio**

Stress (MPa) vs Strain

Conventional

Re-entrant
annealed

Re-entrant
not annealed

Volumetric Compression Ratio

Figure: Poisson's Ratio versus Longitudinal Strain

Longitudinal Strain

Longitudinal Strain

D010103 5.0kV x25.0 1.20mm

D010105 5.0kV x40.0 750μm

25H-28